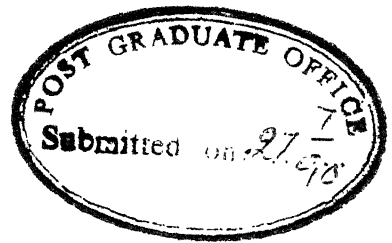# ELECTRON TRANSPORT AND MAGNETIC STUDIES OF CuMn BINARY ALLOYS

A Thesis Submitted
in Partial Fulfilment of the Requirements
for the Degree of

DOCTOR OF PHILOSOPHY

by

ALOK BANERJEE

to the

DEPARTMENT OF PHYSICS

INDIAN INSTITUTE OF TECHNOLOGY, KANPUR

July, 1990

C E R T I F I C A T E

It is certified that the work contained in the thesis entitled "ELECTRON TRANSPORT AND MAGNETIC STUDIES OF CuMn BINARY ALLOYS" by Alok Banerjee has been carried out under my supervision. This work has not been submitted elsewhere for a degree.

(Alak Kumar Majumdar)
Professor
Department of Physics
IIT Kanpur, INDIA.

July, 1990

Name of Student :   ALOK BANERJEE   ROLL NO. 8310962

Degree for which submitted : Ph.D., Department of Physics

Thesis Title : **ELECTRON TRANSPORT AND MAGNETIC STUDIES OF CuMn BINARY ALLOYS.**

Thesis Supervisor : Dr. A.K. Majumdar, Professor of Physics, I.I.T. Kanpur - 208016, India.

Month and year of thesis submission : July 1990

The fascinating magnetic, thermodynamic and electron transport properties exhibited by noble metal-transition metal alloys have kept them in the limelight of condensed matter physics for many decades till now. They have thrown tough challenges to experimentalists and theoreticians which resulted in diverse experiments and their interpretations. CuMn alloys, by virtue of their properties, won an important place in the family of the above class of materials. They have shown a variety of magnetic orders which raised apparently unending controversies about their nature and origin. Over the years, the low Mn concentration range belonging to Kondo and canonical spin-glass regimes were thoroughly studied experimentally as well as theoretically. But the studies on the high concentration regime, especially near the percolation threshold, are far from being satisfactory. The dependence of the magnetic properties of CuMn alloys on their metallurgical conditions is well known. Alongwith these, the complicated nature of the binary phase diagram poses serious problems about crystallographic phases in these concentrated

alloys. The existing magnetic phase diagram, constructed by taking scattered experimental results on different sets of samples, looks more like a collage.

This motivated us to study the $Cu_{100-x}Mn_x$ alloys in large x region. We started our study with the following aims in mind :

a. To identify the magnetic phases through their characteristic properties within the same crystallographic phase and metallurgical conditions.

b. To look for a mixed phase on the antiferromagnetic side.

c. To study the effect of magnetic phases on electron transport.

d. To determine the magnetic contribution to electrical resistivity.

e. To construct an improved magnetic phase diagram and compare it with the existing theoretical one.

We introduce the subject in Chapter I of the thesis followed by a sketch of the theoretical work and a brief review of experimental results. This chapter provides the motivation behind the work alongwith some complications associated with the problem.

The setting up of experimental facilities and the experimental procedures are described in Chapter II. $Cu_{100-x}Mn_x$ alloys with x = 4.4,9,35,45,55,65,72,80 and 85 are prepared by induction melting of spectroscopically pure elements in pure argon atmosphere followed by homogenization at appropriate high temperatures. Then they are swaged, rolled, shaped and quenched from suitable temperatures to preserve the f.c.c. (γ) phase. We have performed chemical and spectroscopic analyses together with x-ray diffraction studies to characterize the samples.

A low cost, high accuracy mutual inductance bridge is constructed using only operational amplifiers to measure low-field ac-susceptibility. The superiority of this bridge over the existing ones is because of the use of low-pass and high-pass active filters. These filters act as phase splitters and give the bridge better frequency response since they replace all inductors from the circuit. The measurement is done using a closed-cycle helium refrigerator (cryotip) from 16 to 300K. The interfacing with the cryotip gives enormous problem and limits the minimum detectable moment to 6×10^{-7} emu. The bridge could be made more sensitive ($\sim 1 \times 10^{-7}$ emu) with the use of liquid coolant and glass cryostat. This is indeed found with liquid nitrogen as coolant. The bridge is calibrated with paramagnetic salts and standardized with other magnetic and superconducting materials.

An automated electrical resistivity set-up is developed during the course of this study. It consists of a cryotip, a $7\frac{1}{2}$ digit multimeter, a temperature controller and an IBM PC-XT. In this set-up we can measure the resistivity from 8 to 300K. The temperature can be stabilized to within 0.1K and the relative accuracy in resistivity is better than 1 part in 10^5.

The dc-magnetization was measured with a vibrating sample magnetometer attached to an electromagnet and a liquid nitrogen cryostat. We have also used a standard high temperature oven assembly. Some of the results are checked using a Faraday balance and a SQUID magnetometer elsewhere.

Chapter III deals with the results and discussion of our experimental observations. The analyzed compositions of the alloys are quite satisfactory and the samples are found to exhibit

a single f.c.c.(γ) phase with lattice parameters ~ 3.757 A.

The ac-susceptibility (χ_{ac}) vs temperature (T) measurements on $Cu_{100-x}Mn_x$ with x = 4.4 and 9 have shown typical spin-glass cusp at temperatures T_f which match very well with the literature values. χ_{ac} vs T curves for alloys with x = 35-80 exhibit broad peaks at T_f and are affected by external dc field. The peak value of χ_{ac} has decreased with the increase in x. These results are discussed with the help of the superparamagnetic model. These alloys are thought to have antiferromagnetic clusters of spins and the broad peaks in χ_{ac} vs T indicate the blocking of these clusters.

The dc-magnetization measurements are done to find the effect of field-cooling (FC) and zero-field-cooling (ZFC) up to 15 kOe field and to observe time-dependent magnetization. The dc-susceptibility (χ_{dc}) vs T curves display broad peaks at T_f in the ZFC state for samples with x = 35-80 but the peaks get flattened out in the FC state. The time-dependent magnetization, M(t), which shows a $\ln t$ behavior for x = 35 - 72 has been justified. The sample with x = 80 has also shown some remanence. These kinds of behavior are similar to what is observed in canonical spin-glasses. The effective number of Bohr magneton per Mn atom, calculated from χ_{dc}, shows a decrease with the increase in Mn concentration indicating antiferromagnetically coupled spin clusters. Apart from these, x = 80 and 85 show small antiferromagnetic peaks at T_N ~ 275 and ~ 484K respectively. We have seen a clear-cut evidence of both cluster-glass and antiferromagnetism in x = 80 sample through a double transition. If we couple the above observation with neutron diffraction

results we can conclude that the alloy with x = 80 exists in a mixed cluster-glass and antiferromagnetic phase below 130K.

We finally construct a magnetic phase diagram from the χ_{ac} and χ_{dc} measurements and compare it with the latest theoretical phase diagram. The agreement is quite satisfactory.

A quantitative analysis of resistivity (ρ) vs temperature (T) has been made to estimate the magnetic contribution. We have assumed the validity of Matthiessen's rule and Bloch-Grüneisen law for the phonon contribution (ρ_{ph}). We have considered two well known forms of magnetic contributions (ρ_{mag}) for spin-glass, namely, $AT^{3/2}$ and $AT^2 - BT^{5/2}$. Our data have been fitted to equations consisting of terms for static disorder (ρ_o), ρ_{ph} and ρ_{mag}. For ρ_{mag} both the above forms are used separately. For all our samples in the spin-glass range of temperature ($T < T_f$), a better fit is obtained with the form of $\rho_{mag} \sim AT^2 - BT^{5/2}$. From this fit below T_f we have extracted the coefficients of the ρ_{ph} term and the ρ_o term. These two values and the data above T_f are used to estimate the ρ_{mag} for all temperatures. We find that for samples x = 35-72, ρ_{mag} has maxima at temperatures which increase with x while for x = 80 and 85, ρ_{mag} increases monotonically with T. This is the first report of a systematic study of magnetic scattering in concentrated crystalline alloys.

In conclusion chapter IV highlights the important findings and the scope of future work.

ACKNOWLEDGEMENT

Manu, Sastry and Raje. We shared many enjoyable moments and weathered many storms with solidarity.

During my Ph.D. I could manage to have many adventures with my friends but the most memorable one I had was with Venkey, Sen and Sudhir in our boat trip. Those five days on the Ganges were moments of pure thrill and high danger.

I pay my tribute to my friends in the action committee and many persons who actively supported from out side in our struggle for a better environment for research in this institute. I was fortunate to be in the company of Amit, Anbu, Bala, Bhat and family, Bipin, Boga, Brijesh, Dada, Damu, Danial, Debanand,Dharampal, Emmanuel, Ghantu, Gill, Godre, Govind, Ilango, Islam, Kanetkar, Kartikeya, Mishra, Prateek, Rajput, Ranjit, Razee, Sajan, Sandy, Sanjay, Sankaranarayanan, Santosh, Sanyal, Siddartha, K.S.Singh, Shuklaji, Srini, the Subbaraos,Tenka VC, Vijayan and many others. They proved to be really friends in need.

I could never feel that I am away from home whenever I was in Prof. Majumdar's residence, with the members of his family.

It is difficult to put in words all that my family has done for me and my feeling towards the members of my family. They always encouraged me to achieve my goals in life by sacrificing their needs.

I am indebted to the people of India whose silent encouragement and unconditional support to this endeavor can never be acknowledged in words.

Alok Banerje

To

My Parents

CONTENTS

LIST OF FIGURES

LIST OF TABLES

CHAPTER I

Introduction

1.1 Preamble

Condensed matter physics has remained a lively branch of science for the exciting and challenging problems it tackles in different fronts using many possible experimental methods and theoretical techniques. The alloys of noble metal and transition metal elements belong to a brighter front of the field for the fascinating magnetic, thermodynamic and electronic properties exhibited by them. CuMn and AuFe alloys are the two important systems belonging to the above class of materials. The glories lie on the diverse interpretations of the exhaustive studies made on them. The magnetism of intermediate concentration regime of these systems, from time to time, has been interpreted in terms of "ensemble of mutually interacting ferromagnetic and antiferromagnetic domains" [1]; "mictomagnetism" [2], "rock magnetism" [3] and "superparamagnetism" based on phenomenological model of Néel [4] and developed as "magnetic clusters" or "magnetic clouds" [5]; and finally "spin-glass" [6] and "cluster-glass"[7].

In noble metal hosts like Au or Cu, when we keep on substituting randomly transition metals with unpaired 3d-electrons like Fe or Mn, first we encounter the Kondo regime where the 3d-electrons of the magnetic ion interact antiferromagnetically with the conduction electrons. At low temperatures, this interaction makes the isolated magnetic ion non-magnetic and

enhances the electron scattering cross-section giving rise to resistivity minimum. When we add more of magnetic ions in the system, they start interacting with each other through RKKY interaction. This indirect inter-impurity interaction opposes the weakening of moment due to Kondo effect, and beyond a certain concentration of magnetic ions we see the stabilization of magnetic moments where, what is called "good" moment is formed. Here we encounter a magnetic phase which is commonly known as spin-glass. In this case, below a certain temperature, many interesting magnetic phenomena like irreversible effects, time-dependent magnetic properties resulting from the randomly frozen (for time intervals over which experiments are carried out) magnetic moments with a degenerate ground state, etc. take place. Also, we come across the effect of "measurement time" on the freezing in a particular experiment, indicating non-equilibrium phenomena, often referred to as non-ergodicity [8]. The manifestation of the irreversible effects, time-dependent magnetic properties and effect of "measurement time" on the freezing can be seen from the experimental signatures shown in Figure 1.1 (a)-(c). The state of randomly frozen spins can give rise to a quenched disorder in an otherwise crystalline solid. The randomly distributed magnetic ions interact with one another through RKKY interaction, whose magnitude and sign depend on the distance between the magnetic ions. Thus, spins interact with one another ferro- or antiferromagnetically, depending on their distances. As a result, we find that contradictory interactions coming through different paths are experienced by a magnetic ion. This
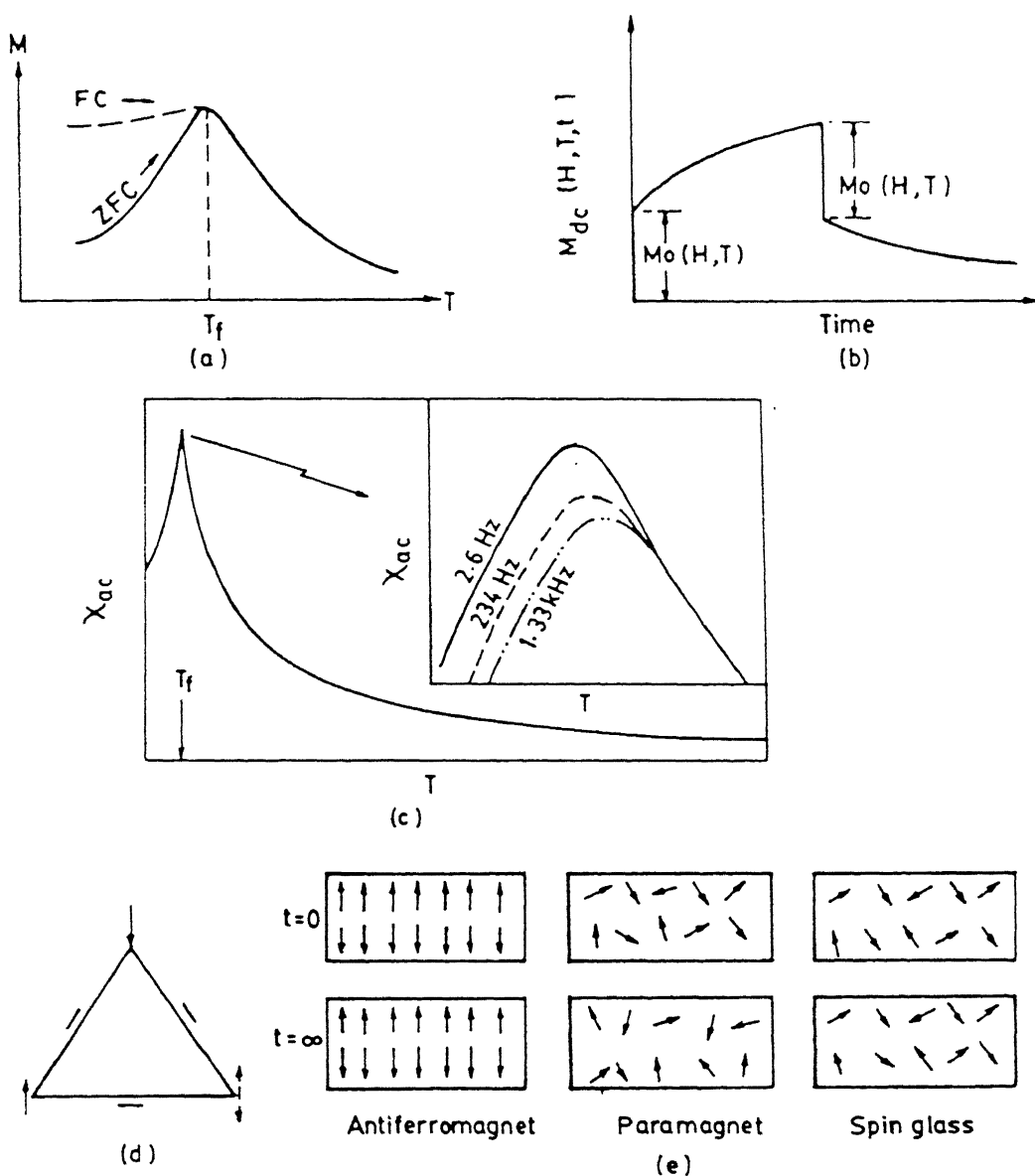
Figure 1.1   (a) Reversible   and   irreversible
magnetization   vs   temperature   for   a
spin-glass. (b) Time-dependent magnetization
of   a   spin-glass.   (c)   Frequency-dependent
ac-susceptibility   vs   temperature   of   a
spin-glass. (d) A   frustrated   lattice.   (e)
Example of random freezing in a spin-glass.

conflicting situation is called "frustration" [9]. Thus, quenched magnetic disorder and frustration are the basic ingredients of the spin-glass phase, which is achieved without having a spatial long-range magnetic order. In Figure 1.1(d) we show that, if we define a triangular lattice with antiferromagnetic interaction and put three spins at the vertices, the third spin cannot simultaneously satisfy both the interactions coming from the two different paths. This makes the third spin and as a matter of fact the whole lattice frustrated.

The meaning of random freezing may get clarified in Figure 1.1(e) where we see that, though the spins in both the paramagnet and the spin-glass are randomly oriented, unlike paramagnet the spins in spin-glass are frozen in time. The spins in an antiferromagnet seem to be frozen but they are not random and have a long-range order. Quenched disorder and frustration are the two important common features of all the spin-glasses, irrespective of the origin of these two characteristics. This is the reason why we observe spin-glass phenomenon in conducting crystalline and amorphous alloys as well as in insulating systems. Mydosh [10] has classified various types of spin-glasses. Here we give typical examples of some spin-glasses :

    a)   Noble metal-transition metal alloys, i.e., canonical spin-glasses ⇒ AuFe, CuMn, AgMn etc.

    b)   Transition metal-transition metal alloys ⇒ PdMn, VFe, etc VFe, etc.

    c)   Rare earth alloys ⇒ $La_{1-x}Gd_xAl_2$, $La_{80}Th_{20}Ce$, etc.

    d)   Transition metal compounds ⇒ $(Ti_{1-x}V_x)O_3$

e) Amorphous metallic alloys $\rightarrow$ $(A_x\bar{B}_{1-x})_{75}$ $P_{16}B_6Al_3$ where $A \equiv (Fe,Co)$ and $\bar{B} \equiv (Mn,Ni,Cr,Mo)$ and LaGd, etc.

f) Amorphous semiconductors $\rightarrow$ $(Sb_2S_3)_x(SbI_3)_y$ Fe_z, Si

g) Insulators and semiconductors $\rightarrow$ $Eu_xSr_{1-x}S$, $Eu_{1-x}Gd_xS$, $Fe_{1-x}Mg_xCl_2$, etc.

h) Intercalated graphite $\rightarrow$ Intercalating $FeCl_3$ into ordered graphite

i) Induced moment systems $\rightarrow$ Pr $P_{0.9}$.

In spin-glasses, at low concentration of magnetic ions, we come across the scaling regime which is a result of strictly RKKY interaction. Here the spin-freezing temperature is proportional to the concentration of magnetic ions, and different experimental quantities are universal functions of T/c and H_{ext}/c, where c is the concentration of magnetic ions and T and H_{ext} are temperature and external magnetic field, respectively. As we increase the concentration, there is a greater probability for a magnetic ion to be first or second nearest neighbour of another magnetic ion. In Figure 1.2(a), we have shown a 2-dimensional square lattice of a noble metal host where 10% of the lattice sites are randomly substituted by transition metal impurities. Here we can see that most of the transition metal ions are well separated (beyond second nearest neighbour). If the spins are not well separated then since the wave functions of 3d electrons of the magnetic ions have a finite extent, there is a considerable interatomic overlap resulting in a direct exchange. This produces a short-range interaction, which couples the neighbouring magnetic ions ferro- or antiferromagnetically depending on the nature of

$\odot \rightarrow$ *transition-metal atom*

(a)

$\odot \rightarrow$ *transition-metal atom*

(b)
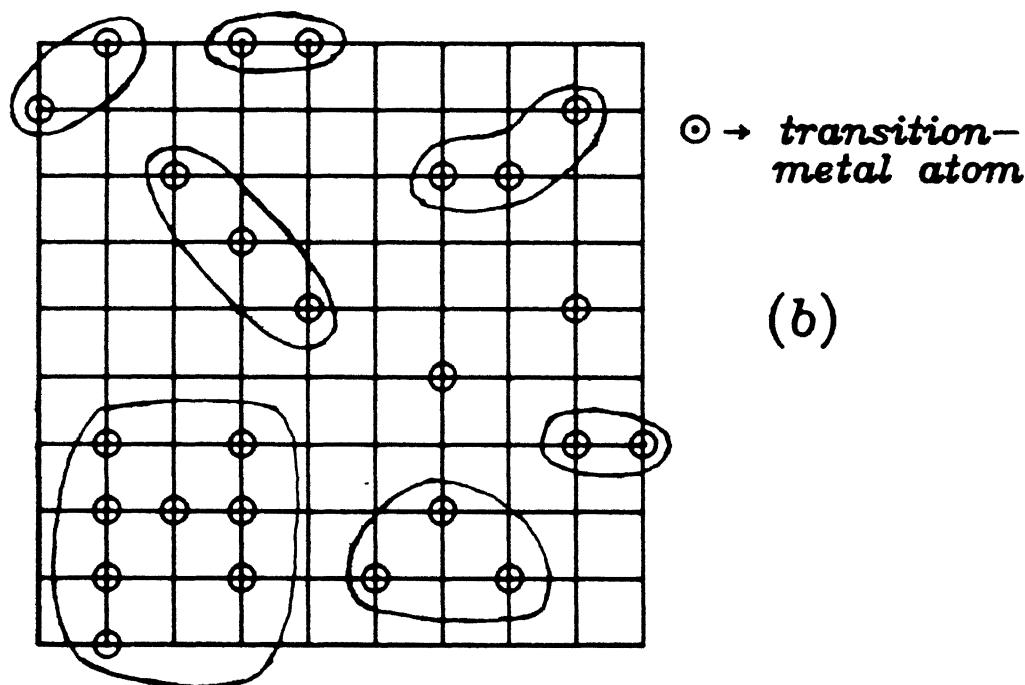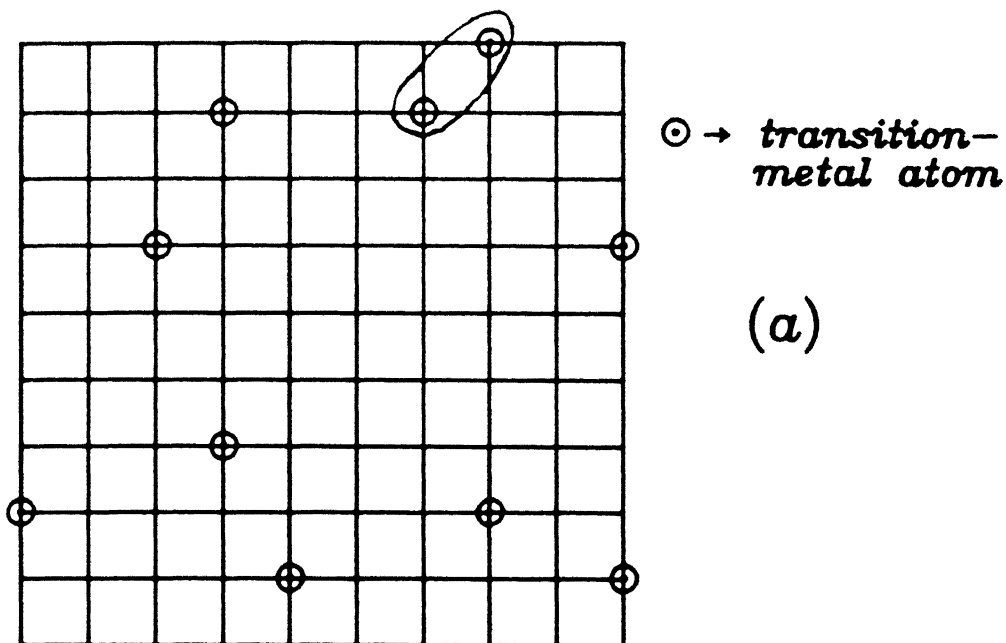
Figure 1.2 (a) A 2-dimensional square lattice of noble metal host where 10% of the lattice sites are randomly substituted by transition metals. (b) A 2-dimensional square lattice of noble metal host where 25% of the lattice sites are randomly substituted by transition metals.

the 3d ion. At still higher concentrations, this short-range magnetic interaction will lead to the formation of magnetic clusters because of the concentration fluctuation in these random alloys. In Figure 1.2(b) 25% of the noble metal sites are randomly substituted by transition metal ions. This is done by random number generator in a computer. Here we can see that the magnetic clusters of various shapes and sizes can be identified considering only the first and the second nearest neighbour interactions between magnetic ions. In addition, at these large concentrations, chemical or atomic order may give rise to chemical clustering affecting the local magnetic order . The magnetic response of these alloys are dominated by large magnetic clusters and they are termed as mictomagnet or cluster-glass, though it carries most of the important signatures of spin-glass resulting from quenched disorder and frustration. These mictomagnets or cluster-glasses form larger and larger magnetic clusters with the addition of magnetic ions, and finally percolate to long-range magnetic order.

Though AuFe and CuMn are well studied in the low concentration spin-glass range, the high concentration range up to the long-range ordered state, and concentrations near and around the critical concentration have their own glories and difficulties. As the system proceeds towards long-range order, it goes through a state which tries to retain the signatures of spin-glass, while manifestation of long-range order is also evident. Hence the phenomena like coexistence of different magnetic phases and double transitions show up. If the long-range

order is a ferromagnetic one, then it is not very difficult to isolate it from the spin-glass state. But the coexistence of long-range antiferromagnetism and the spin-glass state is very difficult to observe, at least through bulk property measurements. This may be one of the reasons why the phase boundary between the spin-glass and ferromagnetic states appears to be more often studied than the spin-glass to antiferromagnetic one. CuMn alloys belong to the latter class and we would like to concentrate on the electron transport and magnetic properties of this alloy system near the percolation threshold.

1.2 Motivation

As we have said earlier, the difficulties of experimental studies on the coexistence of antiferromagnetism and spin-glass can justify the scarcity of such studies in the literature especially on the metallic systems. On top of that CuMn, which is expected to show such behaviour, is not very systematically studied near the percolation threshold. The dependence of the magnetic properties of CuMn alloys on their metallurgical conditions like annealing, quenching, aging, plastic deformation, etc. is well known. Alongwith this the complicated nature of the metallurgical binary phases creates serious problems regarding the crystallographic phases in the concentrated CuMn alloys. These problems throw serious doubt on the interpretation of experimental results from different groups on different sets of samples. The construction of magnetic phase diagram on the collated data thus makes it unsound.

This motivated us to study the electrical and magnetic properties of $Cu_{100-x} Mn_x$ alloys in the large x region on samples which are subjected to the same metallurgical conditions (quenching) and having the same crystallographic phase (γ-phase). We started our study with the following aims in mind :

a.   To identify the magnetic phases through their characteristic properties within the same crystallographic phase and metallurgical conditions.

b.   To look for a mixed phase on the antiferromagnetic side.

c.   To study the effect of magnetic phases on electron transport.

d.   To determine the magnetic contribution to electrical resistivity.

e.   To construct an improved magnetic phase diagram and compare it with the existing theoretical one.

1.3   Complications of the Problem

Before we get into the actual system we should study the problems and novelties of γ-phase (fcc) CuMn alloys.   A few of them are discussed below :

(1) Magnetism of Mn :   Mn shows first nearest neighbour antiferromagnetic and second nearest neighbour ferromagnetic interactions. This is the reason for the increase in effective number of Bohr magneton in CuMn alloys with the addition of Mn at low concentrations of Mn, since the second nearest neighbour, which is ferromagnetically coupled, is more probable than the first nearest neighbour simply on statistical grounds. With the addition of more Mn the first nearest neighbour interaction starts

growing and we observe a decrease in the effective number of Bohr magneton. The magnetic moment falls drastically which makes magnetic measurements difficult [11,12].

(2) Metallurgical Condition : It has been shown that metallurgical conditions like quenching, aging, annealing and plastic deformation have got remarkable effects on the magnetism of CuMn [12].

(3) Crystallographic Phase : Figure 1.3 is the binary metallurgical phase diagram of CuMn alloys. It may become clear from the figure that above 25 at% Mn, γ-phase CuMn can be produced only by fast quenching from high temperature near the liquidus curve.   In the intermediate temperature range, there is a crystallographically complex phase($\gamma+\alpha$).   Hence the quenched γ-phase CuMn remains a metastable structure, making the high temperature studies difficult and unreliable. On top of that, a change from cubic to tetragonal phase is observed around Mn concentration of 74 at% [11,13].

(4) Antiferromagnetic Structure : A change in the antiferromagnetic structure is observed in neutron diffraction studies of CuMn. On the long range antiferromagnetic side it is the AF1 structure, where the first nearest neighbour is antiferromagnetically coupled while the second nearest neighbour is ferromagnetically coupled.   But as we cross the critical concentration from Mn rich side, CuMn shows an AF3 antiferromagnetic structure where both first and second nearest neighbours are antiferromagnetically coupled. This change in the magnetic structure appears to coincide with the change from

BINARY PHASE DIAGRAM of Cu Mn
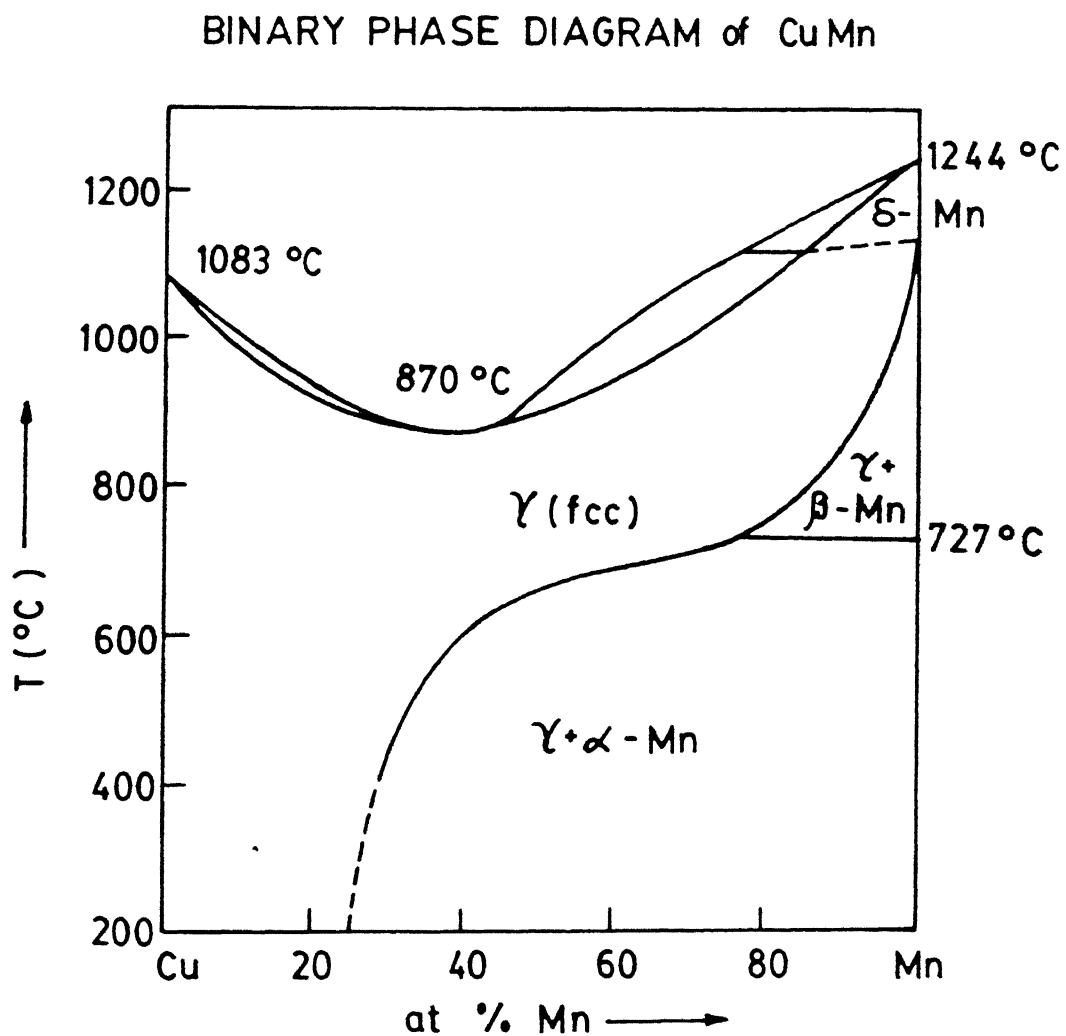
Figure 1.3   Binary phase diagram of CuMn alloys.

long-range to short-range magnetic order at the critical
concentration [11].

(5) Percolation Concentration : Theoretical calculations
show that antiferromagnetically coupled spins in f.c.c lattice
requires ~ 46 at% of magnetic atoms to give rise to a long-range
order. But in CuMn, experiments suggest a much higher
concentration of 72 at% Mn to get to a long-range
antiferromagnetism [11,14,15].

1.4 Theoretical Status

In this section we give a brief sketch of the
theoretical work done on the substitutional alloys focussing on
the spin-glass aspect. For a detailed discussion one may consult
the recent review articles [16,17].

The earlier theories which tried to explain some of the
spin-glass properties are based on the idea of random distribution
of the local magnetic fields. The first among these was proposed
by Marshall [18]. Later on Marshall's intuitive theory was put on
a rigorous basis by Klein and Brout [19]. Blandin made the first
attempt to derive the scaling-law behaviour of the canonical
spin-glasses from the power-law behaviour of exchange interaction.
Later on Souletie and Tournier [20] applied it effectively for
dilute alloys. The basic idea of these theories is to evaluate the
free energy from the distribution of local random magnetic fields,
and then calculate the thermodynamic and magnetic properties from
them. But these theories suffer from theoretical complications
and also they cannot explain many experimental results.

A new era in the field of randomly substituted noble metal-transition metal alloys started with the observation of a sharp cusp in the ac-susceptibility and its interpretation as a magnetic phase transition. Various theories came into the field which considered the spin-glass transition as a phase transition. Though it is difficult to give an account of all those theories, we will mention a few points which have been considered in order to study the phase transition.

i. Identification of the relevant physical property that distinguishes the two phases of the system, in other words, the identification of a suitable order parameter.

ii. Finding the distribution of exchange interaction.

iii. Developing a mean field theory in terms of the free energy as a function of the order parameter.

iv. Verification of the result that, in the limiting case, the mean field approximation gives an exact answer.

v. Improvement of mean field theory results by incorporating critical fluctuations in the theory.

No theory has so far fully satisfied all the above mentioned points while dealing with spin-glass transition. This is the reason why, apart from running into theoretical complications, their predictions do not match with many experimental observations. All theories of this class suffer from one or the other inconsistency out of a few listed below.

a) Prediction of a strong specific heat anomaly which is not observed experimentally.

b) Do not explain the observed shape of low temperature

susceptibility.

c)   Theoretically the slope of magnetization vs temperature curve does not approach zero as T → 0. This implies a violation of the third law of thermodynamics.

d)   Violation of Maxwell's relation except in field-cooled samples.

A different class of theories is also proposed which do not consider the spin-glass transition to be a true thermodynamic phase transition. It is similar to the phenomenon of blocking of superparamagnetic particles in rock magnetism [5,21]. This class of theories originated from the phenomenological theory proposed for rock magnetism by Néel [4]. Here the magnetic material is considered to be made up of magnetic domains or clusters of various shapes, sizes and spontaneous magnetization. Each cluster is characterized by an anisotropy energy or a coercive field. Wohlfarth [22] has suggested the following possible sources of anisotropy :

   i)   Surface anisotropy,

  ii)   Magneto-crystalline anisotropy,

 iii)   Shape anisotropy,

  iv)   Magnetostrictive strain anisotropy,

   v)   Other magnetostatic dipole-dipole effects,

  vi)   Anisotropic exchange effects.

The anisotropy acts like a potential barrier for the particle or cluster magnetization. The thermal activation of the cluster magnetization over the barrier leads to the relaxation of the remanent magnetization given by

$$M_r = M_s \exp(-t/\tau) , \tag{1.1}$$

where M_s is the spontaneous magnetization of the cluster and τ is the relaxation time given by

$$\frac{1}{\tau} = \frac{1}{\tau_0} \exp\left[-\frac{vH_c M_s}{2k_B T}\right] . \tag{1.2}$$

Here v is the volume of the particle, τ_0 is a constant $\simeq 10^{-9}$ second, H_c is the coercive field, k_B is the Boltzmann constant and T is the temperature. Below a certain temperature T_B , called the blocking temperature of a given cluster, the relaxation of magnetization becomes difficult. This process of thermal activation and blocking of cluster magnetization can explain many experimental observations. We have discussed different aspects of these theories in Chapter III in connection with our experimental results. Here we give some results deduced from these class of theories.

Wohlfarth has calculated the magentic susceptibility which is given by

$$\chi(T) = \frac{C}{T} \int f(T) \, dT , \tag{1.3}$$

where C is the Curie constant and $f(T)$ is the distribution of blocking temperatures for the clusters. The physical implication of Equation (1.3) is that only those clusters contribute to the susceptibility which are not yet "frozen", or where blocking temperature $T_B < T$. In the absence of a first principle

calculation of $f(T_B)$, it is estimated [23] from the experimentally measured value of $\chi(T)$ using the relation,

$$f(T_B) = \frac{1}{C} \frac{d(\chi T)}{dT} .$$ (1.4)

Murani [24] has reframed Equation (1.4) in terms of a distribution of relaxation times of the clusters $N(\tau)$ as,

$$\chi(\tau) = \frac{C'}{T} \int N(\tau) \, d\tau .$$

The distribution of relaxation times gives rise to a logarithmic decay in remanent magnetization [25] and hysteresis [26].

The characteristic time or the probe time τ_m of a particular measurement, decides the blocking temperature T_B of a cluster of volume v. The lower the τ_m, the higher is the T_B for a given cluster. This can explain qualitatively the frequency dependence of the peak in the ac-susceptibility curve. The difference in the spin-glass transition temperature (T_f) in different experiments can also be explained on the above basis. Since τ_m (neutron scattering) < τ_m (Mössbauer) < τ_m (ac-susceptibility) we would expect T_f (neutron scattering) > T_f (Mössbauer) > T_f (ac-susceptibility). Such variations of T_f with time scale of the experimental probes are in qualitative agreement with the corresponding results for canonical spin-glasses [27].

Though the above class of theories can explain many experimental observations, the main criticism comes from the phenomenological origin and lack of first principle calculations.

Though there are many other models proposed for spin-glasses like hydrodynamic model, percolation model, localization-delocalization model etc., we will not go into the details of them. Instead , we will mention some calculations done on the transport properties of spin-glasses.

Rivier and Adkins [28] have obtained a $T^{3/2}$ type of magnetic contribution to the resistivity in spin-glass at low temperatures. Their results are deduced from the calculation of scattering of conduction electrons by the elementary excitation of spin-glass which are the spin diffusion modes. This $T^{3/2}$ temperature dependence of resistivity has been used to explain the experimental resistivity behaviour of canonical spin-glasses.

Fischer [29] calculated the resistivity of spin-glasses from the scattering of conduction electrons by the static disorder of the impurity spin and by the low temperature spin excitations. The exchange interaction between the conduction electrons and the spins of the magnetic impurity leads to elastic and inelastic scattering. The elastic contribution is determined from the atomic positions as well as the frozen-in spin configuration. The inelastic contribution is determined by the dynamics of the impurity spins. Fischer considered a model with N spins S_i, which interact with the conduction electrons through an exchange interaction J and a spin-independent potential V. The expression for the resistivity is found to be

$$\rho(T) = \frac{m^*}{ne^2} \left[\tau_{el}^{-1} + \langle \tau_j^{-1} \rangle + \tau_{el} \langle \tau_j^{-2} \rangle \right] \quad , \quad (1.5)$$

where n is the conduction electron density, m^* is the effective mass of electrons, τ_{el} is the relaxation time for elastic electron-spin scattering process, τ_j is the relaxation time for inelastic electron-spin scattering. The third term in Equation (1.5) comes from the interference between magnetic and non-magnetic scattering. This cross term vanishes in a spin-glass in zero external field. <···> denotes summation over all modes.

Taking into account the spin diffusive modes the resistivity is calculated to be of the form

$$\rho(T) = \frac{m^*}{ne^2} c\pi N(0) \left[V^2 + \frac{J^2}{4} \left\{ q(T) + \frac{18}{\pi} \chi \left(\frac{(k_B T)^2}{k_0^2 D} J_2 - \frac{\pi (k_B T)^{5/2}}{2\sqrt{2}(k_0^2 D)^{3/2}} J_{5/2} \right) \right\} \right],$$

(1.6)

where $N(0)$ is the density of states near the Fermi level, c is the concentration of magnetic ions, $q(T)$ is the spin-glass order parameter, k_0 is the wave vector for electrons in the conduction band, D is the diffusion constant and

$$J_n = \int_0^\infty dx \frac{x^n}{(e^x - 1)(1 - e^{-x})} \quad .$$

In Equation (1.6), χ is taken to be the temperature-independent equilibrium susceptibility of the spin-glass.

Hence the temperature dependence of electrical resistivity of spin-glass below the transition temperature $(T < T_f)$ is of the form $AT^2 - BT^{5/2}$ with the constants $A, B > 0$. This form is valid, for spin-glasses where there is no ferromagnetic clustering

or ferromagnetic short-range order.

1.5 Earlier Studies

A brief mention of the earlier studies done in CuMn alloys is already given in section 1.3 of this chapter. Here we will discuss some findings in concentrated CuMn.

Beck and co-workers [12] made detailed study in the intermediate concentration range for CuMn alloys and established the dependence of magnetic properties on the metallurgical conditions and existence of short-range orders. The magnetic short-range order is also inferred from the earlier neutron diffraction studies [30]. The recent study by Cowlam and Shamah [11], near the percolation threshold, reveals many interesting aspects about the nature of short-range order and the arrangement of spins. In this study, the long-range antiferromagnetism is found to exist above 72 at % of Mn. Wiltshire et al.[31] have studied single crystals of γ-$Mn_{90}Cu_{10}$ by neutron diffraction and found the antiferromagnetic magnons to be isotropic and damped. Kouvel [1] proposed a model for CuMn alloys with Mn concentration $\leq$ 25 at % , in terms of mixed ferromagnetic and antiferromagnetic domains. But Beck [2] interpreted these "mictomagnetic" alloys as stable ferromagnetic clusters embedded in a spin-glass matrix.

Gibbs et al. [32] have constructed the magnetic phase diagram from magnetic studies over the whole concentration range They have reproduced the phase diagram constructed by Cowlam and Shamah but detailed studies of the magnetic phases are lacking in their work. Vedyaev and Cherenkov [33] have studied

ac-susceptibility, Hall effect, magnetoresistance and ESR in a wide composition range of CuMn alloys. They have observed a "short-range-antiferromagnetism" with Mn content $\geq$ 14 at % . They have concluded that at low temperatures the alloys with high concentration of Mn show a "cluster-glass" phase with short-range antiferromagnetism but the alloys with 70 to 80 at % of Mn do not show a clear-cut magnetic phase. They have constructed the magnetic phase diagram from their data and the data collected from other groups. This phase diagram is different from that of Cowlam and Shamah or that of Gibbs et al..

CHAPTER II

Experimental Details

2.1 Sample Preparation

The alloys are prepared by induction melting of required
amount of spectroscopically pure Cu and Mn obtained from
Johnson-Mathey, Inc. (England). The elements are cleaned with
organic solvent and etched with dilute HNO_3. Then the required
quantities are weighed. Generally we have taken a little more Mn
than the required amount anticipating some Mn loss by
evaporation. The chosen compositions for $Cu_{100-x}Mn_x$ alloys have
x = 4.4,9,35,45,55,65,72,80 and 85.

The melting is performed in a water-cooled coil type
induction furnace, with a maximum power of 7 kW, fed by an "Ajax
Magnethermic Converter" which converts line current of 50 Hz to a
value between 20 to 40 kHz. The elements are taken in a high
quality alumina crucible which is placed in a graphite susceptor
and the whole thing is put in a vacuum-sealed quartz tube. This
zone was repeatedly evacuated to 10^{-3} torr and flushed with high
purity argon gas. Finally, this quartz tube is filled with argon
gas at less than atmospheric pressure. During heating process the
temperature is monitored with an optical pyrometer. The furnace is
switched off as soon as the melting of the constituents is
completed. The alloy ingot thus prepared is subjected to a
homogenization process. The ingot is put in a quartz capsule
which is then repeatedly evacuated and flushed with argon gas and
finally sealed in a partial pressure of argon. The capsule is

then heated for 2 days in a vertical furnace at a temperature which is roughly 100^OC less than the melting point of the alloy, decided from the binary phase diagram. The alloy is then dropped in a bucket full of brine to quench it to room temperature. Then the alloy ingot is swaged, cold-rolled and cut into various shapes for different measurements. The sample pieces are then sealed in quartz tubes in argon atmosphere and heated for a day in a vertical furnace at temperatures close to their melting points and then fast quenched in brine. This heat treatment is very important since this process helps in preserving both the high temperature crystallographic phase (γ-phase) and the random substitutional disorder in polycrystalline samples and preventing any possible chemical clustering. The quenching process has to be as fast as possible. Slow quenching will introduce other lower temperature crystallographic phases as discussed in section 1.3.

2.2 X-ray Diffraction

The powder x-ray diffraction pattern for the samples are recorded using a Rich Seifert Isodebyeflex 2002 diffractometer with CrK_α radiation. The same condition is set for all the samples and the scanning is done from 2θ = 20 to 150°.

2.3 Chemical Composition

A rough check of chemical composition is done from the change in weight of the samples before and after any heat treatment including the melting process. Then the chemical analysis is performed to find out the amount of individual

components in a sample. This is done after the final heat treatment. The presence of any Fe impurity is also checked chemically. Then a uv-visible spectrometer (Simadzu UV-160) is used to measure the amount of Cu and Mn as well as any trace of Fe in a sample. For this spectroscopic analysis we have used standard physical chemistry methods [34].

2.4 AC-Susceptibility Apparatus[*]

To measure the low-field ac-susceptibility of the samples we have constructed a high-accuracy, low-cost mutual inductance bridge. This bridge is used with a closed-cycle helium refrigerator or cryotip (Cryosystems and CTI-Cryogenics, model 21) to measure ac-susceptibility from 16 to 300K. Here we give the details of the principle and construction of the bridge and the calibration and measurement procedure using the apparatus.

Principle

In the mutual inductance bridge we have one primary coil and inside that there are two identical but oppositely wound secondary coils connected in series as shown in Figure 2.1(a), except that the primary and the pair of secondaries are actually coaxial. In the absence of a sample the resulting induced voltage in this system of secondaries is zero. When we introduce a sample in one of the secondaries then, because of the magnetization induced in the sample by the exciting ac field the
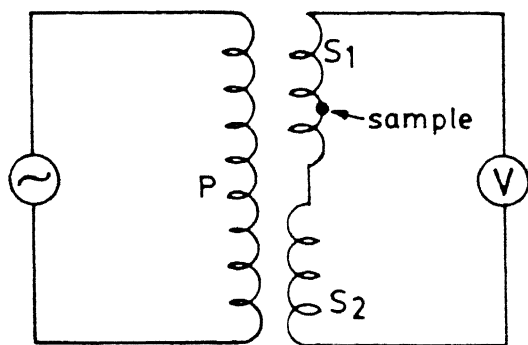
(a.)
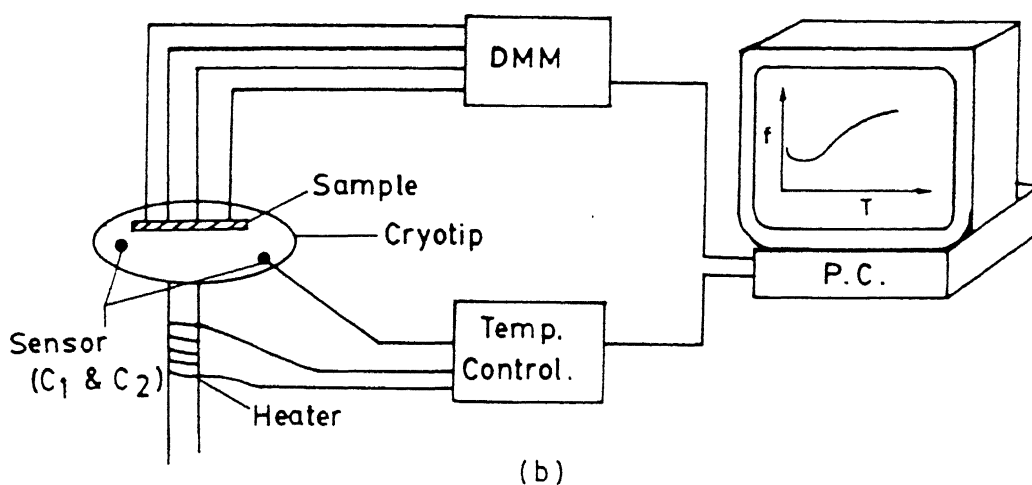
(b)

Figure 2.1 (a) The coil system for the ac-susceptibility bridge.(b) Block diagram of the automated resistivity set-up.

magnitude of the induced voltage in the two secondaries are no longer equal. As a result we get an off-balance voltage, V. We can easily find out that the voltage in a single coil containing the sample is

$$\overline{V} = - \frac{\partial \phi}{\partial t} .$$

or, $\overline{V} = - N A \mu_o \frac{\partial}{\partial t} (fM + H) = - N A \mu_o \left[f \frac{\partial M}{\partial H} \frac{\partial H}{\partial t} + \frac{\partial H}{\partial t} \right]$.

or, $\overline{V} = - N A \mu_o (f\chi + 1) \frac{\partial H}{\partial t}$, $\qquad$ (2.1)

where ϕ is the magnetic flux, N is the number of turns of the secondary coils, A is the area of the secondary coils, μ_o is the relative permeability of free space, f is the filling factor, M is the magnetization of the sample, H is the magnetic field due to the primary current and the ac-susceptibility $\chi = \partial M/\partial H$.

Now, if we consider the sinusoidal ac field to be of the form

$$H = H_o e^{i\omega t} , \qquad (2.2)$$

where H_o is the amplitude and ω is the frequency of the field, then from Equations (2.1) and (2.2) we get

$$\overline{V} = - iNA\mu_o \omega H_o (1 + f\chi). \qquad (2.3)$$

Since N,A and μ_o are constants and the constant term in Equation (2.3) is subtracted out during the process of measurement, we can

write the off-balance voltage as

$$V = i \, K \, \omega \, H_o \, \chi \, , \qquad (2.4)$$

where K is the calibration constant and i implies that the signal, which is proportional to the susceptibility of the sample, is in quadrature to the primary current. Hence once we calibrate the bridge and find out K, then by knowing ω and H_o, we can find out χ of the sample from the off-balance voltage. One can also find out χ from the change in mutual inductance after the sample is introduced in the coil.

In practice the secondaries cannot be made identical to the extent that the induced voltage can be neglected. Usually this inherent off-balance voltage is quite large compared to the voltage which is induced when a sample with low χ is placed in one of the coils. To overcome this problem we have to design a bridge which is employed to nullify the off-balance voltage present without the sample. Most of the efforts in this measurement is devoted in nullifying this inherent off-balance voltage. After this adjustment the measurement of the additional induced off-balance voltage or the change in mutual inductance, with the introduction of the sample, becomes almost trivial.

This method of measurement was first introduced by Hartshorn [35]. Then there were many modifications made to increase the sensitivity [36,37,38]. But all these earlier bridges used expensive ratio transformers to minimize the noise. In recent designs [39,40,41] operational amplifiers and Kelvin-Varley voltage dividers are used to electronically simulate

the mutual inductance. Here we have designed a mutual inductance bridge using only operational amplifiers. We have replaced the Kelvin-Varley voltage divider by a set of Butterworth active filters which act as a phase splitter. This replacement makes the bridge more sensitive with a better frequency response and reduces the cost.

Bridge design

To measure the ac-susceptibility from 16 to 300K we insert the coil assembly inside the cryotip. The problem of using a cryotip, for ac susceptibility measurement, is two-fold. It has a cylindrical pure copper tube (Figure 2.2) of 12 mm inner diameter. This narrow space limits the number of turns in the primary and secondary coils. Again, this highly pure copper tube produces enormous eddy currents which reduce the applied ac magnetic field [42]. This high conductivity copper tube cannot be replaced by less conducting ordinary materials since this establishes the thermal link between the sample zone and the cold head of the cryotip. The reduction of magnetic field depends upon temperature since eddy current varies with conductivity of the copper tube enclosing the coils. This problem is eliminated by monitoring the voltage of one of the secondary coils in the absence of the sample. By adjusting the primary current, this secondary coil voltage, which is proportional to the ac magnetic field, is kept constant. It is this very eddy current in the copper tube which prevents us from putting the coils outside and thereby able to have a large number of turns for obtaining large
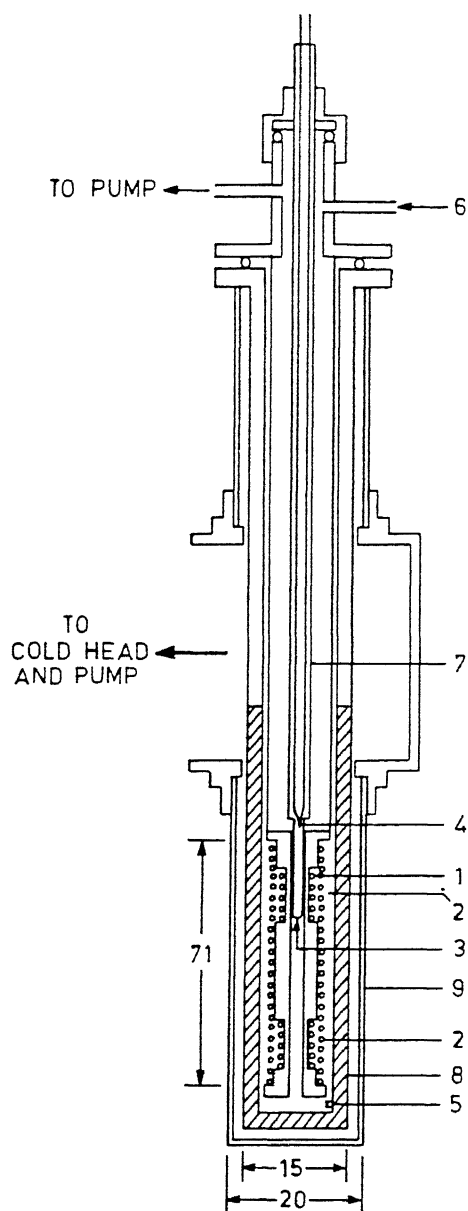
Figure 2.2   Cryostat assembly: 1. primary coil   2. secondary coil   3. sample holder   4. thermocouple 5. silicon diode temperature sensor 6. electrical feed through   7. stainless steel tube 8. highly conducting copper tube 9. Be-Cu tube. All lengths are in mm.

secondary signals. The coils are wound coaxialy on a polymer tube and the specifications of the primary and secondary coils are given in Table 2.1.

Table 2.1

Length of each secondary	=	15 mm
Length of primary	=	71 mm
Number of turns of each secondary	=	5875
Number of turns of primary	=	2711

The two secondaries are connected in series opposition so that the output of the bridge is nearly balanced without the sample. The small off-balance signal is balanced electronically. The circuit diagram of the bridge is shown in Figure 2.3.

A voltage proportional to the primary current i_p across R_1 is passed directly or through the inverter A1 and then resolved into a set of reference and its quadrature components by a pair of low-pass (A2) and high-pass (A3) Butterworth active filters with identical time constants. Each phase-splitted component is amplified by A4 and A5 and then fed into the voltage divider stage. The voltage dividers (A6 and A7) are basically inverting amplifiers whose gain can be varied by using standard decade resistance boxes R_2 and R_3 (General Radio, Type 1432B). These decade boxes have a good frequency characteristics ($\Delta R/R$ < 1%) in the audio frequency range. The mutually 90° out-of-phase components are then added by A8 and fed into the secondaries S_1 and S_2. The voltage across R_1 is fed to the phase-splitter directly
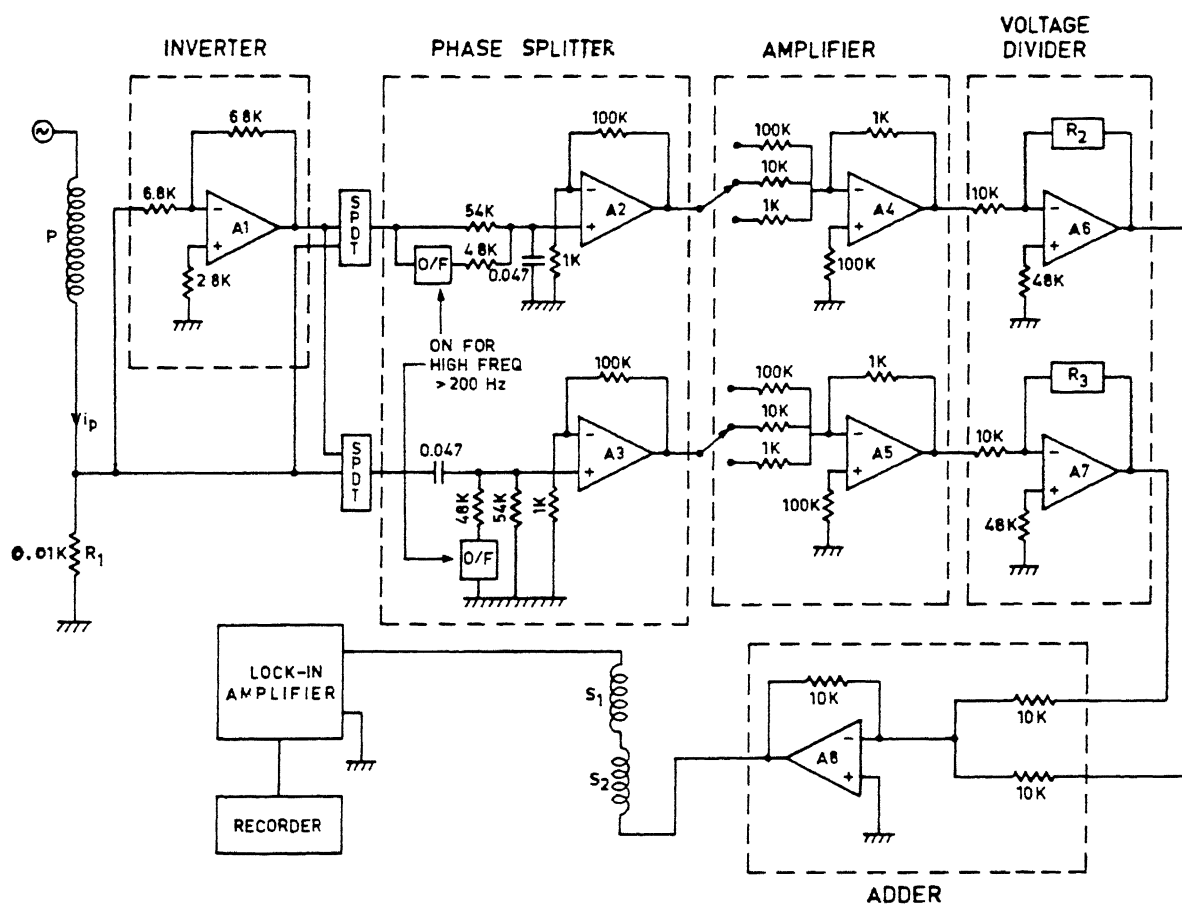
Figure 2.3   Detailed circuit diagram of the bridge. All
              ICs are 741, resistances are in Ω and
              capacitances are in μF, P is the primary
              coil, S_1 and S_2 are the two secondaries.

or after passing through the inverter depending on whether addition or subtraction is needed to the second secondary coil voltage to make the off-balance signal null. Two SPDT (single pole double throw) switches are provided for this purpose. By adjusting the gain of two amplifiers A6 and A7, the in-phase and the quadrature components of the off-balance secondary voltage can be balanced. A lock-in amplifier (PAR, model 5208), whose reference is set with the phase of the primary current, is used as a null detector for this purpose. The bridge can be balanced down to $1\mu v$(full scale) of the lock-in amplifier. The sample, placed in a polymer holder, is held from the top by a stainless steel tube (Figure 2.2). The sample can be moved in and out of the coil by moving the tube through an O-ring coupling. A copper-constantan thermocouple is placed near the sample. This voltage is measured to an accuracy of $1\mu v$ (corresponding to a temperature stability of about 0.2K) by a digital multimeter (Keithley, Model 174). A chromel/AuFe (0.03%) thermocouple would give a more realistic sample temperature since it could be placed very near the sample without introducing any unwanted signal in the secondary coil. A copper-constantan thermocouple gives, on the other hand, sizable signal below 80K due to the presence of nickel in constantan if it is placed inside the secondary alongwith the sample.

Measurement procedure and calibration

The reference phase of the lock-in amplifier is first adjusted with the phase of the primary current which in turn

determines the ac magnetic field. The bridge is then balanced without the sample using the two decade boxes R_2 and R_3. It is observed that the balancing point does not depend on the primary current. The sample holder, containing a known quantity of the sample, is then placed in one of the secondaries and moved in and out of it several times and the average off-balance signal is noted for both in-phase and quadrature components at any given temperature.

If $(R+j\omega M)$ is the impedance of the mutual inductance coils, the voltage induced in the secondary will be $V = (R + j\omega M)i_p$. Thus the quadrature component of the secondary voltage gives the mutual inductance and hence the real part of the ac-susceptibility (χ_{ac}). The in-phase component will be the dissipative part and is proportional to the imaginary part of the ac-susceptibility (χ_{ac}').

It turns out that there is a temperature gradient along the length of the copper tube of the cryotip. This gradient depends upon the temperature of the sample zone. The normalized temperature gradient $1/T \, dT/dx$ is roughly 6×10^{-2} cm^{-1}. Thus the bridge is to be balanced without sample at each temperature. If liquid helium or nitrogen is used as a coolant the balancing of the bridge without sample is not necessary at each temperature and hence susceptibility can be recorded continuously. The bridge is found to be frequency independent ($\pm 3\%$) from 20 Hz to 1.2 kHz outside the cryotip. But for very accurate measurements using the cryotip, and where the signal is smaller than 1.2×10^{-5} emu, calibration has to be done for each frequency specially for temperatures higher than 70K.

The bridge is calibrated with three standard paramagnetic salts Gd_2O_3, Er_2O_3 and $HgCo(NCS)_4$ at a field of 2 Oe and frequency 73 Hz. During measurements the background dc field due to the earth is not shielded. The plot of inverse ac-susceptibility (χ_{ac}^{-1}) with temperature is shown in Figure 2.4. The data is fitted to the Curie-Wiess law : $\chi = C/(T - \theta)$ using a standard least-squares programme and the best fitted parameters C and θ alongwith their confidence limits are listed in Table 2.2. The Curie constant C is calculated taking the standard value for Gd_2O_3. The agreement with the literature values is quite reasonable. However the discrepancy could be due to the uncertainty in thermocouple calibration, temperature gradient, purity of the salt and measurement of temperature. The error bars, shown in Figure 2.4, denote the r.m.s deviation of the experimental data from the best fitted straight lines.

Table 2.2

Sample	$\theta(K)$		C (cm^3 K / mole)	
	fitted	literature	fitted	literature
Gd_2O_3	-(20.0±1.2)	-18.4 [43]	-	8.3 [43]
Er_2O_3	-(19.3±1.2)	-13.4 [43]	12.3±0.1	11.1 [43]
$HgCo(NCS)_4$	-(10.5±1.9)	-10.0 [44]	3.2±0.1	2.5 [44]
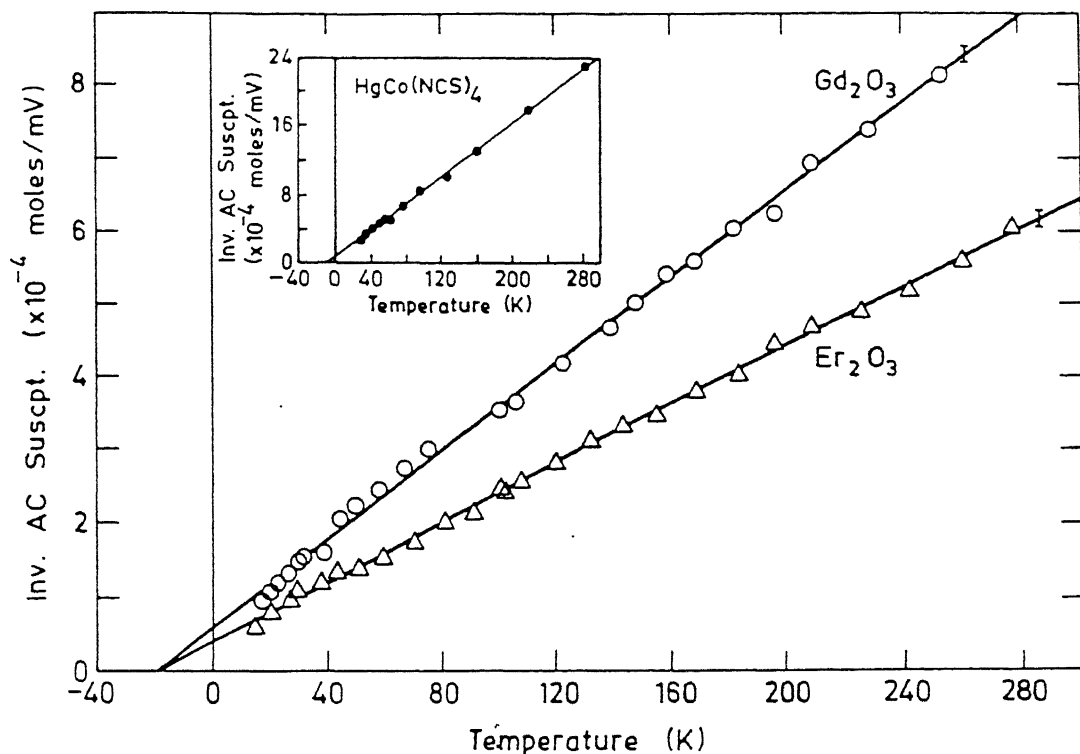
Figure 2.4 Temperature dependence of inverse ac-susceptibility of standard paramagnetic salts Er_2O_3 (Δ) and Gd_2O_3 (O). The inset shows the ac-susceptibility of $HgCo(NCS)_4$.

The data are fitted to the Curie-Weiss law. The best fitted straight lines are shown.

Performance of the bridge

We have measured the susceptibility of various kinds of magnetic materials using this bridge. Figure 2.5 shows the temperature dependence of susceptibility of a ferromagnetic ($Fe_{50}Ni_{30}Cr_{20}$) and a superconducting ($YBa_2Cu_3O_{7-\delta}$) material. The inset of Figure 2.5 shows the temperature variation of susceptibility of a spin-glass alloy, CuMn (4.4 at %). The measurements are done at 2 Oe r.m.s. field with a frequency of 73 Hz. The characteristic temperatures of these systems are given in Table 2.3. We can detect moment values down to $6x10^{-7}$ emu. The bridge can be made more sensitive (~ $1x10^{-7}$ emu) with the use of liquid coolant and glass cryostat. This is indeed found with liquid nitrogen as coolant.

Table - 2.3

Sample	Transition from	Transition temperature(K)	
		present data	literature
$Fe_{50}Ni_{30}Cr_{20}$	para-to ferro-magnetic	152	144 [45]
$YBa_2Cu_3O_{7-\delta}$	normal to superconducting	88	91 [46]
CuMn(4.4 at %)	paramagnetic to spin-glass	26	25 [47]

One could reach a temperature of 14K and also get better stability by keeping the tail of the cryostat immersed in liquid nitrogen.
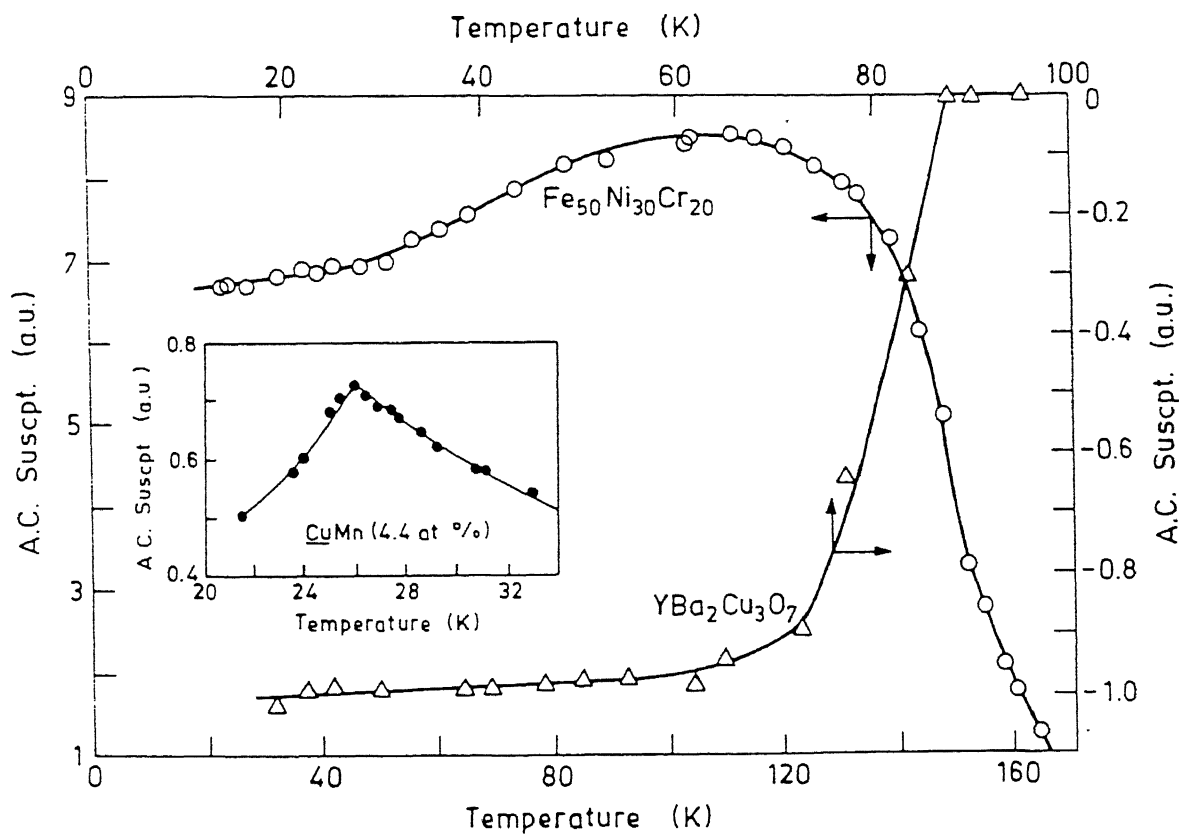
Figure 2.5   Temperature dependence of ac- susceptibility of $Fe_{50}Ni_{30}Cr_{20}$ (O) and $YBa_2Cu_3O_7$ (Δ). The inset shows the susceptibility vs temperature curve of the spin-glass CuMn (4.4 at %) alloy.

2.5 DC-Magnetization Set-up

The dc-magnetization measurements are carried out with a Princeton Applied Research Inc. (USA), model 155 vibrating sample magnetometer (VSM). The magnetic field with a maximum of 18 kOe is provided by a 15 inch Varian electromagnet with a 2.5 inch pole gap. We have used a Janis model 153 variable temperature cryostat with liquid nitrogen to measure magnetic moments from 77 to 300K. The high temperature measurements from 300 to 900K are carried out using a model 151 high-temperature oven assembly in place of the cryostat. The VSM gives directly the magnetic moment of the sample in a 3-digit digital display. However, using a null method moments could be read up to four digits. By a suitable choice of sample mass, change in moment up to 1 part in 10^4 can be detected. The VSM is calibrated against a standard Ni sample and paramagnetic Er_2O_3 before any measurement.

The cryostat is equipped with a copper-constantan thermocouple but we have also attached a platinum resistance thermometer to the sample rod rather close to the sample for more accurate measurements of temperature. The sample zone is connected to the liquid reservoir through a capillary which can be opened or closed from outside. The liquid from the reservoir comes to a vaporizer where a heater is placed. We can maintain the temperature of the sample zone at a constant value within 0.2K by controlling the liquid flow in the vaporizer and manipulating the heater power. Since the cryostat is basically designed for use with liquid helium, it creates some problem when it is used with liquid nitrogen. Because of the bubbling of liquid nitrogen in

the sample chamber fluctuations are observed in magnetic moment measurements near 77K. However, this disappears as soon as all liquid nitrogen in the sample chamber is evaporated out and measurements above about 85K are perfectly in order.

Besides these some magnetic measurements are done in KFK, Karlsruhe using a Faraday balance (Oxford Instruments) and in I.I.T., Madras using a SQUID magnetometer (Quantum Design). Both are equipped with superconducting magnets. These measurements were done using liquid helium.

2.6 Electrical Resistivity Set-up

During the course of this study an automated 4-probe electrical resistivity set-up is developed (Figure 2.1 (b)). The experimental set-up consists of a closed-cycle helium refrigerator or cryotip (Cryosystems and CTI-Cryogenics, model 22), a Lake-Shore Cryotronics temperature controller (model DRC- 82C), a $7\frac{1}{2}$digit Datron (model 1071) digital multimeter, an IBM compatible PC-XT and a GPIB (General Purpose Interface Bus) card.

A circular OFHC (Oxygen Free High Conductivity) copper plate is attached to the tip of the second stage of the cryotip, called the cold head. The sample is mounted on this cold head with GE varnish which gives both good thermal contact and electrical insulation between the sample and the cold head. Two calibrated silicon diodes (C_1 and C_2) are attached to the cold head with indium contacts to monitor the temperature. A heater is wound with a non-inductive winding just below the cold head. A typical sample dimension is 2.0 x 0.1 x 0.01 cm^3. Four thin copper

wires are soldered on to the sample with non-superconducting CdZn solder material. Without any heater power the cold head reaches ~ 8K.

The temperature of the cold head and hence of the sample is controlled by the temperature controller by sensing the temperature through the silicon diodes and giving the required current to the heater. The heater current is controlled by the proportional-integral-derivative (PID) control parameters of the controller. By a proper choice of PID the temperature of the sample can be controlled to within 0.1K from 8 to 300K. After the stabilization of temperature the multimeter, which passes a 10 mA current through the current leads of the sample, measures the voltage developed across the voltage leads and displays the resistance directly. The current is then passed in the opposite direction and again the resistance is noted. The average of both these values is taken as the actual resistance. Reversing the current is essential to eliminate the effect of any thermo-emf. The cold head is taken to another temperature and again the same process is repeated. The relative accuracy of the resistance measurement is better than 1 part in 10^5. Though this resistance measurement is not very complicated, it is extremely time consuming and prone to human error. Hence the automation here is not an extravaganza but a genuine need.

The automation is achieved by attaching a GPIB card to an IBM compatible PC-XT and IEEE 488 interfacing attached to the respective instruments. The low level software support is provided by a device driver, GPIB.COM, supplied by the

manufacturer of the GPIB card. The next level of software is written in Turbo Pascal to make a link between the device driver and the high level language. Though the automation implementation programme is relatively simple, there are two tricky points worth mentioning. The first is about reversing the direction of the current through the sample. The digital multimeter does not have any command to accomplish this. Interfacing a switch would require additional instrumentation. However, the multimeter does have separate "front panel" and "rear panel" inputs, which are isolated by a relay operated switch. From outside one can choose either the "front panel" or the "rear panel" inputs and the relay will work according to the choice. We have connected the sample to both the inputs with the current leads reversed. Therefore, to change the direction of the current we have to simply change the input panel by the programme. Secondly we have to find the criteria for the stability of temperature which are consistent with the following problem of the closed-cycle helium refrigerator. The cycling frequency of closed-cycle helium refrigerator results in a fluctuation of the cold head temperature. This frequency is about 0.5 cycles/second and the fluctuation in temperature is about 0.05 K. The PID temperature controller is unable to control this fluctuation since its sampling frequency is about 1 cycle/second. Besides this, an improper choice of PID, which depends on many external factors, may lead to very large delay in the system to reach a set temperature and a continuous change in temperature during one set of measurements. A simple algorithm is developed to tackle this

problem which is described below.

A small number (typically 5) of temperature readings are taken at equal intervals of time (roughly 2 seconds). Such "cluster" of readings are taken at longer regular intervals (typically 20 seconds). The temperature is considered to be steady if it satisfies the following criteria :

(i) the average of differences between consecutive readings in the last and second last clusters are both less than a specified tolerance limit (t_1). This takes care of short term fluctuations.

(ii) the difference between the average of last and second last cluster is less than another specified tolerance limit (t_2). This process takes care of any long term fluctuations.

(iii) a cluster recorded after the resistance measurement is done at a particular temperature satisfies the condition (ii).

The resistance readings commence when the first two conditions are satisfied. The multimeter outputs the average of a set of last 16 readings which takes about 14 seconds. Generally, two sets of forward and reverse resistance readings are taken. This process needs a time span of nearly 1 minute and therefore, condition (iii) becomes necessary and useful.

CHAPTER III

Results and Discussion

3.1 Characterization of the Samples

The results of chemical and spectroscopic analyses for determining the composition of the alloys alongwith their lattice parameters, determined from the x-ray diffraction studies, are given in Table 3.1.

Table 3.1

Nominal Composition	Actual Composition	Lattice parameter "a" ($\mathring{A}$)
$Cu_{65}Mn_{35}$	$Cu_{64}Mn_{36}$	3.735
$Cu_{55}Mn_{45}$	$Cu_{54}Mn_{46}$	3.756
$Cu_{45}Mn_{55}$	$Cu_{45}Mn_{55}$	3.757
$Cu_{35}Mn_{65}$	$Cu_{40}Mn_{60}$	3.750
$Cu_{28}Mn_{72}$	$Cu_{27}Mn_{73}$	3.759
$Cu_{20}Mn_{80}$	$Cu_{24}Mn_{76}$	3.757
$Cu_{15}Mn_{85}$	$Cu_{17}Mn_{83}$	3.750

Chemical and spectroscopic analyses show that the amount of Fe present is not more than 0.05 % in any sample. In the following discussion, we have referred to the alloys by their nominal compositions but all the calculations and the construction of the magnetic phase diagram are done using the values of the analyzed compositions.

The x-ray studies show lines belonging to only the f.c.c structure (γ-phase) and the quoted lattice constants are the average lattice constants calculated from these lines. These values match quite well with the literature values [11]. When the samples are annealed at $100^{\circ}C$ for 24 hours the x-ray diffraction shows a different pattern which implies the presence of other phases.

3.2 AC-Susceptibility

We have measured the ac-susceptibility, χ_{ac}, in 2 Oe rms ac field of frequency 313Hz from 20K to almost up to room temperature and in external dc fields of 0 to 280 Oe for $Cu_{100-x}Mn_x$ alloys. Figure 3.1 shows χ_{ac} vs temperature (T) in zero external dc field for x = 4.4 and 9 samples. In Figures 3.2 and 3.3 we have shown the χ_{ac} vs temperature for samples with x = 35 and 45 at % in the presence of zero and 280 Oe external dc fields. Figures 3.4 and 3.5 show similar plots for samples with x = 55 to 85 in the absence of any dc field. In these samples the signal is very weak and the effect of low external dc field (~280 Oe) could not be shown as clear-cut as it is for samples with x = 35 and 45. In Figure 3.6 we have shown the effect of different external dc fields on the χ_{ac} of x = 35 sample at different temperatures.

For all the samples with x $\geq$ 35, χ_{ac} vs temperature curves show a broad peak at high temperatures (~150K) except for x = 85. Though x = 72 does not seem to show any clear peak (because of the lack of data points at higer temperatures) the
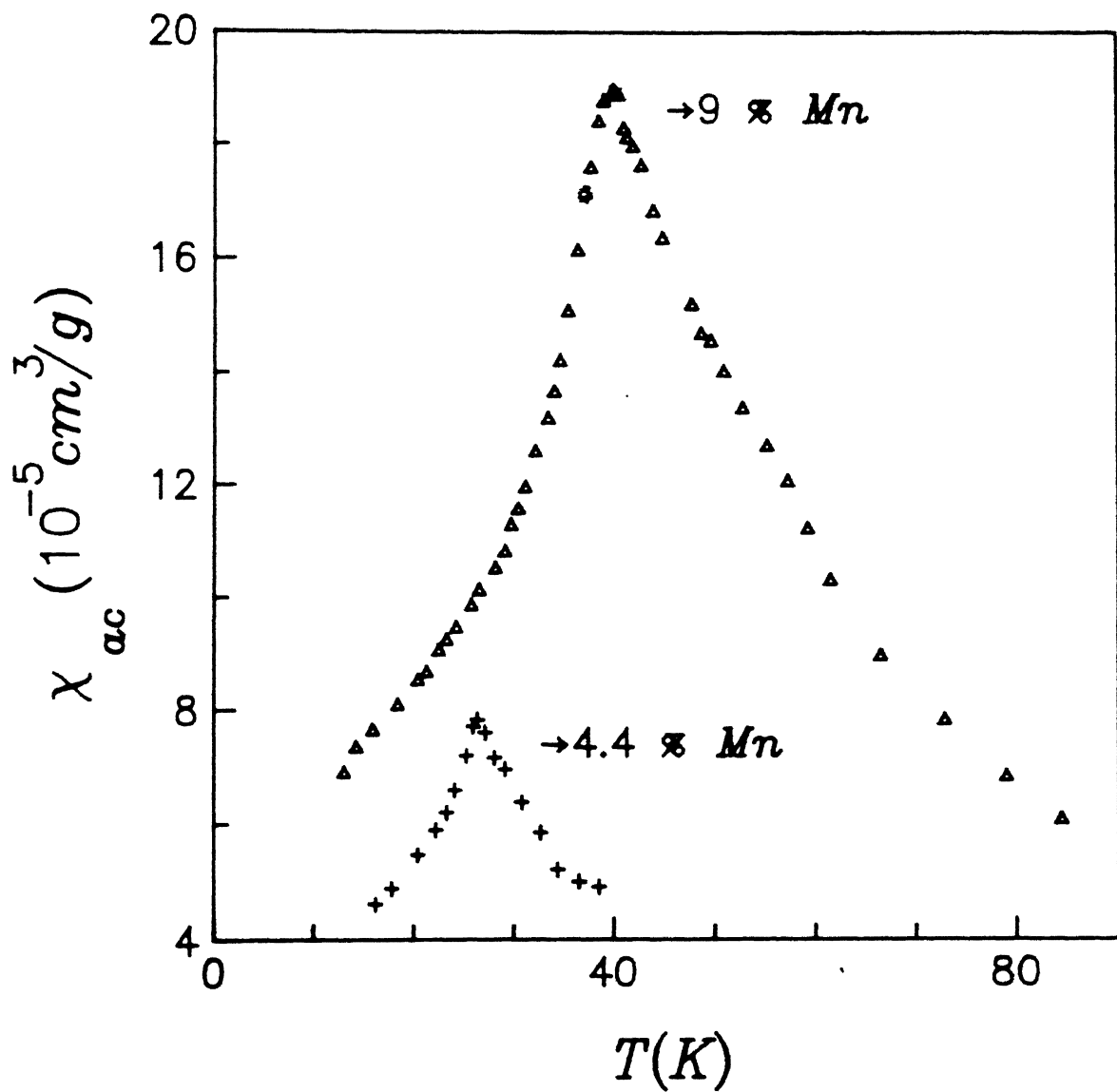
Figure 3.1   ac-susceptibility (χ_{ac}) vs temperature for
$Cu_{100-x}Mn_x$ alloys with x = 4.4 and 9 in zero
dc field.
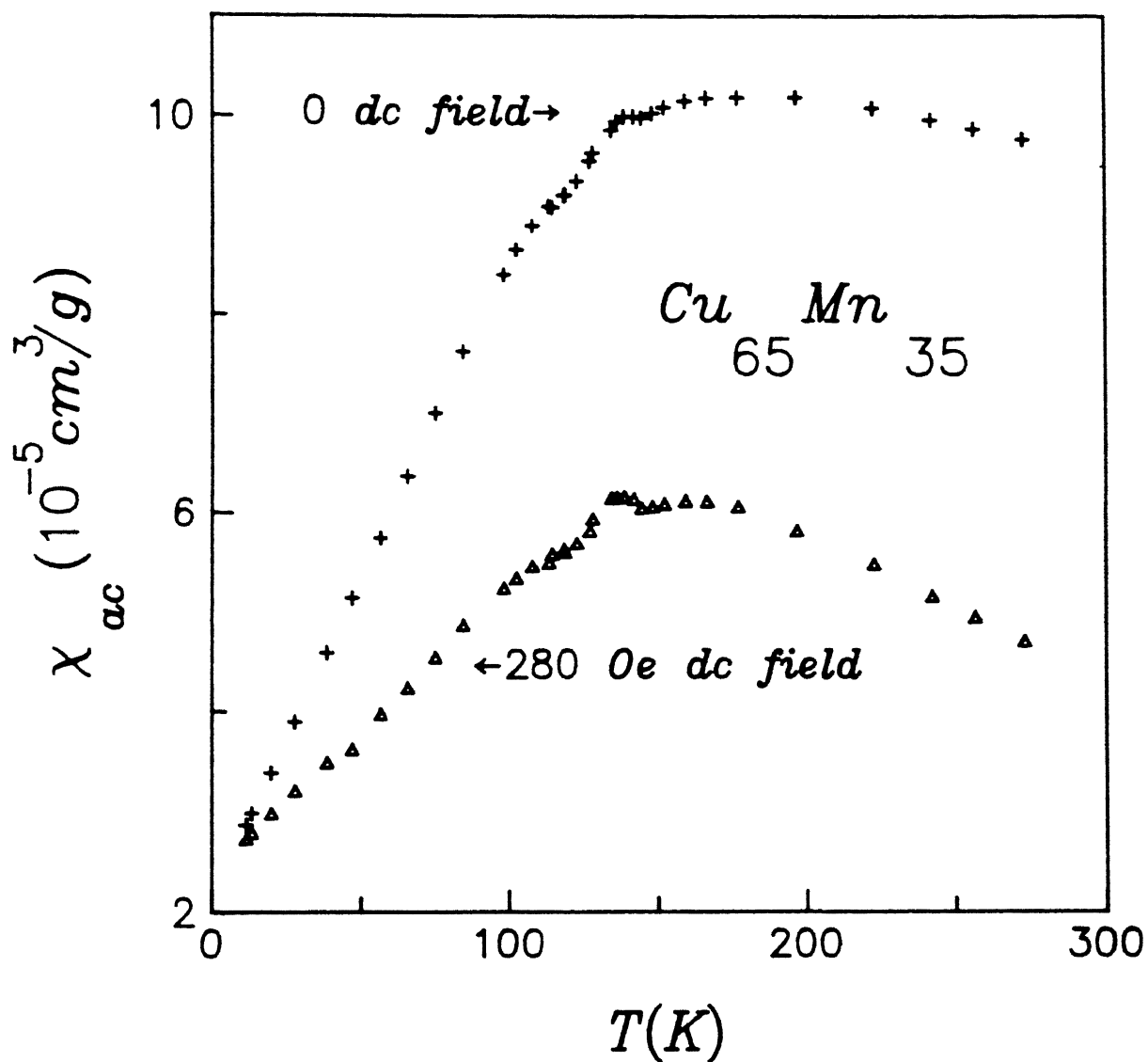
Figure 3.2 ac-susceptibility (χ_{ac}) vs temperature for x = 35 in zero and 280 Oe dc fields.
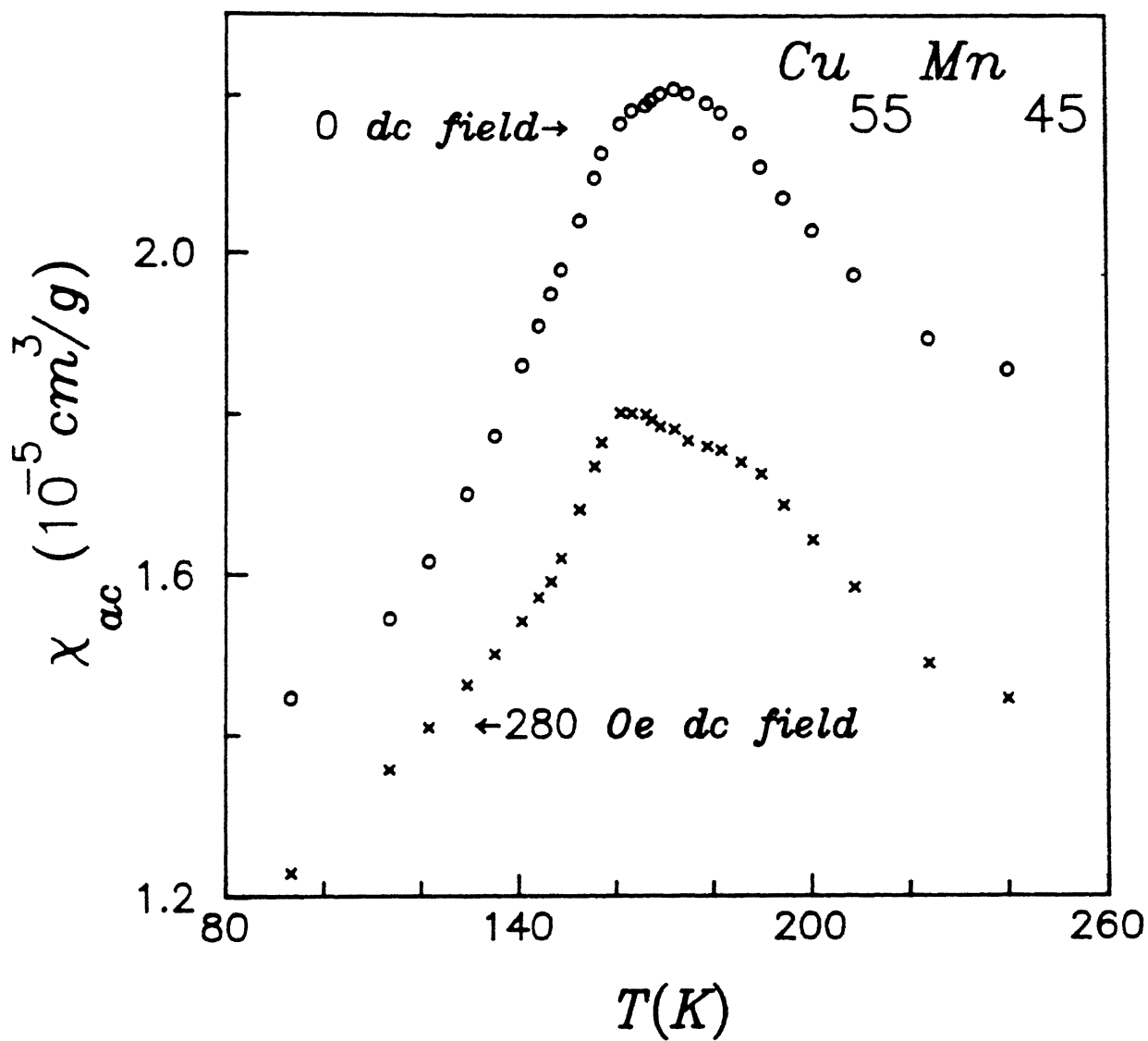
Figure 3.3 ac-susceptibility (χ_{ac}) vs temperature for x = 45 in zero and 280 Oe dc fields.
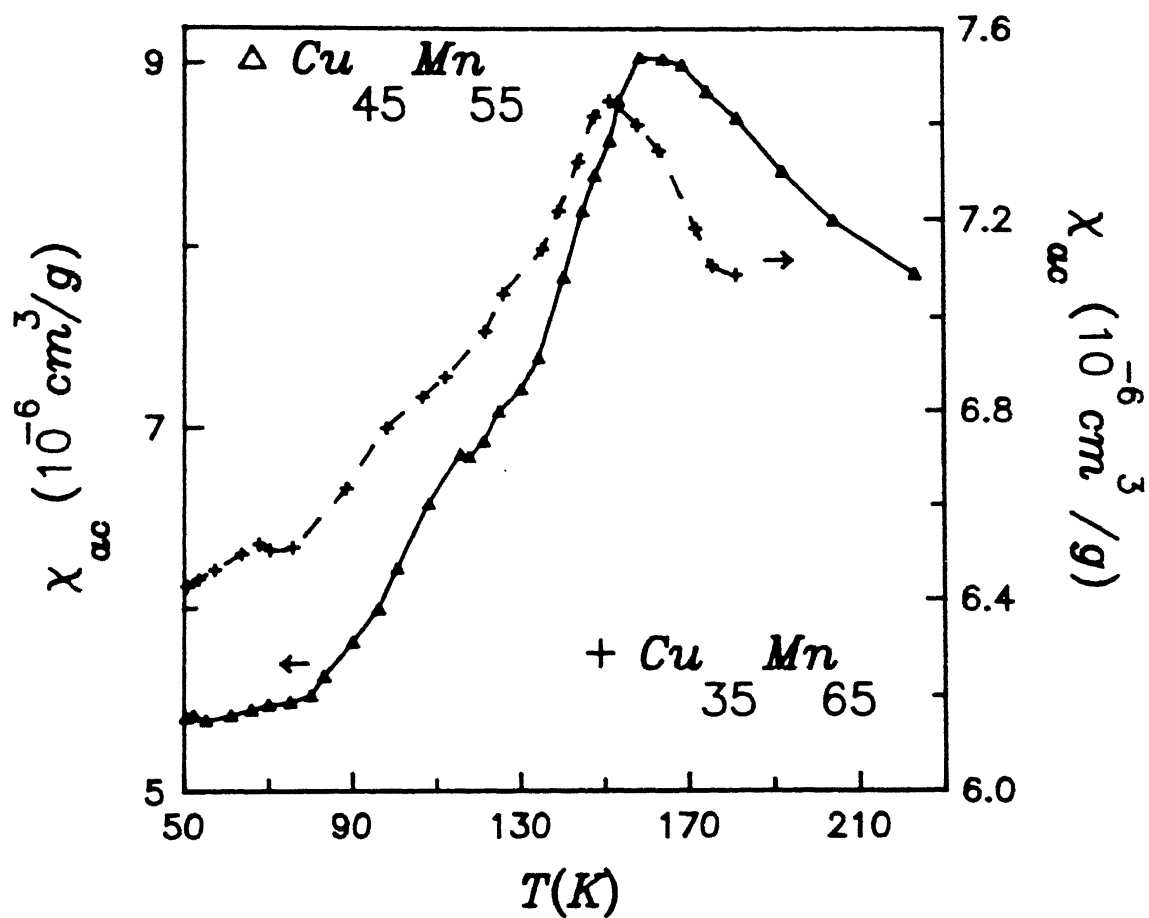
Figure 3.4 ac-susceptibility (χ_{ac}) vs temperature for x
= 55 and 65 in zero dc field. The lines
joining the points are just guides to the
eye.
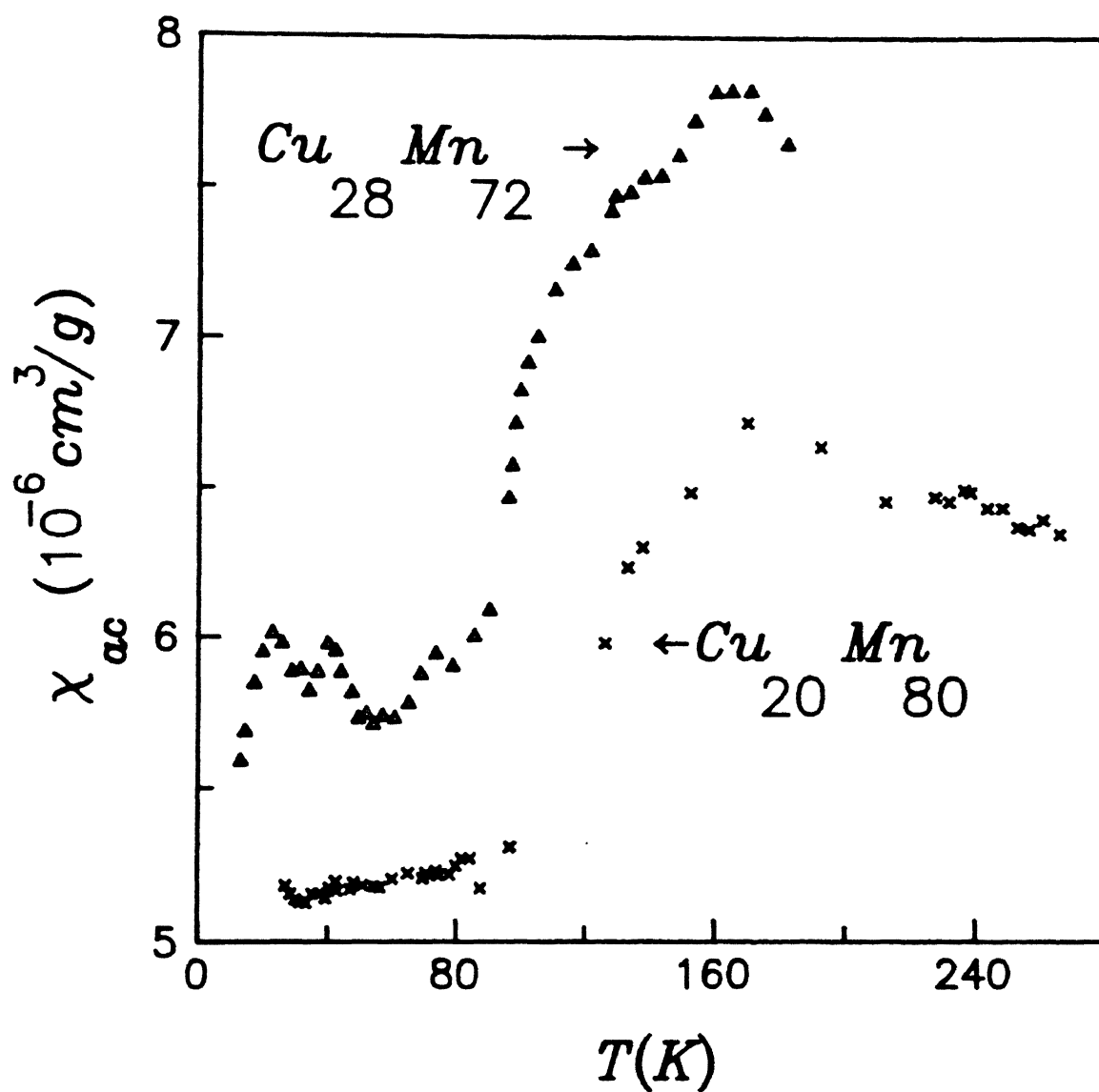
Figure 3.5 ac-susceptibility (χ_{ac}) vs temperature for x
= 72 and 80 in zero dc field.
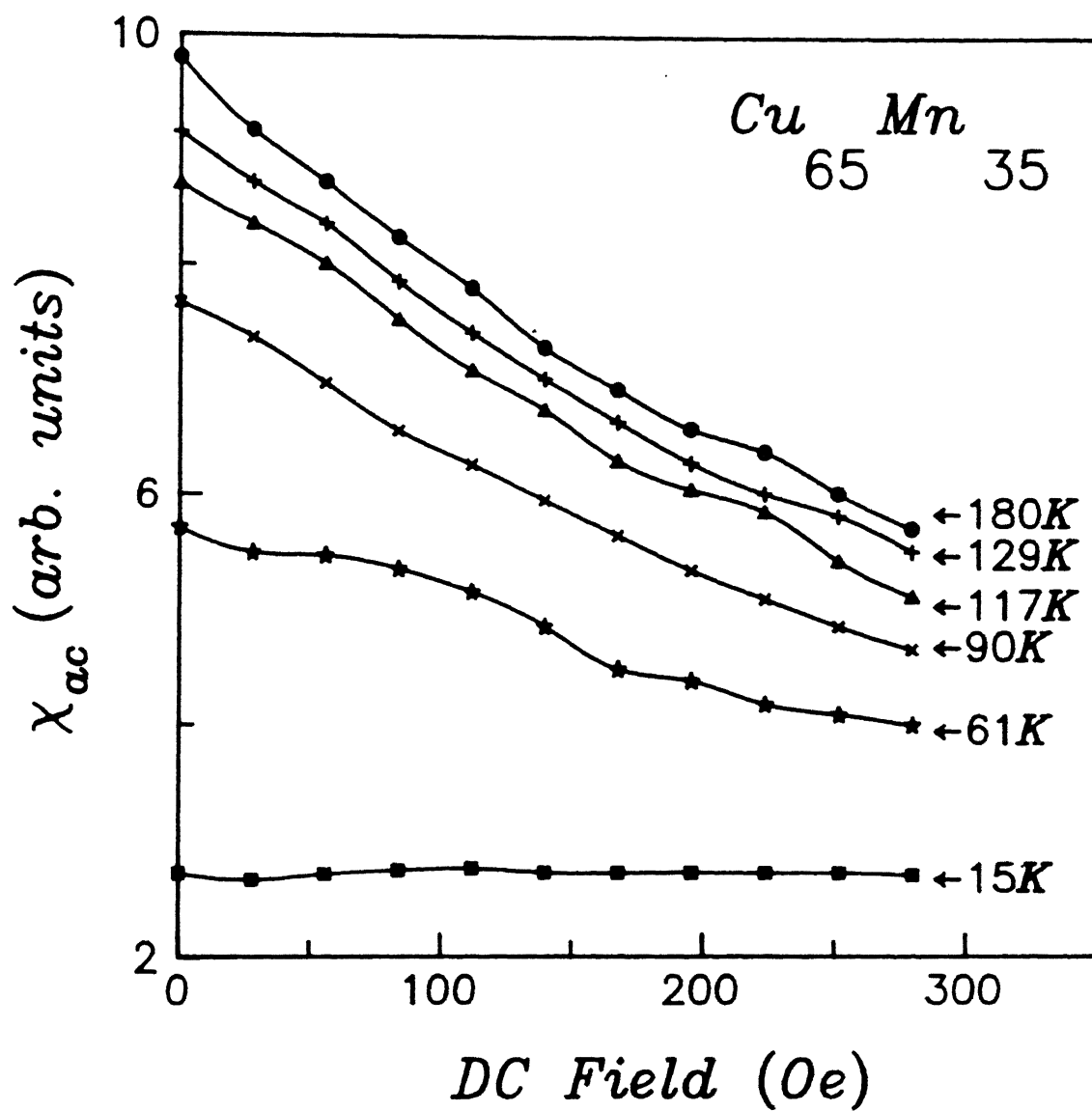
Figure 3.6 ac-susceptibility (χ_{ac}) vs external dc field
for x = 35 at different temperatures.

value of χ_{ac} at ~170K is certainly more than that at room temperature implying that a peak exists even for x = 72 somewhere around 170K. The peak value of χ_{ac} decreases monotonically with the increase in Mn concentration for x > 9. In Table 3.2 we have listed the variations of the peak values of χ_{ac} and the peak temperature, T_f, with concentration.

Table   3.2

Mn concentration x	χ_{ac}^{max} $(10^{-5}cm^3/g)$	T_f (K)
4.4	7.7	26
9	19.0	39
35	10.5	160
45	2.2	175
55	0.92	165
65	0.74	165
72	0.76	~170
80	0.6	~150
85	0.4	–

The χ_{ac} vs T curves for all the samples, except the dilute ones, do not show spin-glass cusps but show broad peaks indicating spin-glass like freezing. The origin of the peaks being ascribed to antiferromagnetic long-range order or other long-range orders is ruled out on the basis of high field dc measurements which will be discussed later. Guy [25] has shown

that there is no great significance attached to the sharpness of the peaks even in canonical spin-glasses like AuFe (Fe from 0.25 to 7 at %). His experiments with AuFe in low dc fields make this point clear. The sharpness seems to be a question of temperature scale and here we have gone only up to ~ 2 T_f. For our samples any temperature above 300K is almost forbidden because the samples are crystallographically metastable and a second phase crystallises above room temperature as explained earlier.

It is difficult to explain some of the observations like the broad peak in χ_{ac} vs temperature, a non Curie-Weiss behaviour above the peak temperature, etc., on the basis of a phase transition or a cooperative phenomenon involving a single order parameter. A plausible explanation can be given on the basis of the phenomenological theory of superparamagnetism proposed by Néel [4] and later on applied to similar kinds of systems by Tholence and Tournier [5], Wohlfarth [3,21] , Guy [25] and many others. Here we attempt to understand the results of χ_{ac} measurements in the framework of superparamagnetic cluster model. This model assumes that a magnetic system is made up of clusters of spins or domains of various sizes and shapes. Each cluster is characterized by an anisotropy energy which acts as a potential barrier for the magnetization of the system. The thermal activation of respective domain walls and cluster magnetization will enable them to overcome the respective potential barriers they face. This will lead to a relaxation process for magnetization of the clusters. The relaxation time τ depends on the thermal energy $k_B T$. Higher the temperature the smaller is the

relaxation time. Now if the observation time τ_m is smaller than τ, then the magnetization of the cluster will appear to be blocked. Hence below a certain temperature, where $\tau > \tau_m$, the particle will appear to be blocked and this temperature is called the blocking temperature, T_B. The system as a whole consists of a distribution of such potential barriers following from the distribution of size and magnetization of the clusters in the system. This leads to a distribution of relaxation time and hence a distribution of blocking temperatures. A typical distribution of blocking temperatures, $f(T_B)$, is shown in Figure 3.7 which is calculated from Wohlfarth's model [21,23] for our x = 55 sample.

The peak in χ_{ac} vs T indicates the presence of competing interactions and it is a matter of one winning over the other. In this case it is the anisotropy energy of individual clusters vs the thermal energy. According to Néel's model, each cluster has an intrinsic or spontaneous magnetization M_s. The magnetic moment vM_s (where v is the volume of the cluster) in the absence of any applied magnetic field can take up two orientations of equal energy : $\theta = 0$ and $\theta = \pi$ with respect to the anisotropy axis of the cluster. The height of the potential barrier between these two states is given by $vH_cM_s/2$ (where H_c = coercive field for the given cluster). Now if the height is very large compared to the thermal energy k_BT, thermal fluctuations cannot move the magnetic moment from one position to the other. So, it always remains fixed in the direction in which it was originally brought by a magnetic field. However, since the height of the potential barrier is $vH_cM_s/2$, a value of v can always be found which is so small that
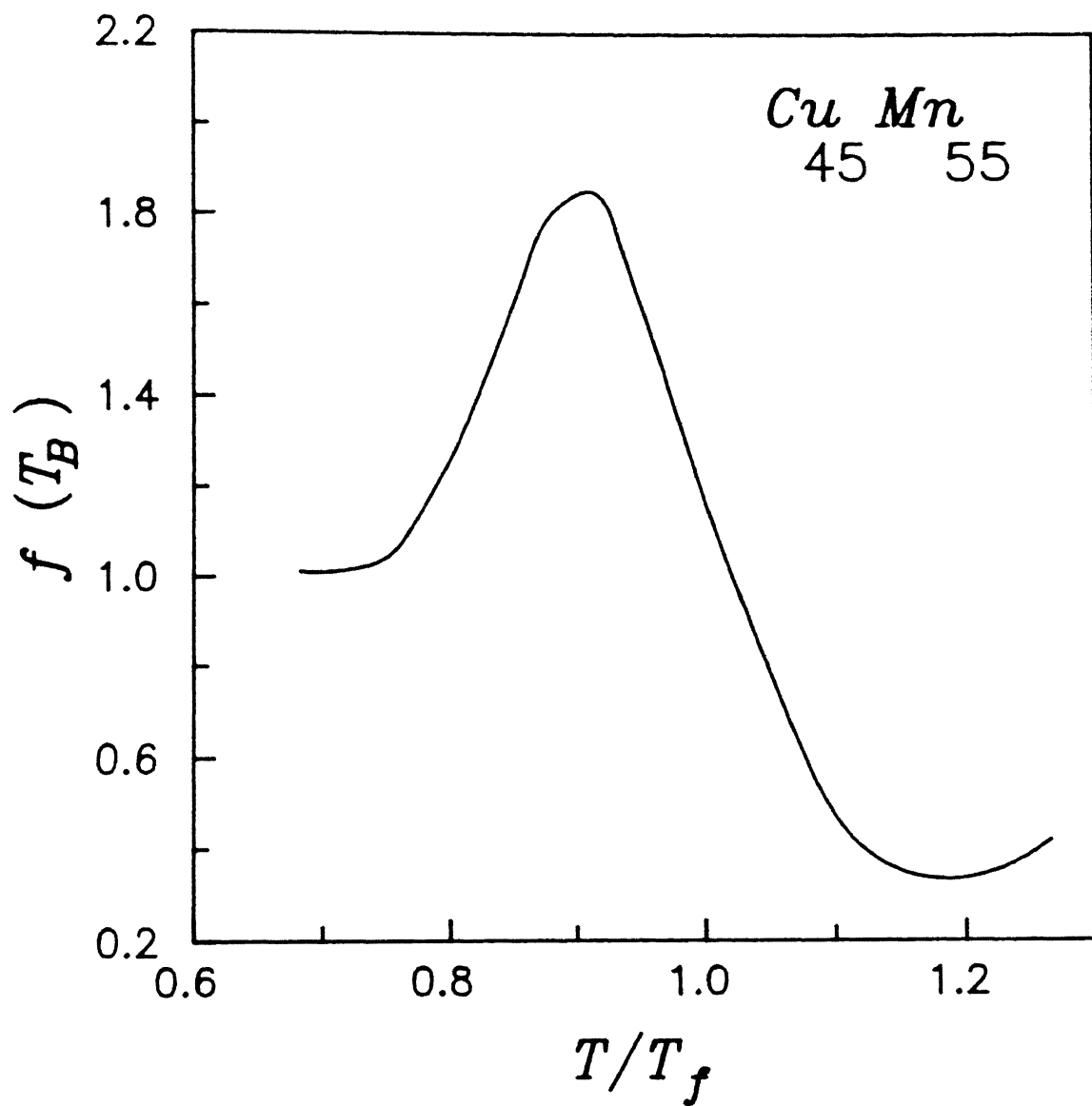
Figure 3.7 Distribution of blocking temperatures vs normalized temperature (T/T_f) for the sample with x = 55.

its height is of the order of $k_B T$. In that case, thermal
fluctuations can cause the moment to change spontaneously from one
position to the other. When we come from the high temperature
side of χ_{ac} vs T curve most of these clusters are free because of
high thermal energy and their response to the field is randomized
by thermal fluctuations. As we decrease the temperature the
response of the superparamagnetic clusters to the field becomes
more and more coherent because of the reduction in thermal
fluctuations and the susceptibility increases. With further
decrease in temperature, the bigger clusters facing higher
potential barriers start getting frozen or blocked because of the
non-availability of the required thermal energy to cross the
barriers. As a result they cannot respond to the field and the
competition comes into play. On one hand the reduction of thermal
fluctuations with the decrease in temperature enhances the
susceptibility and on the other hand the decrease in thermal
energy blocks the bigger clusters where the blocking temperature
is higher and so the susceptibility decreases with the decrease
in temperature. The result of these two opposing effects is the
broad peak in the susceptibility. To justify the above statement,
let us consider that our alloy consists of N independent clusters
of spins. Let M be the magnetic moment of individual clusters and
we have N clusters with a distribution P(M) of their magnetic
moments. In thermal equilibrium the mean magnetization of N
clusters in a magnetic field H is given, in terms of Langevin
function L(x), by

$$\bar{M} = N \int_{0}^{\infty} M\, P(M)\, L\left(\frac{M\,H}{k_B T}\right) dM .$$

For small fields it would lead to the Curie law

$$\chi = \frac{\bar{M}}{H} = \frac{N\,\overline{M^2}}{3k_B T} \text{ where } \overline{M^2} = \int_{0}^{\infty} M^2 P(M)\, dM . \qquad (3.1)$$

Now because of the anisotropy energy $E_A = KM$ where K is the anistropy constant, the response of the clusters to the ac magnetic field may be blocked over the time scale of our measurements, namely, $\tau_m = 1/f$, where f is the frequency of the ac field. Hence the system exists in an incomplete thermal equilibrium. The typical time of response of a cluster is given by $\tau = \tau_0 \exp(KM/k_B T)$, where τ_0 is a constant. Only those clusters will contribute to χ_{ac} for which $\tau \leq \tau_m$. So from Equation (3.1) we get

$$\chi_{ac} = \frac{N}{3k_B T} \int_{0}^{(k_B T/K)\,\ln(\tau_m/\tau_0)} M^2 P(M)\, dM .$$

Hence χ_{ac} will exhibit a peak at a temperature where $(k_B T/K)\ln(\tau_m/\tau_0)$ roughly equals the peak position of the distribution $M^2 P(M)$ which is of the same order as $\overline{M^2}$.

When we look at the results of the effect of dc field on the χ_{ac} we observe that for samples with x = 35 and 45, χ_{ac} is always less in the presence of a dc field and this difference persists even at temperatures much higher than the peak

temperature. It is also difficult to explain this discrepancy on the basis of theories which suggest a phase transition at the peak temperature, T_f. The decrease in χ_{ac} in the presence of a dc field for all temperatures indicates the existence of short-range order or d-d overlap even at temperatures much higher then the freezing temperature. This is more than likely in the concentration range of our present interest. The effect of short-range order, leading to the formation of magnetic clusters, is difficult to handle in first principle theories of spin-glasses. We attempt to understand this effect on the basis of the above mentioned phenomenological theories of superparamagnetism.

The external dc field defines the quantization axis of the spins and the ac field excites the spins. To respond to the ac field the spins or the clusters of spins have to reverse their orientation and thus they must lose and gain energy from the lattice, involving spin-lattice relaxation time. Hence only those clusters can respond to the ac field and contribute to χ_{ac} whose time constant for spin reversal is less than the time constant of the existing ac field. The relaxation rate λ [4,25] is given by

$$\lambda = 1/\tau = 1/\tau_o \exp(-E/k_B T),$$

where E is the height of the potential barrier given by

$$E = (2E_A \pm vM_s H_{ext})^2/4E_A . \qquad (3.2)$$

Hence we see that the application of a dc field parallel to the ac

field increases the time constant for spin reversal and thus causes the decrease in χ_{ac} (Figures 3.2 and 3.3). When τ becomes longer than a typical measuring time τ_m, then the moment is frozen and the temperature at which this freezing of a particular cluster takes place is called the blocking temperature (T_B) which can be found out from

$$E(T_B) = k_B T_B \ln (\tau_m/\tau_o). \qquad (3.3)$$

Our results on the effect of dc field on χ_{ac} shows that the blocking temperature has wide distribution over the whole temperature range and confirms the result of our calculation of $f(T_B)$ from the data of χ_{ac} in one of our samples (Figure 3.7). This broad distribution of T_B justifies the broad peak in χ_{ac} and the effect of dc field on χ_{ac}. The peak in χ_{ac} vs T is described on the basis that T_f is the temperature at which roughly maximum number of spins get blocked. Figure 3.6 shows that the dc field dependence of χ_{ac} is more pronounced at higher temperatures. The barrier height E, at a given temperature, increases as vH_{ext} where v is the volume of the cluster (Equation (3.2)). At lower temperatures, only smaller clusters respond to the ac field contributing to the susceptibility and thus the change in E is not significant for these clusters. At higher temperatures, on the other hand, larger clusters are also involved and the change in E shows up through a decrease in χ_{ac} with dc field.

When we look at the peak values of χ_{ac}, we observe a decrease in the peak susceptibility with increase in Mn

concentration. Though we have added more magnetic atoms the decrease in susceptibility value at the peak indicates that the addition of more magnetic atoms only tries to cancel the magnetic moment of each other, that is, they are orienting themselves antiferromagnetically. Hence we conclude that within the magnetic clusters, the spins are antiferromagnetically ordered.

3.3 DC - Magnetization

We have measured the magnetization (M) as a function of temperature (T) for x = 35-85 at % alloys in magnetic fields ranging from 500 Oe to 15 kOe. For all the samples the temperature range being liquid nitrogen temperature to almost up to room temperature and for x = 85 we have gone up to 700K to find the Néel temperature.

To obtain M vs T curves we have taken two different routes. First, we cooled the sample in the absence of any magnetic field to the lowest temperature. Then the field was switched on and the measurement M(T) started as the sample was warmed up. This path is called the zero-field-cooled (ZFC) branch of M(T). The second path is known as the field-cooled (FC) branch of M(T). Here we cool the sample from room temperature in the presence of a magnetic field to the lowest temperature. Then keeping the field constant we warm up the sample and measure M(T) in the same field. The results of these measurements are given in Figures 3.8-3.13. Here we have plotted M/H vs T where H is the measuring field and we call M/H the dc-susceptibility, χ_{dc}.

To measure the time dependence of magnetization, we have
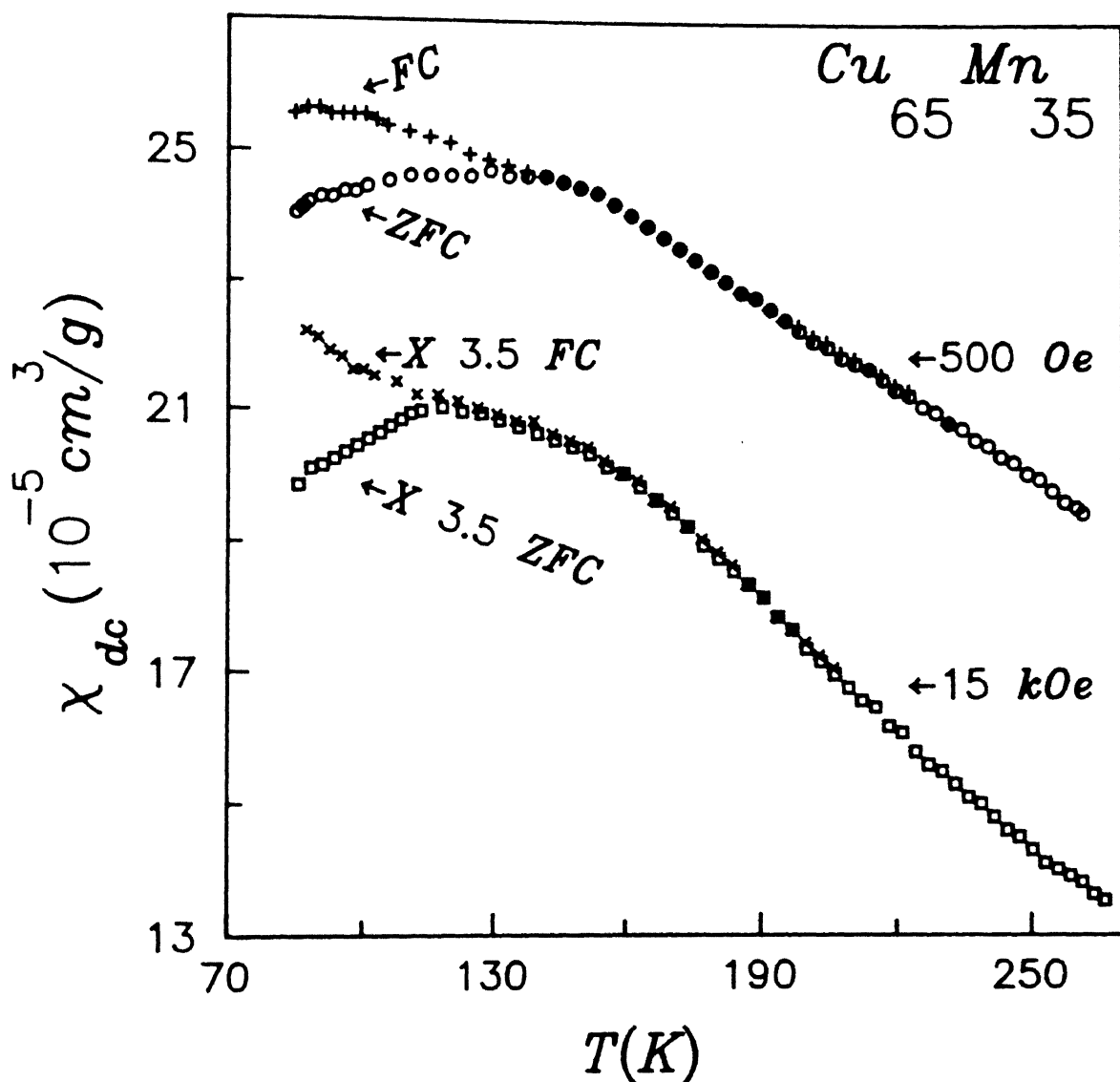
Figure 3.8   dc-susceptibility (χ_{dc}) vs temperature for sample with x = 35 in 500 Oe and 15 kOe dc fields. χ_{dc} at 15 kOe is multiplied by a factor 3.5. Both FC and ZFC branches are shown.
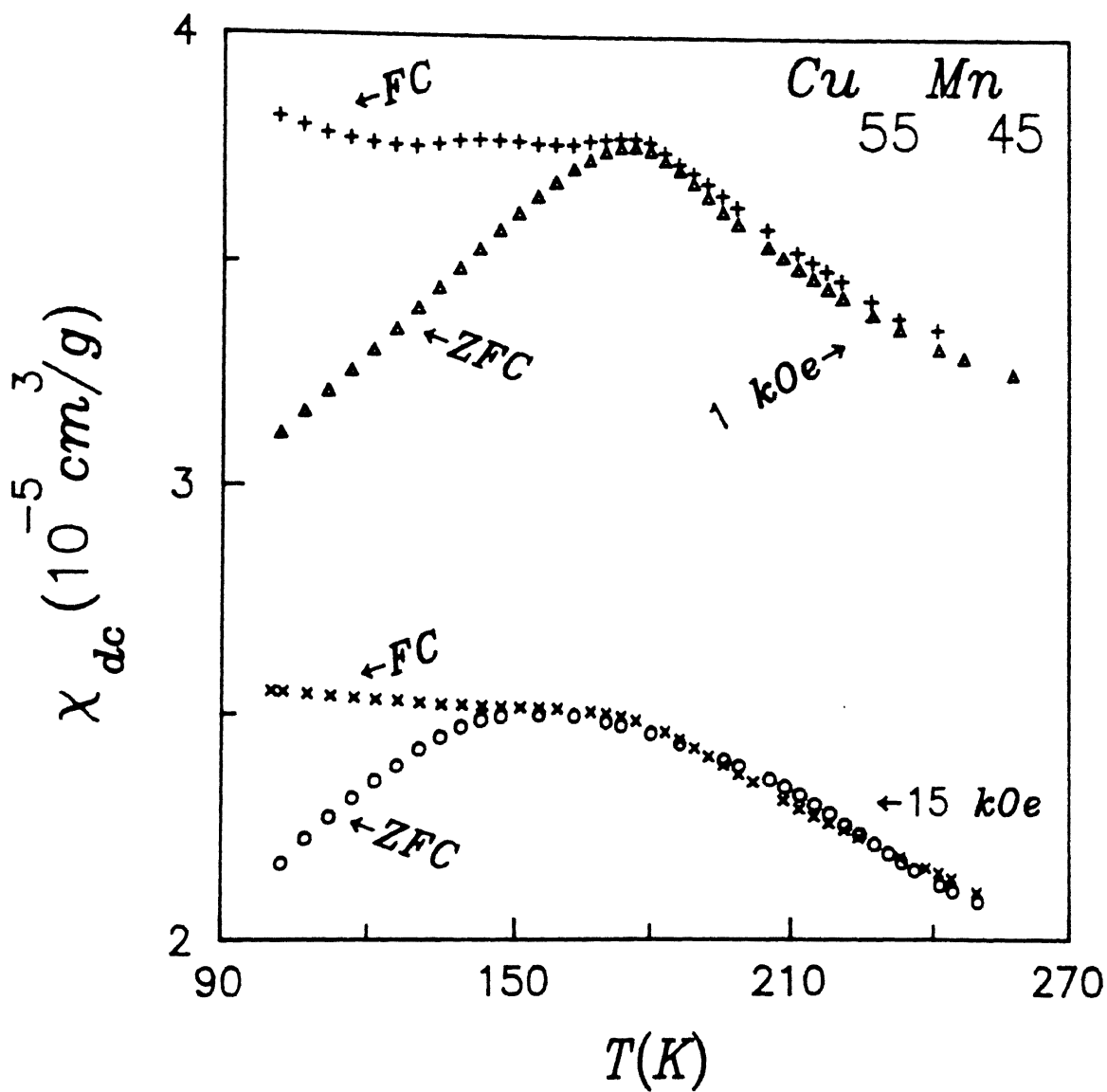
Figure 3.9   dc-susceptibility (χ_{dc}) vs temperature for x
= 45 in 1 and 15 kOe dc fields.
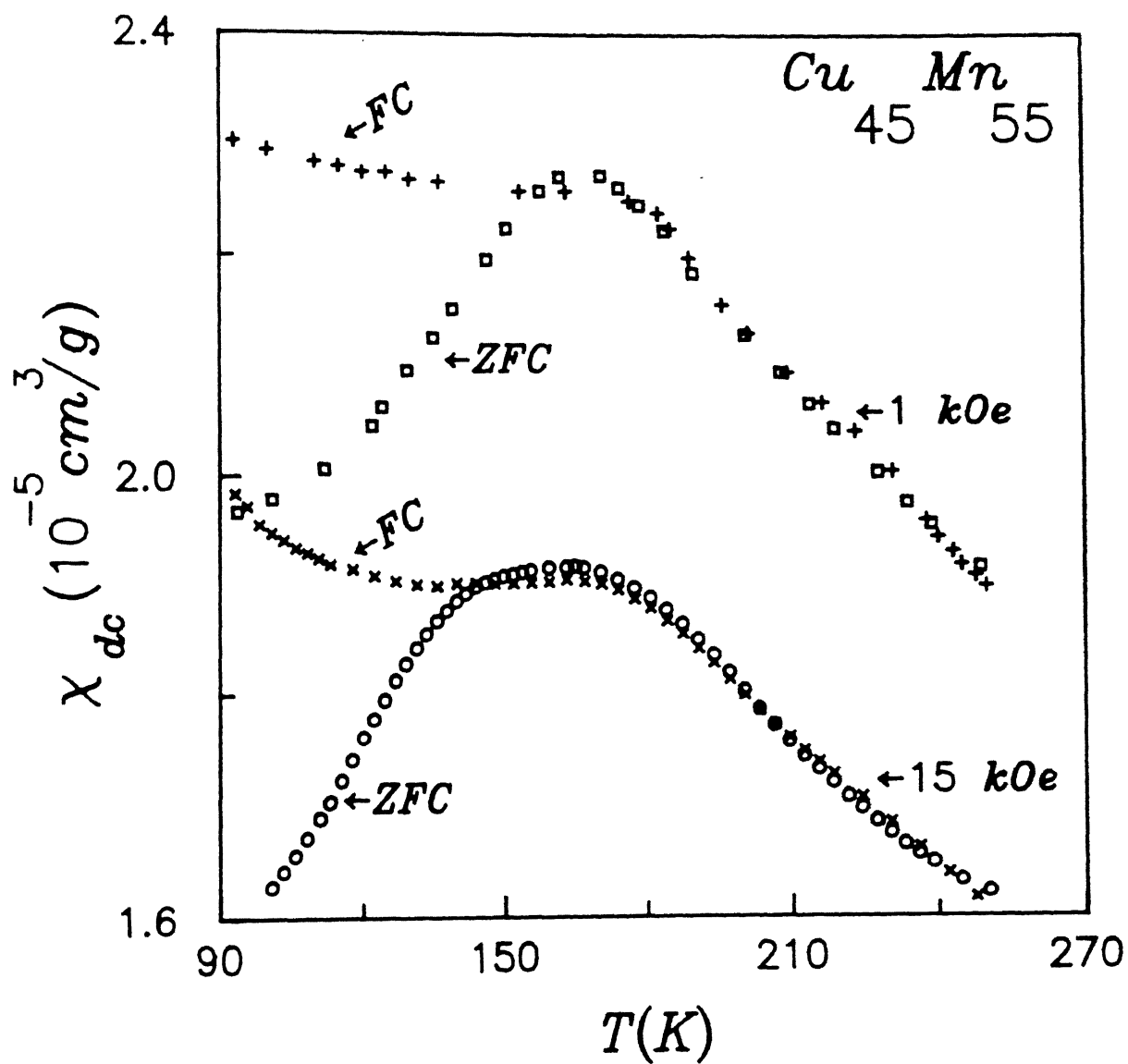
Figure 3.10 dc-susceptibility (χ_{dc}) vs temperature for x = 55 in 1 and 15 kOe dc fields.
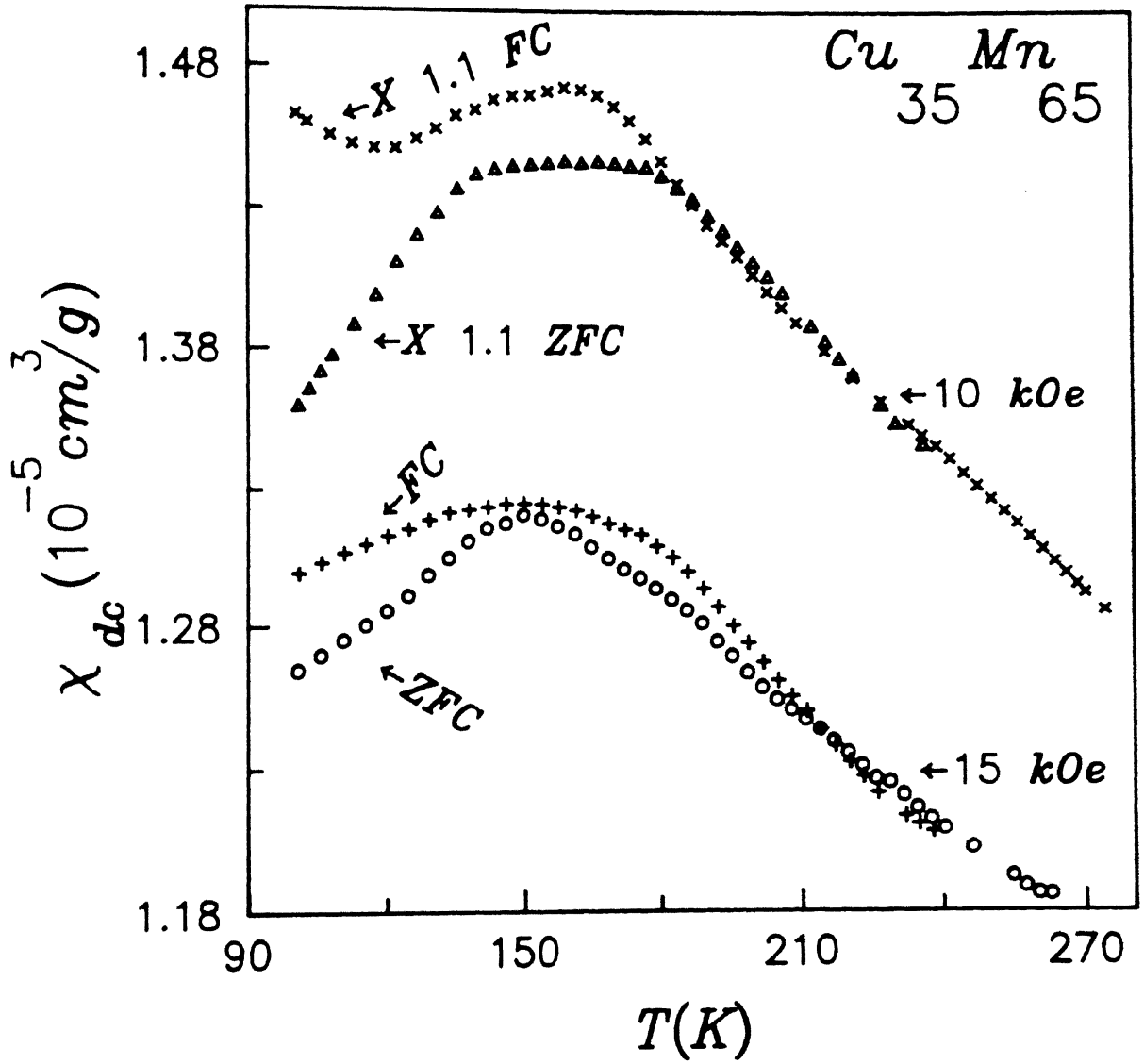
Figure 3.11 dc-susceptibility (χ_{dc}) vs temperature for x = 65 in 10 and 15 kOe dc fields. χ_{dc} at 10 kOe field is multiplied by a factor of 1.1.
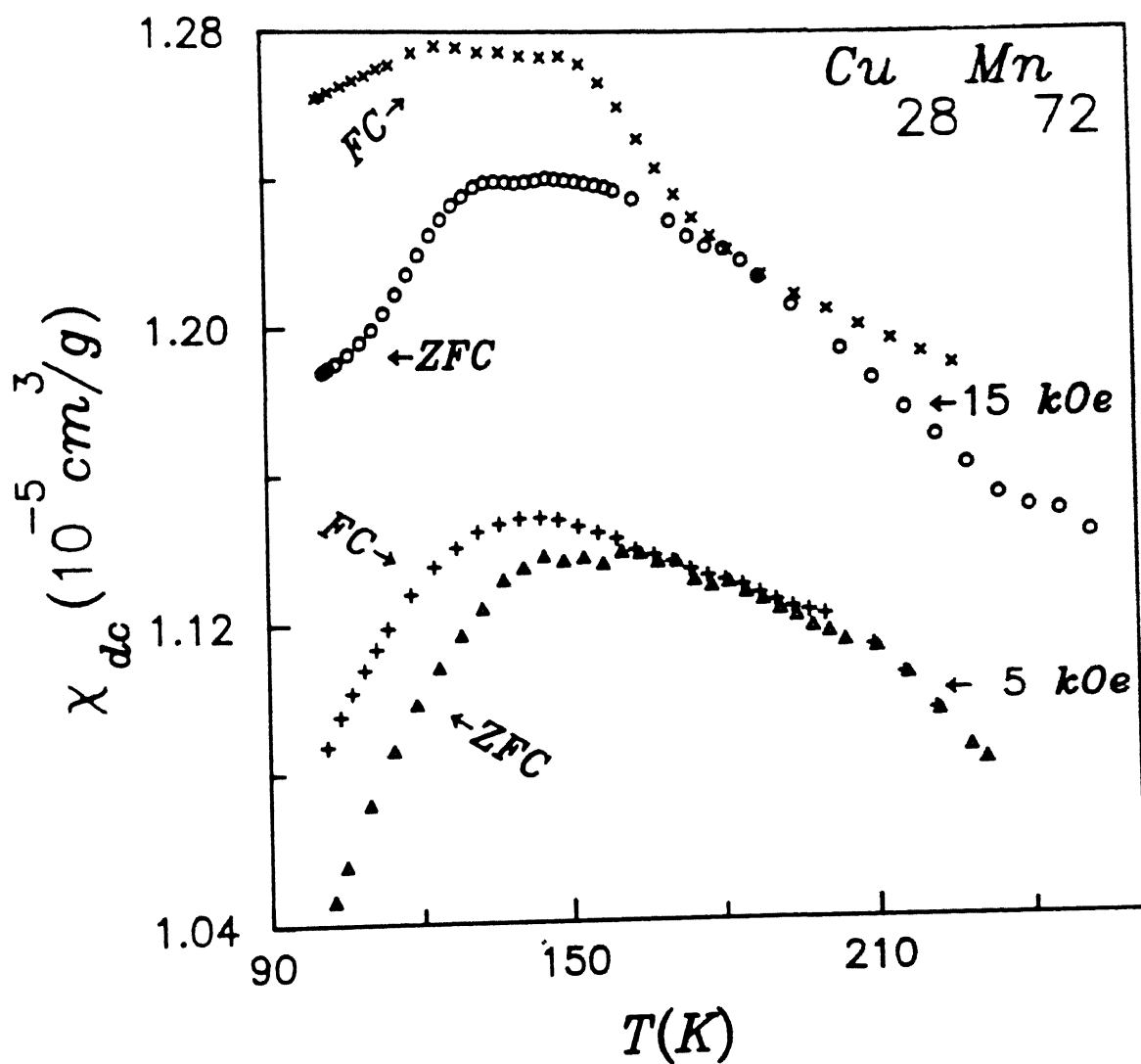
Figure 3.12 dc-susceptibility (χ_{dc}) vs temperature for x = 72 in 5 and 15 kOe dc fields.
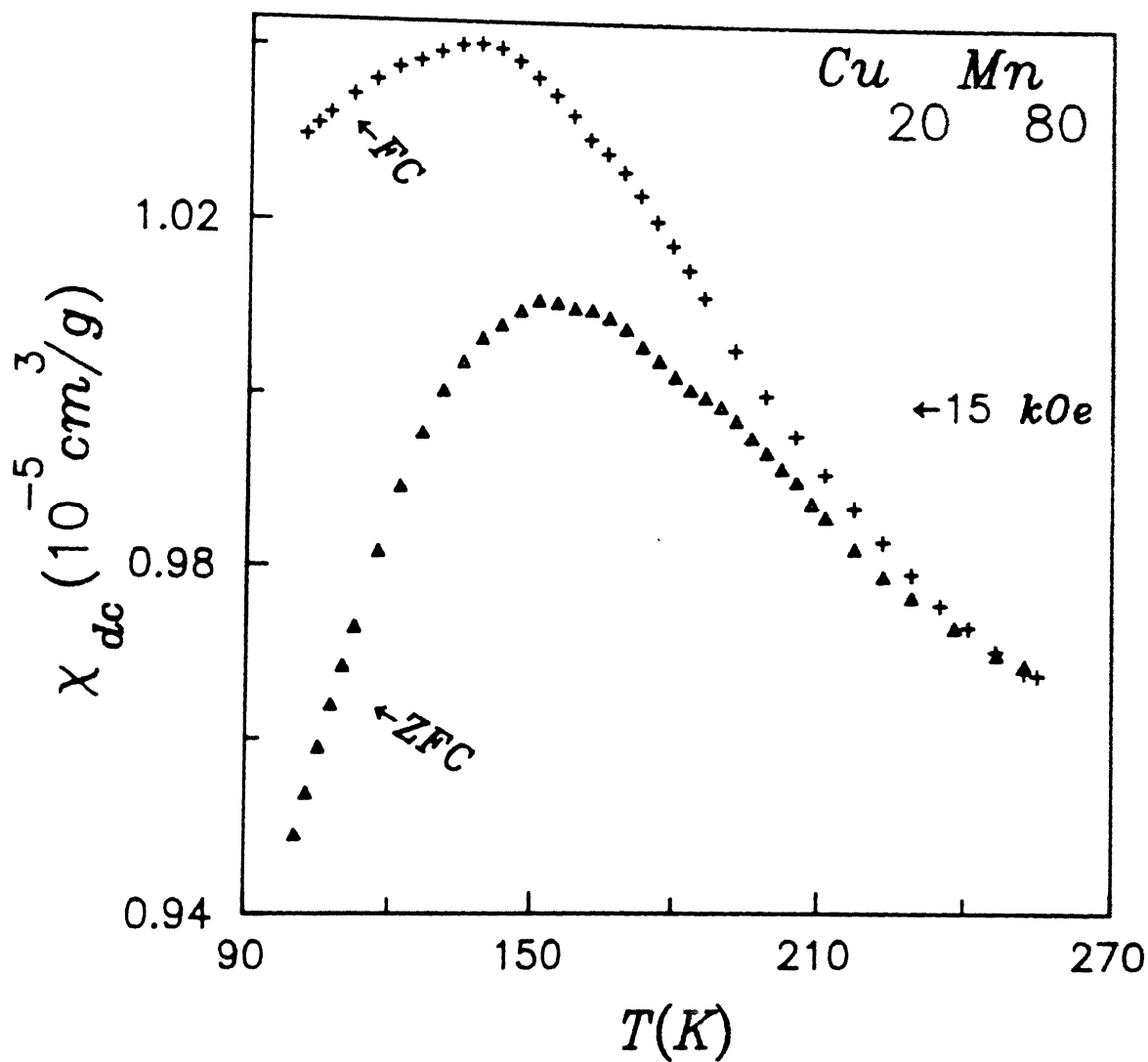
Figure 3.13 dc-susceptibility (χ_{dc}) vs temperature for x = 80 in 15 kOe dc field.

cooled the samples in the presence of 15 kOe field from room temperature to a temperature (T) which is much below the temperature where the peak of χ_{dc} occurred. Then we switched off the magnetic field and started measuring magnetization with time (t) in the residual field of the electromagnet (~ 30 Oe) keeping the temperature constant. The temperature T was almost the same for all the samples. We have taken the data for t > 10 sec. since the integration time constant of the instrument is 1 sec.. Figure 3.14 gives the variation of M with $\ln$ t for samples with x = 35-72. Although it was very difficult to measure the time-dependent magnetization for the sample with x = 80 because of the small signal, nevertheless a qualitative decay of M with time could definitely be observed.

M vs H for all the samples at room temperature and at the lowest temperature are also measured. Figure 3.15 shows the M vs H for all the samples at 77K after cooling them in zero field. M vs H for ZFC x = 72 sample at 5, 120 and 300K are carried out in fields up to 55 kOe in a SQUID magnetometer. The results are shown in Figure 3.16.

Apart from these, M(T) measurements are also carried in samples with x = 72 and 80 in a Faraday balance. These measurements are made in the zero-field-cooled state. M(T) is measured in 1 kOe field from 30K to room temperature. The result for x = 80 is shown in Figure 3.17. The M vs T measurements for x = 80 sample are also carried out in FC and ZFC states at 10 kOe field from 5 to 300K in a SQUID magnetometer. Inset of Figure 3.17 shows the result.
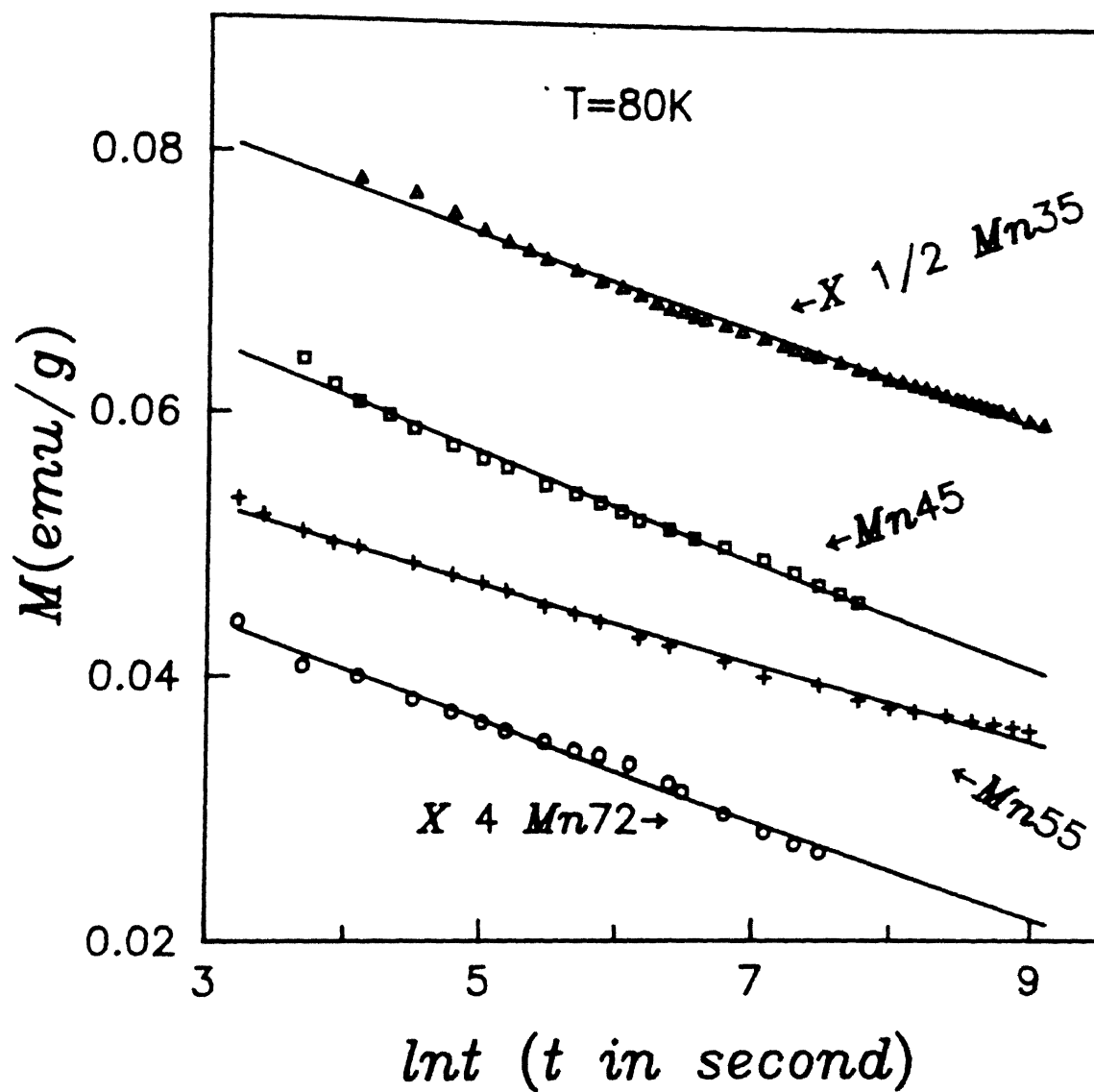
Figure 3.14 Remanent magnetization (M) at 80K vs logarithm of time (t) where t is measured in seconds. The best fitted straight lines are shown. M of x = 35 and 72 are multiplied by factors 1/2 and 4 respectively. Thus the slopes are not the real ones.
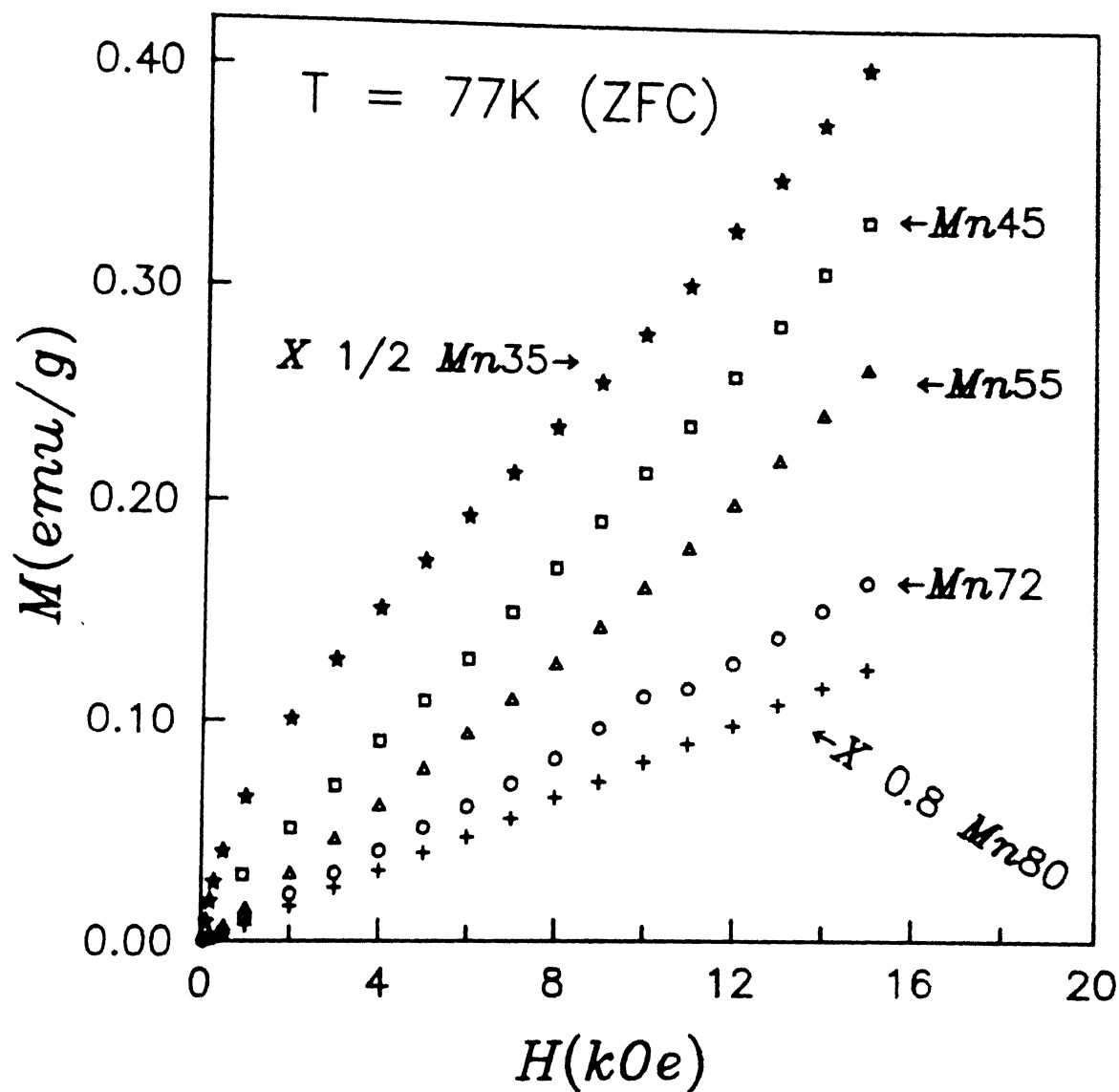
Figure 3.15 Magnetization (M) vs magnetic field (H) of ZFC samples with x = 35, 45, 55 72 and 80 at 77K. M of x = 35 and 80 are multiplied by factors 1/2 and 0.8 respectively.
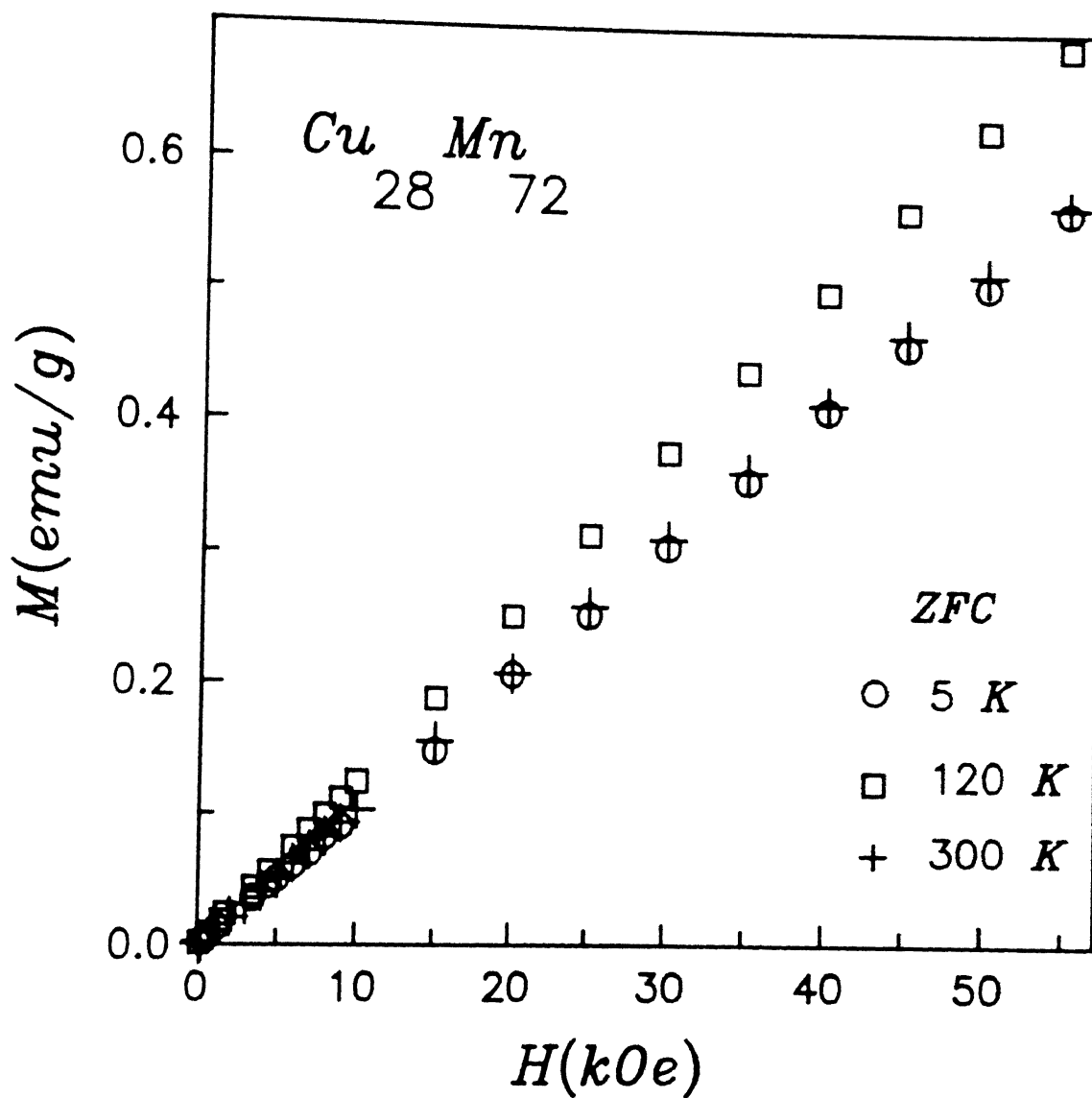
Figure 3.16 Magnetization (M) vs magnetic field (H) of ZFC samples with x = 72 at 5,120 and 300K. Note the overlapping of points for 5 and 300K.
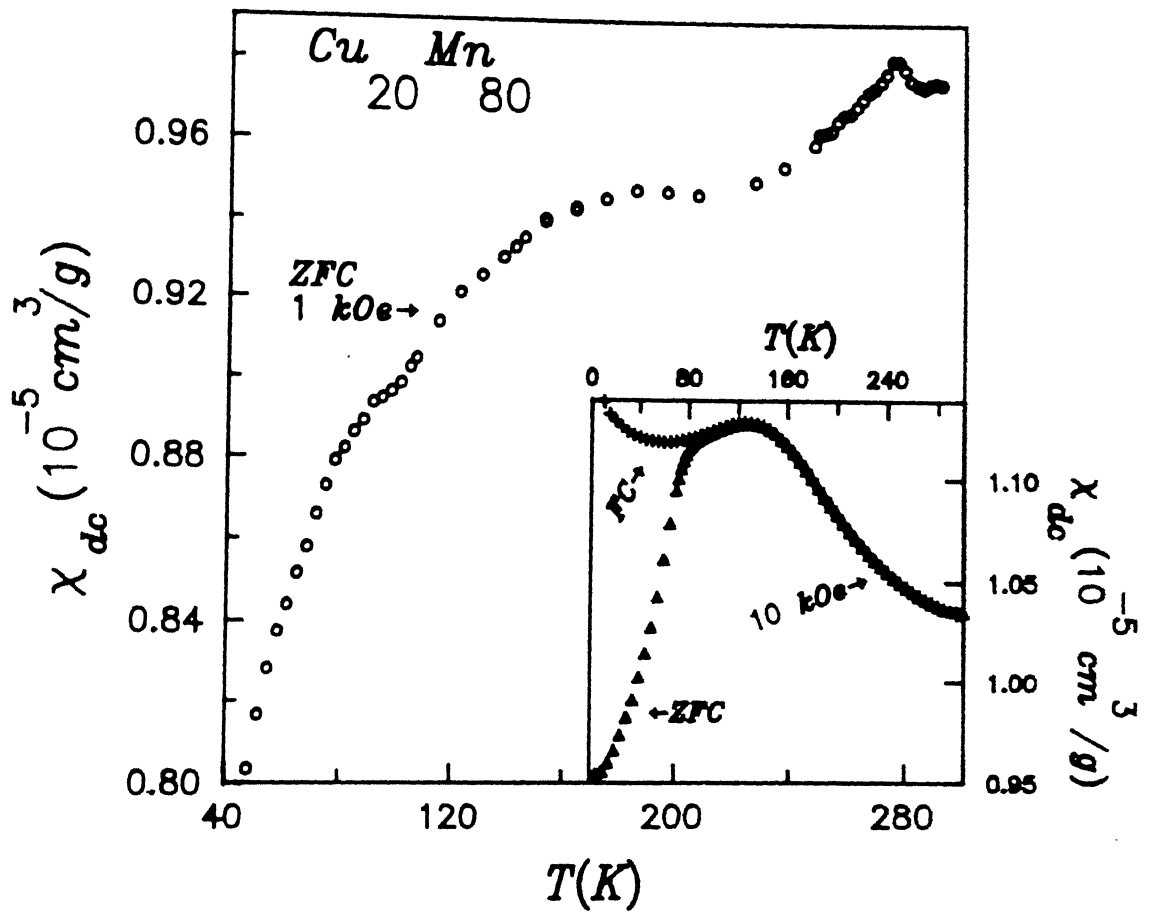
Figure 3.17 dc-susceptibility (χ_{dc}) vs temperature for ZFC sample with x = 80 measured in 1 kOe field. Inset shows the results of M(T) measurement in ZFC and FC samples with x = 80 at 10 kOe field.

From Figures 3.8 - 3.13 we observe that the χ_{dc} vs T curves for the samples with x = 35-80 show broad peaks for the ZFC branch whereas the FC branches tend to flatten out below the peak. The FC branch can be obtained reversibly but the ZFC branch is not reversible. This history dependence gives an indication of a spin-glass like freezing. The temperature where the peak in χ_{dc}(ZFC) has occurred is determined from $d\chi_{dc}/dT = 0$. We call this temperature the freezing temperature (T_f). The temperature T_f and the peak value of χ_{dc}, which we call χ_{dc}^{max}, vary with the measuring field and concentration x. In the high-temperature side of T_f ($T > T_f$) both the ZFC and FC branches of χ_{dc} vs T curve go together and the plot of $1/\chi_{dc}$ vs T (Figure 3.18) shows Curie-Weiss behaviour ($\chi = \frac{C}{T-\theta}$, where C = Curie constant = $N\mu_B^2 p_{eff}^2/3k_B$, θ = Curie-Weiss temperature, p_{eff}= effective number of Bohr magneton (μ_B) per Mn atom in units of μ_B, N = number of Mn atom/g). We have determined p_{eff} from the $1/\chi_{dc}$ vs T plot at high temperatures using Curie-Weiss law. p_{eff} is given by

$$p_{eff} = g \, [J(J+1)]^{1/2} = \left[\frac{3k_B}{N\mu_B^2 \left(\frac{d(1/\chi_{dc})}{dT} \right)} \right]^{1/2} , \qquad (3.4)$$

where g = Lande g factor, J = total angular momentum of Mn atom, and k_B = Boltzmann constant.

We have fitted our $1/\chi_{dc}$ vs T data to Equation (3.4) using a least-squares fitting programme and the lowest temperature of the fitted range is chosen on the basis of the deviation of the data from Curie-Weiss law by an amount exceeding the experimental error. We have calculated p_{eff} from the slope of the best fitted
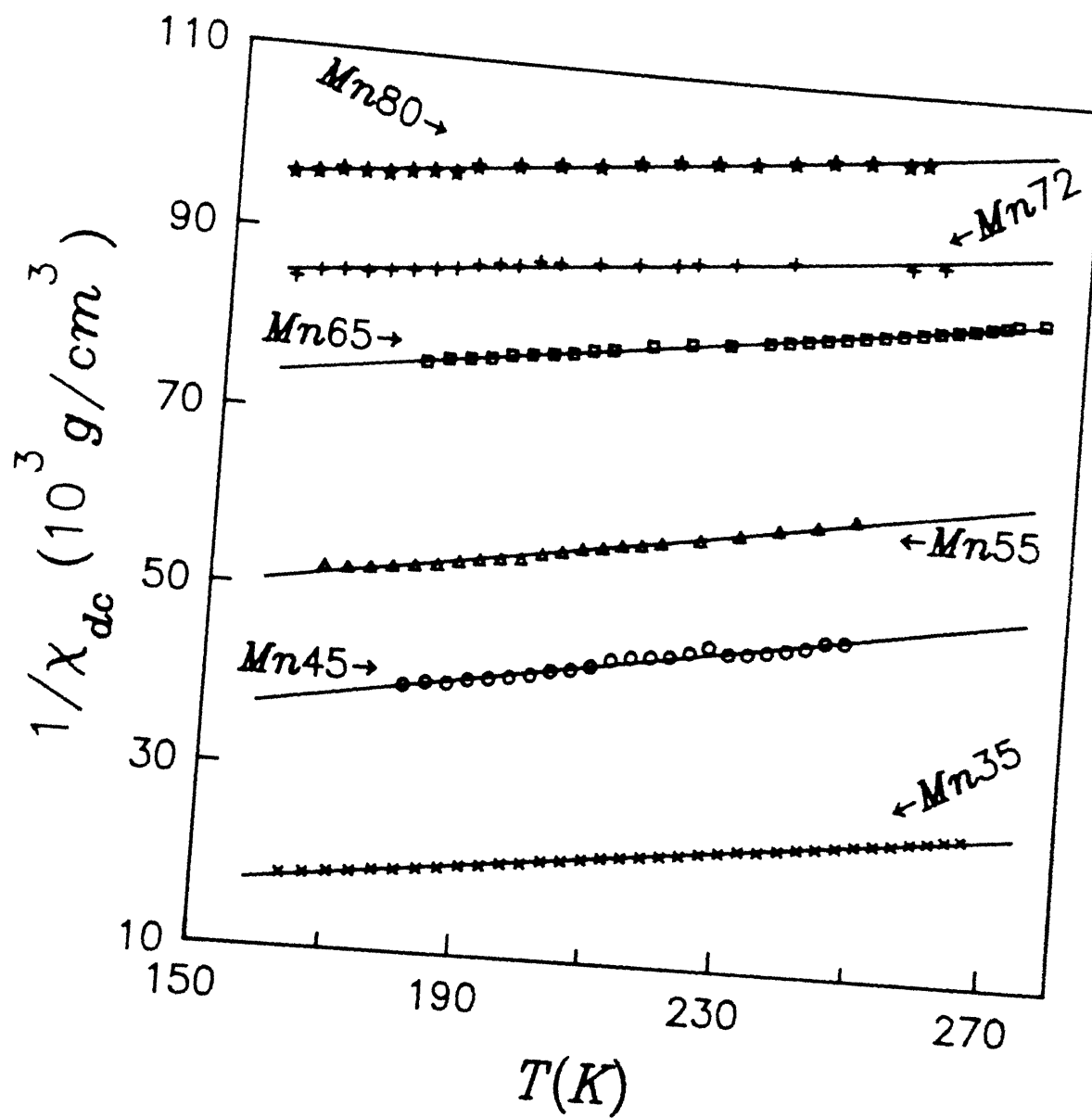
Figure 3.18 A typical example of $1/\chi_{dc}$ vs T for each sample in the paramagnetic region. The best fitted straight lines are shown.

straight lines for both the ZFC and FC branches for H = 10 and 15 kOe and the *average* value was taken as p_{eff}.

Table 3.3 gives the variation of T_f and χ_{dc}^{max} measured at different fields and p_{eff} with concentration x. We have also listed the long-range antiferromagnetic Néel temperature (T_N) for x = 80 and 85. For x = 80 sample we observe a small antiferromagnetic peak at 275K which is 4% above the background χ of $\simeq 10^{-5} cm^3/g$ (Figure 3.17). x = 85 sample has an antiferromagnetic Néel temperature at 484K (Figure 3.19).

Table 3.3

Concentration x (at %)	Field (kOe)	T_f (K)	χ_{dc}^{max} ($10^{-5} cm^3/g$)	p_{eff} (μ_B)	T_N (K)
35	1 10 15	135 127 118	16.8 5.84 6.01	0.55	—
45	1 10 15	176 164 156	3.77 2.56 2.51	0.40	—
55	1 10 15	168 164 156	2.30 1.83 1.91	0.31	—
65	10 15	164 149	1.32 1.32	0.38	—
72	1 5 10 15	172 164 159 148	1.24 1.16 1.15 1.24	0.43	—
80	10 15	130 145	1.12 1.15	0.42	275
85	10	—	0.8	—	484

From Table 3.3 we see that χ_{dc} is very small ($\sim 10^{-5} cm^3/g$) and is close to the sensitivity limit of the
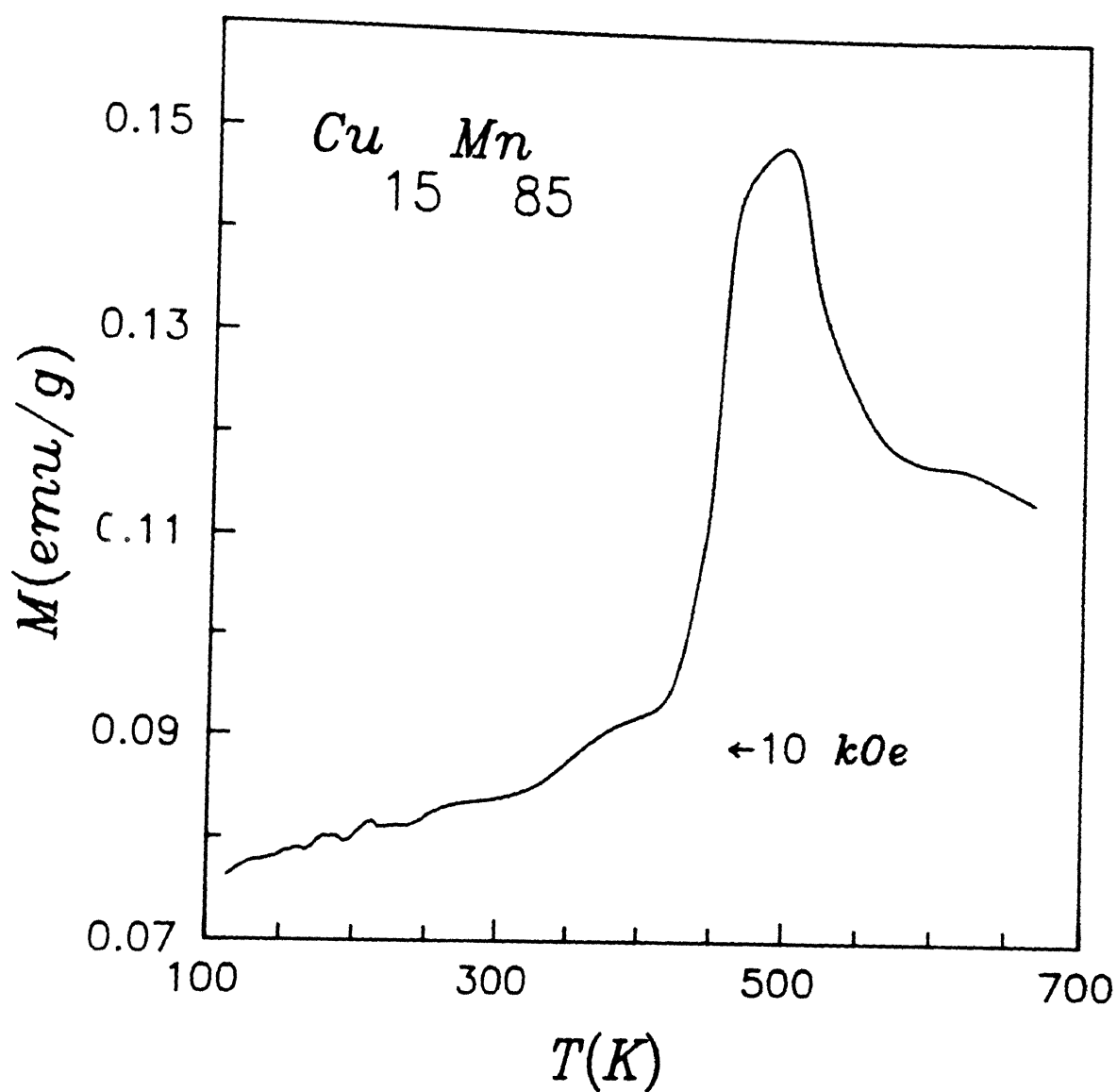
Figure 3.19 Magnetization (M) vs temperature for x = 85 sample at 10 kOe field. The low-temperature and high- temperature data are smoothed out and matched to get a continuity.

vibrating sample magnetometer. It becomes rather difficult to predict from our data the existence of de Almeida and Thouless (AT) line $[(1-T/T_f) \propto H^{2/3}]$ or Gabay and Toulouse (GT) line $[(1-T/T_f) \propto H^2]$. These lines are predicted [16,17] on the basis of the instability in the solution of the infinite-range limit of Sherrington- Kirkpatrick model. The existence of these lines implies a phase transition in the mean field theory for spin-glasses. Wenger and Mydosh [48] have shown that one can get AT-like or GT-like lines even in the case of blocking of clusters in the superparamagnetic theory based on Néel's model which does not assume a phase transition. They have argued that the existence of AT or GT lines in spin-glass does not necessarily mean a phase transition. Their calculations show that $(1-T_f(H)/T_f(0)) \propto H^2$ for low fields and for high fields it goes as $H^{2/3}$. Fiorani et al. [49] have shown the existence of AT line or the $H^{2/3}$ dependence of the blocking temperatures of superparamagnetic clusters of fine iron particles in Al_2O_3 matrix which has shown a spin-glass behaviour. Wohlfarth [21] has also calculated the variation of blocking temperatures with external field and has shown that for small fields $[T_B (H)/T_B (0)]^{1/2} = (1 - H/H_K)$ where T_B is the blocking temperature or the peak temperature (T_f) and H_K is the mean anisotropy field. He also indicated that there may be a change in the behaviour when H becomes comparable to H_K .

It has become more difficult for us to visualize a phase transition, even qualitatively, with a unique Edwards-Anderson (EA) order parameter and its field dependence at T_f. The field dependence of the EA order parameter [16] is given by

$$q(T_f, H) \propto 1 - \frac{\chi_{dc}^{max}(H)}{\chi_{dc}^{max}(0)}$$

and the related critical exponent δ is given by

$$q(T_f, H) \propto (H^2)^{1/\delta}.$$

A close look at Table 3.3, where we have listed the variation of χ_{dc}^{max} with different fields for each sample, will clarify our point. For samples with x = 35-55, q increases with H corresponding to a positive value of δ whereas for others q remains more or less constant giving an unphysically large value of δ.

The variation of the peak value of the susceptibility with field is very complicated in nature. Tholence and Tournier [5] have shown that, when identical monodomains are cooled from $T > T_B$ to $T < T_B$, the resulting magnetic moment in the direction of the field is

$$M = M_s(T_B) \int_0^{\pi/2} \tanh\left[\frac{vM_s(T_B)H}{k_B T_B} \cos\theta \right] \cos\theta \sin\theta \, d\theta. \quad (3.5)$$

Here M_s is the spontaneous magnetization, v is the volume, T_B is the blocking temperature and θ is the angle between the anisotropy axis of the monodomains, and the applied field H. For real systems one has to incorporate the variation of the size of the domain.

Equation (3.5) in the small field limit tends to

$$M = \frac{vM_s^2H}{3k_BT_B}$$

and
$$\chi_{dc} = \frac{M}{H} = \frac{v\,M_s^2}{3k_BT_B} \,. \qquad (3.6)$$

Even in this crude approximation the field dependence comes in through T_B. The applied field H_{ext} increases the barrier height (Equation (3.2)) which, in turn, increases T_B (Equation (3.3)) which results in a decrease of χ_{dc}. Thus the decrease in χ_{dc}^{max} with the increase in field for sample with $x = 35-55$ can be explained.

From Table 3.3 we see that for a particular value of the field, χ_{dc}^{max} has always decreased with the increase in Mn concentration x. This can happen either by a decrease in M_s because of more and more antiferromagnetically coupled spins reducing the uncompensated moment or an increase in T_B because of the increase in anisotropy energy E_A (Equations (3.2) and (3.3)). The dominance of the first effect for $x = 35-55$ is confirmed by the variation of p_{eff} with x, namely, p_{eff} decreases with x. But for $x = 65-80$ the second effect may be more dominant.

Though with the increase in x we have proceeded towards antiferromagnetism, the complex nature of the antiferromagnetic short-range order in the $x=65-80$ range gives a complicated variation in p_{eff}.

The neutron diffraction study by Cowlam and Shamah [11] in γ-phase (f.c.c) $Cu_{100-x}\,Mn_x$ for $x = 72.5 - 82.5$ shows some interesting features about the magnetic short-range order. If J_1 is the first nearest neighbour interaction and J_2 is the second

nearest neighbour one for Mn, then they have shown that for x <
74, both J_1 and J_2 are negative, that is, both are
antiferromagnetic. This is called the AF3 structure. Above x =
74, J_1 is negative but J_2 is positive, that is, the first is
antiferromagnetic while the second is ferromagnetic. This is
called the AF1 structure.

Figure 3.20 shows the variations of χ_{ac}^{max}, χ_{dc}^{max} and P_{eff}
with analyzed Mn concentration x. In this case the decrease in
P_{eff} with the increase in Mn concentration up to about x = 55
shows that the increase in x leads to bigger and bigger
antiferromagnetically ordered clusters with lesser and lesser
uncompensated spins in the AF3 structure. From x = 55 to x = 80
we see an increase in P_{eff} till about x = 72. This may be due to
the change from AF3 to AF1 structure which is accompanied by a
change of J_2 from a negative to a positive value. This implies
that the increase in P_{eff} is due to the ferromagnetically coupled
second nearest neighbour or the positive J_2 in AF1 structure.
Following the above argument the observed P_{eff} should have
increased even beyond x = 72. The constancy of its value for x >
72 indicated dependence of both J_1 and J_2 on Mn concentration x as
well as on the small tetragonal distortion observed for x > 74.
Strictly speaking, the decrease in P_{eff} with increasing x should
have continued till x = 74. Our findings seem to suggest that the
phase boundary between AF3 and AF1 structures may be quite
extended.

An attempt has been made by Tholence and Tournier [5] to
find out the number of spins in a cluster. They assumed that each
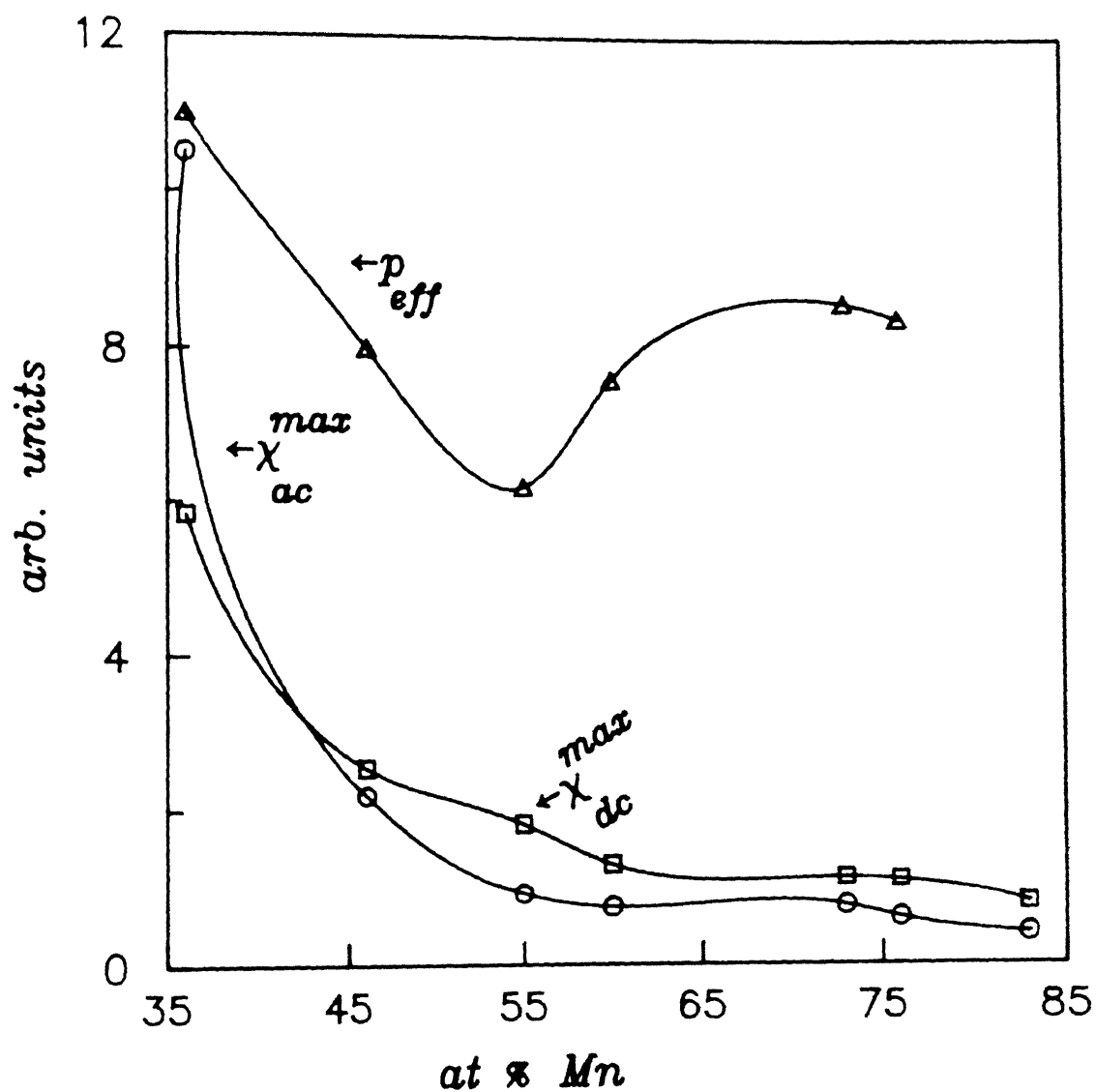
Figure 3.20 Variations of χ_{ac}^{max}, χ_{dc}^{max} and P_{eff} with analysed Mn concentration x. The lines joining the points are just guides to the eye.

cluster consists of n number of Ising spins, parallel or antiparallel. The moment of a cluster is due to the uncompensated spins in the cluster. Using a random walk calculation, they have proved that the effective moment of a cluster containing n antiferromagnetically coupled spins is given by $\sqrt{n}\ p_{eff}^{o}$, where p_{eff}^{o} is the individual magnetic moment of the transition metal atoms. Hence we can say that $p_{eff} = p_{eff}^{o}/\sqrt{n}$. From the above relation we can conclude that the observed decrease in p_{eff} with concentration is related to the increase in n, the number of spins in a cluster. Therefore the decrease in p_{eff} for x = 35 to 55 implies that the average cluster size increases with x or bigger clusters are formed. Since the above calculation does not take care of the change in sign of J_2, which becomes ferromagnetic with the increase in x , the small increase in p_{eff} do not mean a decrease in n above x = 65. Looking at the relative strengths of J_1 and J_2 in AF1 structure we may assume a monotonic increase in the number of spins per cluster or an increase in cluster size.

The shape of the two branches of χ_{dc} vs T (Figures 3.8 - 3.13) for a spin-glass as well as for the alloys of our system can be explained on the basis of Néel's model. When we switch on the magnetic field at $T<T_f$ in the zero-field-cooled branch, only those clusters will respond to the field which have a coercive field less than the applied field or a volume less than some critical volume. In other words, the relaxation time of the cluster has to be smaller than the time of observation so that we can see their response to the field, that is, they can orient themselves in the direction of the field. The response of all the clusters with $T_B<T$

will contribute to the χ_{dc}. As we increase the temperature more and more clusters start responding to the field and the resulting χ_{dc} vs T curve has the same explanation as that of the χ_{ac} vs T curve. To get the FC branch we cool the sample in the presence of a magnetic field from high temperature, that is, $T > T_f$. Since at high temperatures most of the clusters are free, they respond to both the magnetic field and the thermal fluctuations resulting in a susceptibility which follows Langevin function L (vM_sH/k_BT) in the ideal case of non-interacting clusters. As we approach the peak from the high temperature side the clusters slowly proceed towards their blocking temperatures and under the influence of the external field they get blocked in the direction of the field with the lowering of temperature. So the χ_{dc} flattens out at low temperatures. Hence we get a different behaviour in the FC and the ZFC branches of magnetization where the FC χ_{dc} is always more than the ZFC χ_{dc}. For the FC curve, the χ_{dc} below the peak is given by $M_s^2(T)/3K(T)$ for $T<T_B$. Néel has taken the variation of K, the anisotropy constant, as M_s^2 for shape anisotropy or magnetocrystalline anisotropy arising from magnetic dipolar interaction within the cluster. In this case the low temperature χ_{dc} will be independent of temperature. This is the case with the samples with x = 35-55. But the decrease in χ_{dc} for x = 65-80 from the peak value at low temperatures indicates a faster increase in K(T). This may be because of the interaction between the clusters which had been neglected so far. We may note here that this decrease in χ_{dc} has taken place in the concentration range where P_{eff} has an increase with x. So the change in the behaviour of

K(T) may also have the same origin. The χ_{dc} vs T curves for x = 72 and 80 samples, taken at 1 kOe, do not show pronounced peaks near T_f as they show in higher fields (Figure 3.17). This indicates that there are dipolar interactions within the clusters which get suppressed as we apply higher fields. A similar result was obtained in AuFe spin-glasses near the percolation threshold [50].

A time-dependent magnetization is not a unique property of canonical spin-glasses only. It is observed for ferromagnetic and superparamagnetic clusters as well [51]. When a system with superparamagnetic clusters is slowly cooled in a magnetic field H from a temperature which is more than the freezing temperature (T_f) or the blocking temperature (T_B), the system acquires a magnetization M at low temperatures ($T<T_f$) which is almost the equilibrium magnetization at that temperature and field. If at that temperature the field is changed from H to H´ the equilibrium condition is changed. The magnetization M is no longer the equilibrium magnetization for the field H´. Hence the system becomes metastable. The new metastable state and the equilibrium state for H´ are separated by an energy barrier of height E. Due to thermal fluctuations the thermal energy $k_B T$ will help the magnetic cluster to cross the energy barrier and reach the new equilibrium state from its metastable state. The rate of this thermally activated transition is given by $\lambda = 1/\tau_0 \exp(-E/k_B T)$, where τ_0 is a constant ranging from $10^{-8} - 10^{-10}$ sec.. This leads to a change in magnetization with time given by

$$M = Mo \; e^{-\lambda t} \qquad .$$

This type of change in magnetization involves a single relaxation time or barrier height with a constant energy. However, in real systems this type of decay is not observed. To overcome this problem Street and Wooley [52] considered the change in magnetization with time involving a distribution of relaxation times or a distribution of energy barriers ($f(E,t)$). Here we apply their treatment to our case.

At a time t after we have reduced the field at a temperature $T < T_f$, let the number of clusters dN, with activation energies lying between E and E + dE, be $f(E,t)dE$. If the temperature remains constant at T, then the rate of change of N due to thermal activation is

$$\frac{dN}{dt} = \frac{d(f(E,t))}{dt}dE = -1/\tau_0 \; \exp \; (-E/k_BT) \; f(E,t) \; dE \quad . \quad (3.7)$$

Equation (3.7) is satisfied by

$$f(E,t) = f_0(E) \; \exp \; (-\lambda t),$$

where $\qquad \lambda = 1/\tau_0 \; \exp \; (-E/k_BT).$ $\qquad (3.8)$

Let each activation change the magnetization by an average amount $<m>$. Then the mean decrease in initial magnetization for activation of dN ($=f(E,t)dE$) number of clusters is given by

$$\langle m \rangle / \tau_o \ f_o(E) \exp(-\lambda t) \ \exp(-E/k_B T) \ dE \ dt.$$

The rate of decrease of the magnetization for all values of activation energy is

$$\frac{dM}{dt} = - \langle m \rangle / \tau_o \int_{E_{min}}^{E_{max}} f_o(E)(-\lambda t)\exp(-E/k_B T) \ dE. \qquad (3.9)$$

Now let us assume that $f_o(E)$ is independent of E. This means that

$$f_o(E) = p \ \text{for} \ 0 < E < \infty \ .$$

Then,

$$\frac{dM}{dt} = - \langle m \rangle / \tau_o \ p \int_0^{\infty} \exp(-\lambda t)\exp(-E/k_B T) \ dE. \qquad (3.10)$$

Changing variable from E to λ by using Equation (3.8), we get

$$\frac{dM}{dt} = - \langle m \rangle \ pk_B T \int_{\lambda=1/\tau_o}^{\lambda=0} \exp(-\lambda t) \ d\lambda$$

$$= - \langle m \rangle pk_B T \left[\frac{1}{t} \exp(-\lambda t) \right]_{\lambda=1/\tau_o}^{\lambda=0}$$

or, $\qquad \dfrac{dM}{dt} = - \dfrac{\langle m \rangle \ pk_B T}{t} \ [1 - \exp(-t/\tau_o)] \ . \qquad (3.11)$

For $t \gg \tau_o$,

$$M = - \langle m \rangle pk_B T \ \ell n \ t + \text{constant} \qquad (3.12)$$

or,
$$M = M_o - S \ln t, \qquad \qquad (3.13)$$

where
$$S = \langle m \rangle \, p k_B T. \qquad (3.14)$$

Gaunt [53] has shown that the variation of magnetization with time can be approximated to a $\ln t$ variation even when $f_o(E)$ is not constant for time up to 1000 sec.. Figure 3.14 shows that for our samples Equation (3.13) or the $\ln t$ variation is obeyed even for time much more than 1000 sec.. Hence the approximation, that the number of barriers is the same for all energies, is not a bad one for our alloys.

We have fitted our data to Equation (3.13) for time above 40 sec. by a least squares fitting programme and found a good fit with normalized mean-squared deviation χ^2 values consistent with experimental accuracy. The fitted values of M_o and S for different samples are given in Table 3.4.

Table 3.4

Mn conc. x (at%)	M_o (emu/g)	S (emu/g)
35	1.82×10^{-1}	6.9×10^{-3}
45	7.55×10^{-2}	3.8×10^{-3}
55	5.96×10^{-2}	2.7×10^{-3}
72	1.44×10^{-2}	1.0×10^{-3}

One should note here that since M in Figure 3.14 is multiplied by

constants for some samples, the apparent slopes in the figure will not match with the values of S in those cases. From Table 3.4 we see a monotonic decrease in the value of S with Mn concentration. This signifies that the rate of change of magnetization decreases with the increase in Mn concentration. Néel has taken the height of potential barrier $E = vH_cM_s/2$. With the assumption of a single relaxation time, we can show that the rate of change of magnetizaton is proportional to $\exp(-vH_cM_s/2K_BT)$. Hence the increase in Mn concentration leads to an increase in the volume of the clusters. This justifies our earlier conclusion that an increase in x increases the average number of spins in the clusters. One may even try to justify this from the monotonic decrease in M_o with the increase in x.

The zero-field-cooled M vs H for x = 35 sample (Figure 3.15) deviates from a straight line and resembles the results of earlier studies on CuMn with Mn = 19 at % [54]. We observe from Figure 3.15 that for x = 45 to 85 the zero-field-cooled M vs H curves are roughly linear and we have not detected any hysteresis. From Figure 3.16 we can see that the linearity holds for x = 72 at all temperatures even up to a field of 55 kOe. The lack of any structure, especially the absence of saturation, makes any quantitative analysis of the data difficult. We will try to give a qualitative justification of the observed M vs H behaviour in the light of spin-glass domain model proposed by Kouvel and Abdul-Razzaq [55]. They explained the M vs H behaviour of re-entrant NiMn alloys using this model.

We observe from Figure 3.16 that for x = 72, M vs H is

linear for all temperatures. This suggests that there may not be any qualitative difference in the magnetic ordering of the system with temperature. This is consistent with the isothermal magnetization in superparamagnetic cluster blocking model where the dynamics of the clusters are only responsible for magnetic response at all temperatures. The persistence of linearity for all H and the symmetric (undisplaced) M-H loop (not shown) seem to indicate that at least for the zero-field-cooled state the bulk magnetization is achieved by rotation of magnetization of domains or clusters and not by displacement of domain walls and the system is subdivided into randomly oriented domains. This is not unusual since in our system the domains are physically separated.

To explain qualitatively the linearity of M(H) with the domain model [55] we consider that the domains with average magnetization M_{av} are randomly oriented with average anisotropy field H_{av}. Then the magnetization of a domain, M_d, parallel to the external field H is given by

$$M_d = M_{av} \; \frac{(H + H_{av} \cos \theta)}{(H^2 + H_{av}^2 + 2HH_{av} \cos \theta)^{1/2}} \; ,$$

where θ is the angle between H and H_{av}.

Then the bulk magnetization at a field H is given by

$$M(H) = \frac{1}{2} \int_{-1}^{1} M_d \; d(\cos\theta)$$

which gives $$M(H) = \frac{2M_{av}H}{3H_{av}} \qquad \text{for } H \leq H_{av} \qquad (3.15)$$

and $$M(H) = M_{av}\left(1 - \frac{H_{av}^2}{3H^2}\right) \qquad \text{for } H \geq H_{av}. \qquad (3.16)$$

We can see the linearity of M vs H from the limiting case of $H \leq H_{av}$ in Equation (3.15).

It has been shown [55] that the linearity exists even when one assumes a mean field exchange interaction between the domains.

3.4 Magnetic Phase Diagram

We arrive at the magnetic phase diagram by taking the transition temperatures from our magnetic studies. The spin-glass transition temperatures for x = 4.4 and 9 are taken from χ_{ac} data (Table 3.2) and for others from the χ_{dc} data at 10 kOe (Table 3.3). The Néel temperatures(T_N) for x = 80 and 85 are also taken from χ_{dc}. This resulting diagram is shown in Figure 3.21. We are calling the low-x region as spin-glass (SG) and high-x region as cluster-glass (CG). The transition temperatures and the constructed phase diagram including the interpolated line from spin-glass to cluster-glass have qualitative agreements with those of the earlier studies [11,32]. In high Mn concentration regime we have found a double transition from paramagnetic (P) to antiferromagnetic (AF) to cluster-glass phase for x=80. Here below T_f, we have definitely observed some characteristic features of a

EXPERIMENTAL PHASE DIAGRAM
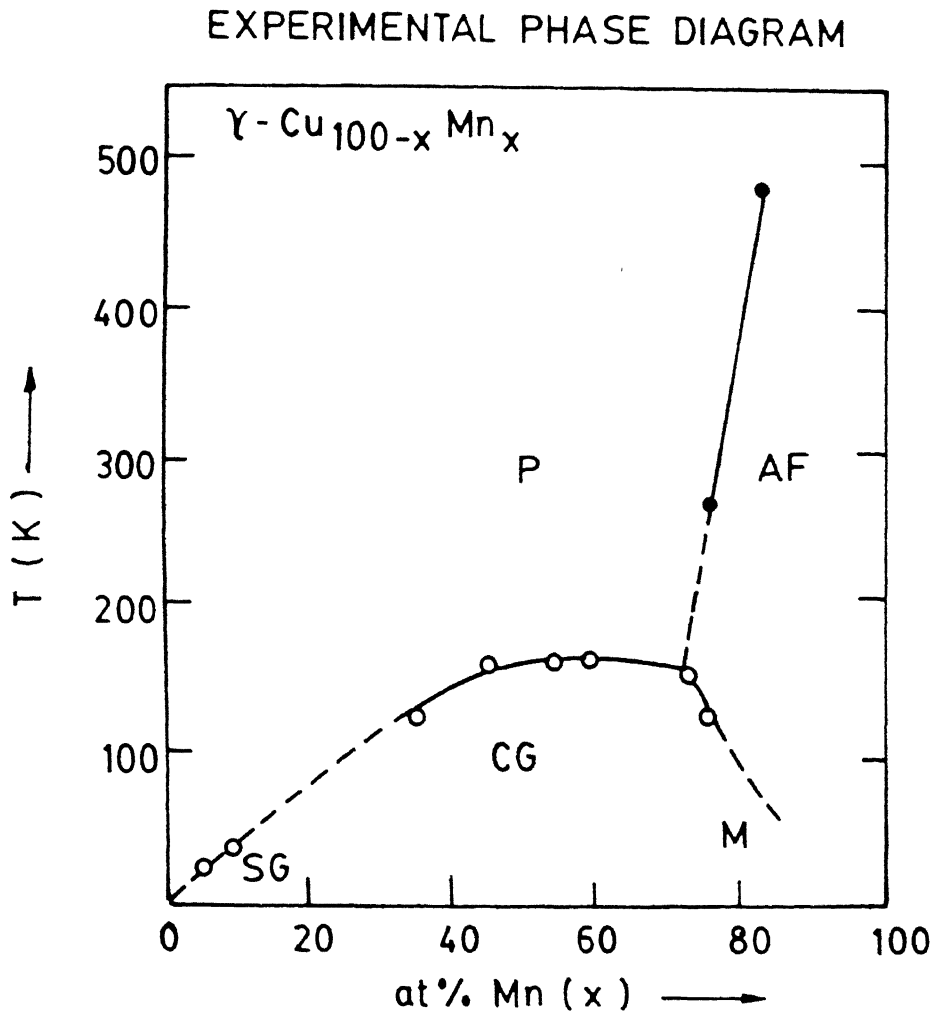
Figure 3.21 Experimental magnetic phase diagram for CuMn alloys.

cluster-glass, viz, the time and magnetic history dependence of magnetization. If we couple this observation to the neutron-scattering data of Cowlam and Shamah which show long-range antiferromagnetism even at 4.2K for alloys in this composition range, then it is clear that below T_f= 130K (Table 3.3), x=80 alloy exists in a mixed(M) antiferromagnetic and cluster-glass phase. Moreover, the alloy with x=72 seems to be a multicritical composition with T_N = T_f =159K. However, the actual phase boundary between CG and M seems to be quite fuzzy. One needs to have more alloys in that region. Also, more accurate and sophisticated low-temperature magnetic studies are expected to throw more light on the exact nature of the cluster-glass to mixed and mixed to antiferromagnetic phase boundaries.

The theoretical magnetic phase diagram has been constructed by Mookerjee and Roy [56] by considering the change in magnetic structure from AF3 to AF1 in the concentration range of 50 to 74 at % Mn. The theoretical phase diagram is shown in Figure 3.22. We see a good agreement with our experimental phase diagram. However, the sharp decrease in antiferromagnetic to mixed phase transition temperature observed by us around x=75 is not present in the theoretical phase diagram. Moreover, although the authors find double transition above x=70, there is no specific mention of the mixed phase in the theory, viz, the co-existence of antiferromagnetism and cluster-glass. One should mention here that experimentally it is easier to detect the co-existence of ferromagnetism with spin-glass from bulk magnetic measurements where one observes both spontaneous magnetization

cluster-glass, viz, the time and magnetic history dependence of magnetization. If we couple this observation to the neutron-scattering data of Cowlam and Shamah which show long-range antiferromagnetism even at 4.2K for alloys in this composition range, then it is clear that below T_f= 130K (Table 3.3), x=80 alloy exists in a mixed(M) antiferromagnetic and cluster-glass phase. Moreover, the alloy with x=72 seems to be a multicritical composition with $T_N = T_f$ =159K. However, the actual phase boundary between CG and M seems to be quite fuzzy. One needs to have more alloys in that region. Also, more accurate and sophisticated low-temperature magnetic studies are expected to throw more light on the exact nature of the cluster-glass to mixed and mixed to antiferromagnetic phase boundaries.

The theoretical magnetic phase diagram has been constructed by Mookerjee and Roy [56] by considering the change in magnetic structure from AF3 to AF1 in the concentration range of 50 to 74 at % Mn. The theoretical phase diagram is shown in Figure 3.22. We see a good agreement with our experimental phase diagram. However, the sharp decrease in antiferromagnetic to mixed phase transition temperature observed by us around x=75 is not present in the theoretical phase diagram. Moreover, although the authors find double transition above x=70, there is no specific mention of the mixed phase in the theory, viz, the co-existence of antiferromagnetism and cluster-glass. One should mention here that experimentally it is easier to detect the co-existence of ferromagnetism with spin-glass from bulk magnetic measurements where one observes both spontaneous magnetization

THEORETICAL PHASE DIAGRAM

Figure   3.22   Theoretical magnetic phase diagram for   CuMn
alloys taken from reference [56].

alongwith time and history dependence as found in γ-FeNiCr ternary alloys [17,45]. But in the case of a possible co-existence of antiferromagnetism with spin-glass, magnetization measurements alone in polycrystalline samples are unable to prove their simultaneous presence. Neutron diffraction studies are essential for the detection of the long-range antiferromagnetic order. However, in the case of single crystals it has been possible to prove their simultaneous presence through magnetization measurements [57]. In the present case of CuMn alloys our bulk magnetization measurements supplemented by neutron diffraction studies establish the presence of mixed antiferromagnetic and cluster-glass phases. We would like to reiterate that, on the basis of neutron diffraction and the present studies, the nature of this phase boundary between cluster-glass and mixed phases is not as clear-cut as depicted in some other experimental studies [11,32]. We believe that this phase boundary could lie anywhere within a range of composition as shown in the work of Vedyaev and Cherenkov [33]. However, we have not included this in our phase diagram (Figure 3.21) since no work, to our knowledge, throws much light on this boundary.

3.5 Electrical Resistivity

We present here the results of the electrical resistivity measurements on $Cu_{100-x}Mn_x$ alloys with x = 35-85 between 8 and 300K. The plots of resistivity ρ vs temperature T are given in Figures 3.23 - 3.29 and $d\rho/dT$ for respective samples are given in the inset of the corresponding figures. We may note here that the experimental error is much less than the width of

Figure 3.23 Resistivity (ρ) vs temperature for sample with x = 35. Inset shows the derivative dρ/dT vs T.

Figure 3.24 Resistivity (ρ) vs temperature for sample with x = 45. Inset shows the derivative dρ/dT vs T.
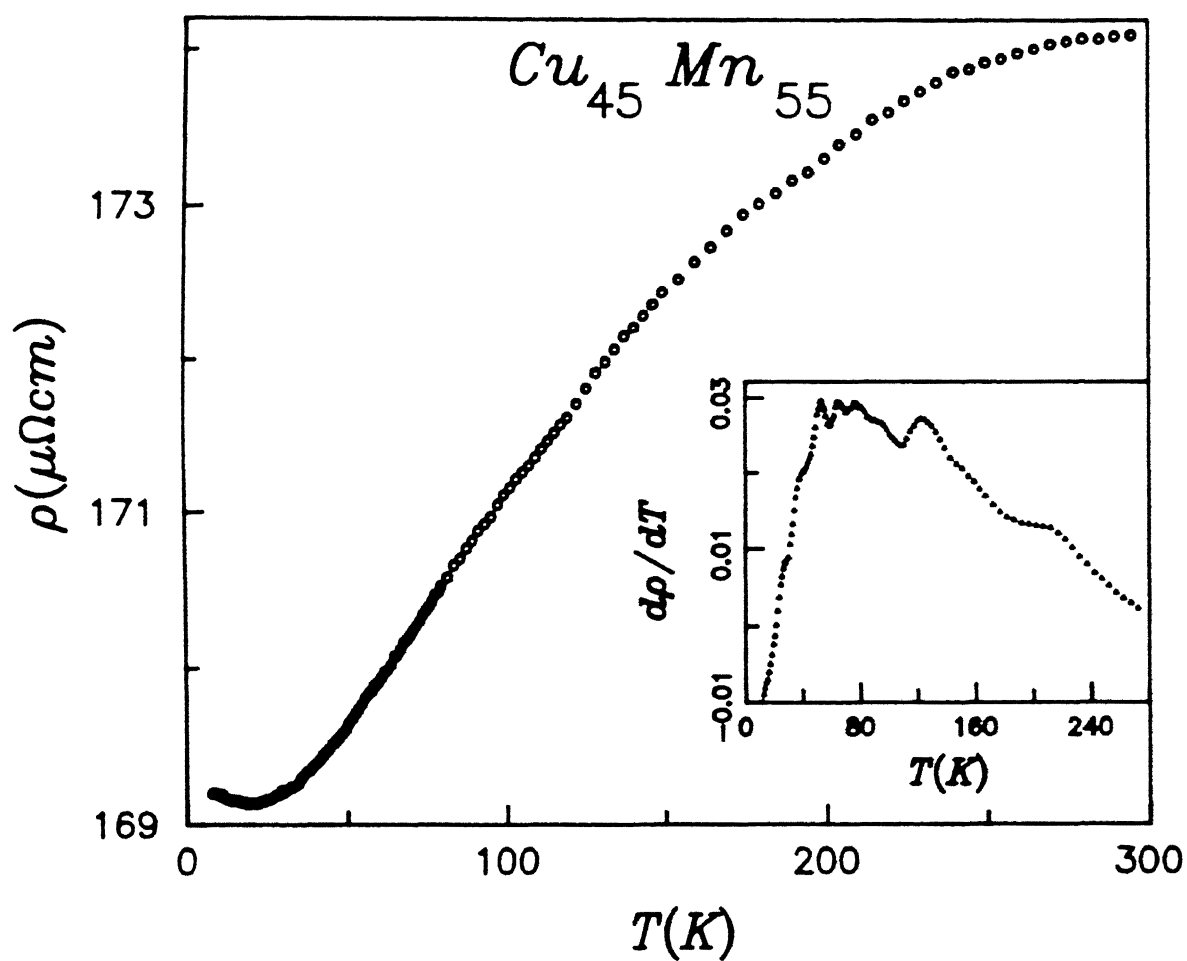
Figure 3.25 Resistivity (ρ) vs temperature for sample with x = 55. Inset shows the derivative dρ/dT vs T.
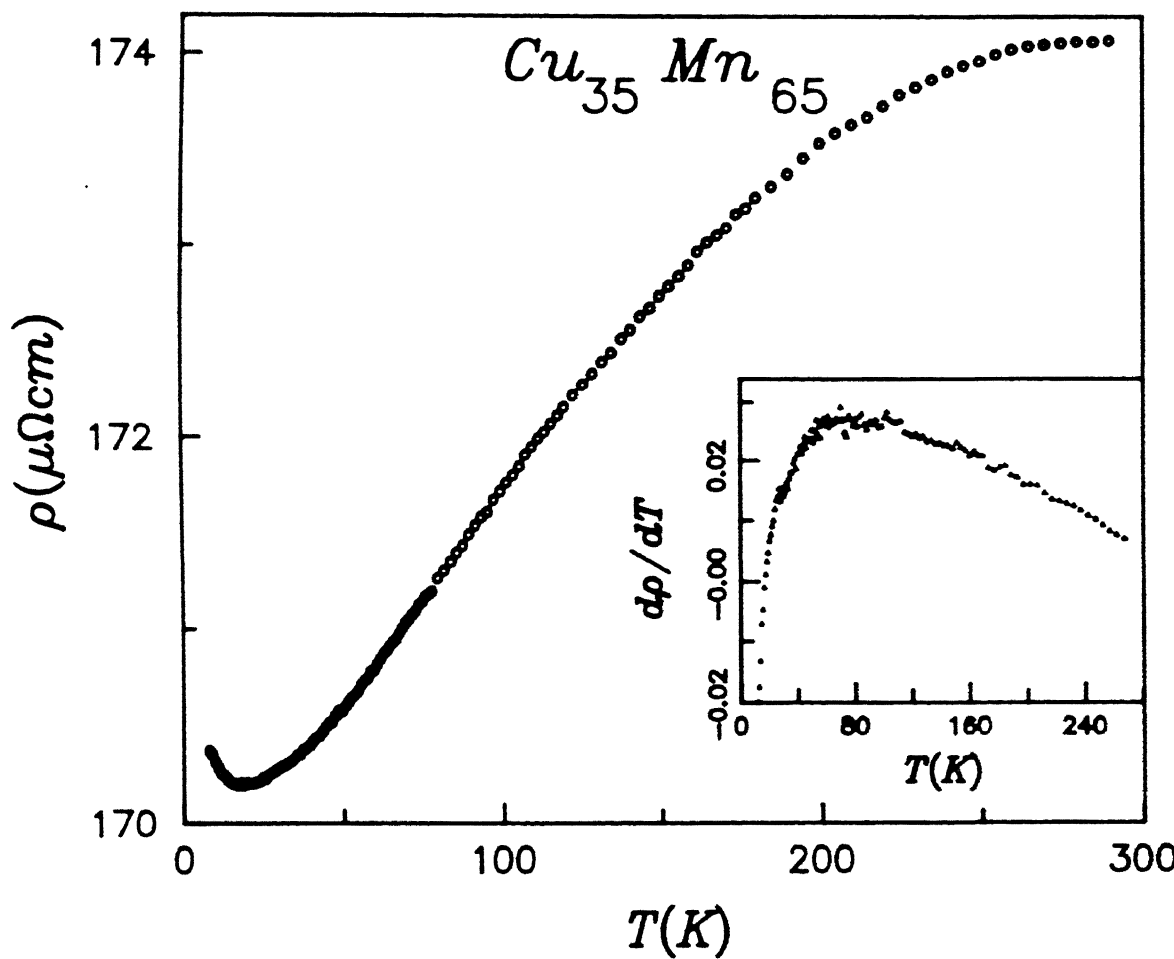
Figure 3.26 Resistivity (ρ) vs temperature for sample with x = 65. Inset shows the derivative dρ/dT vs T.
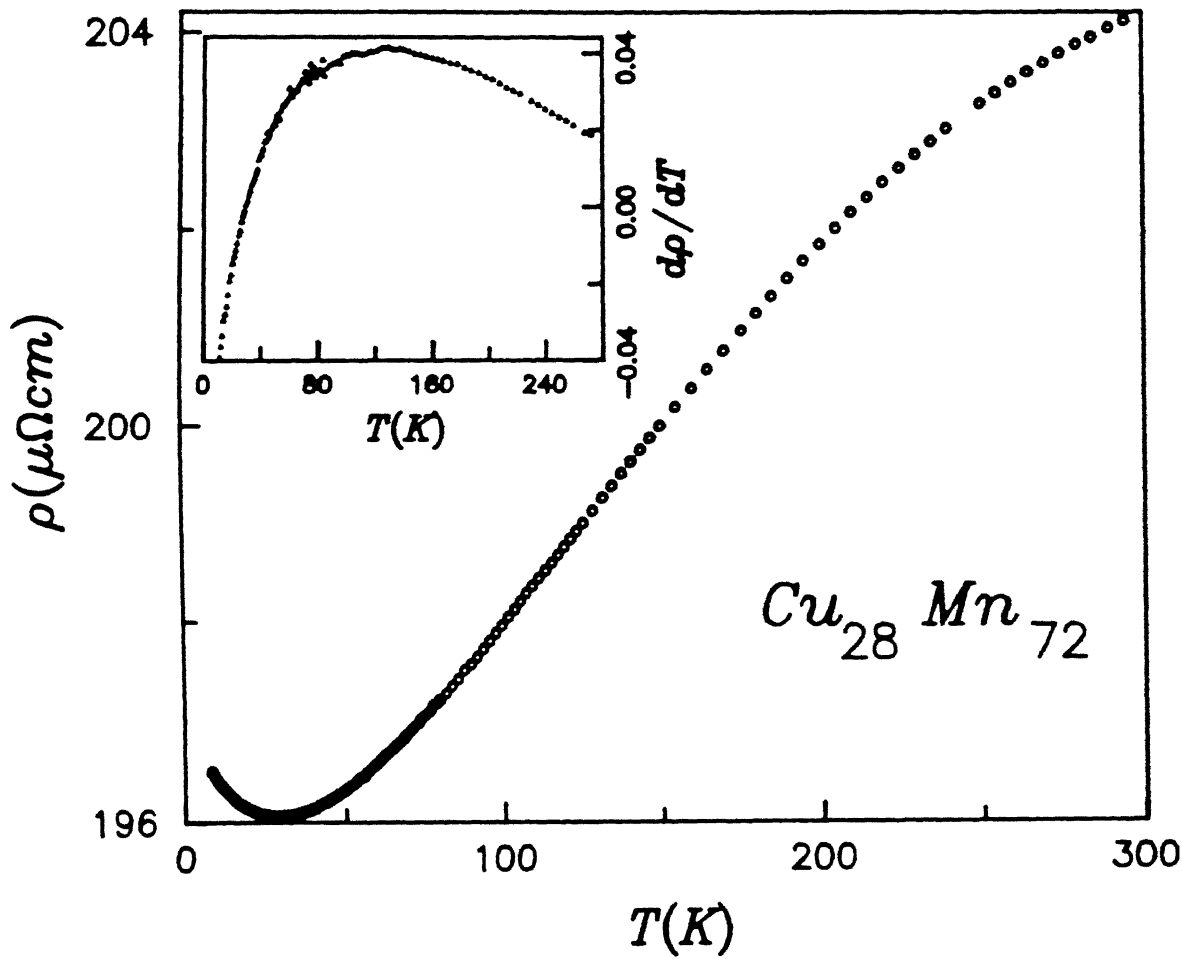
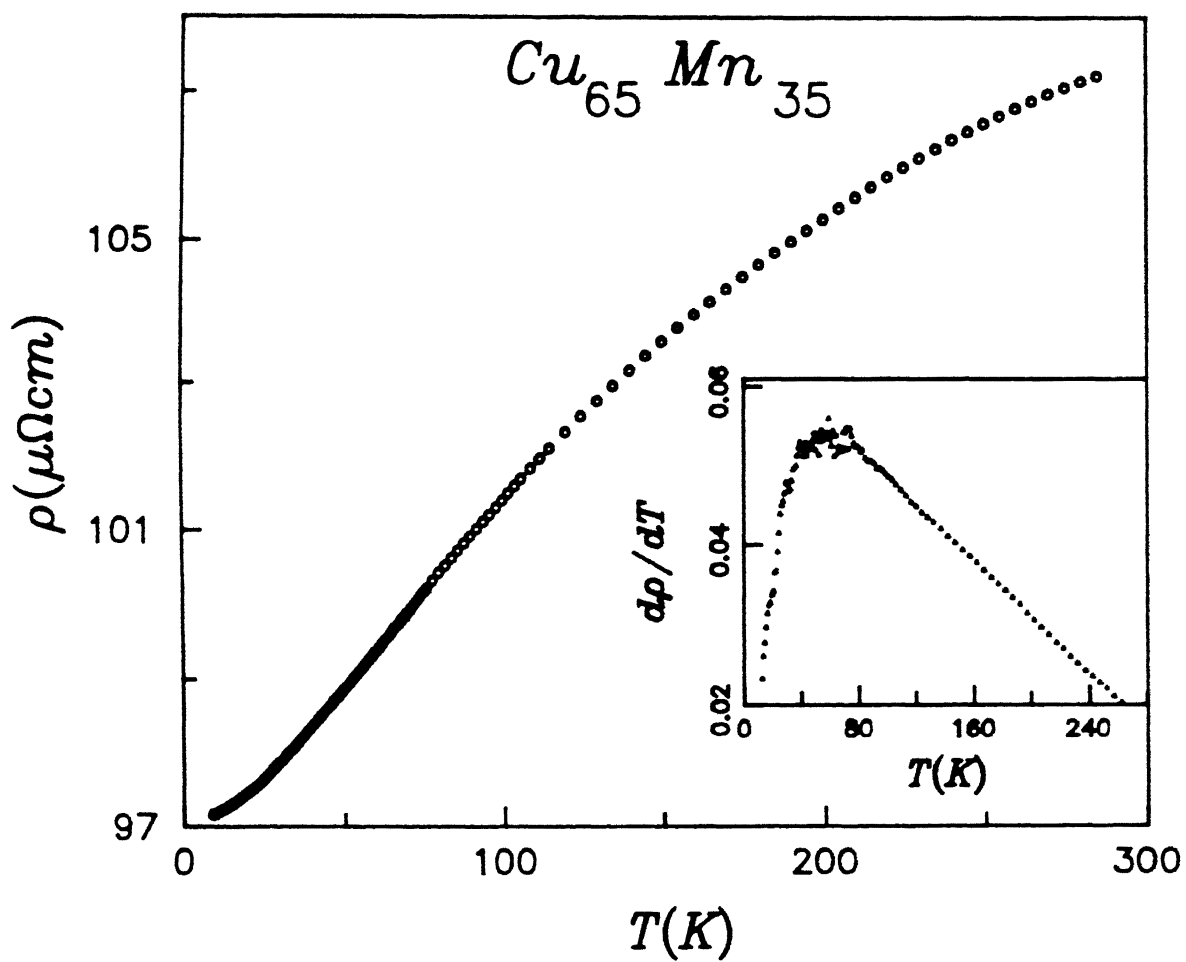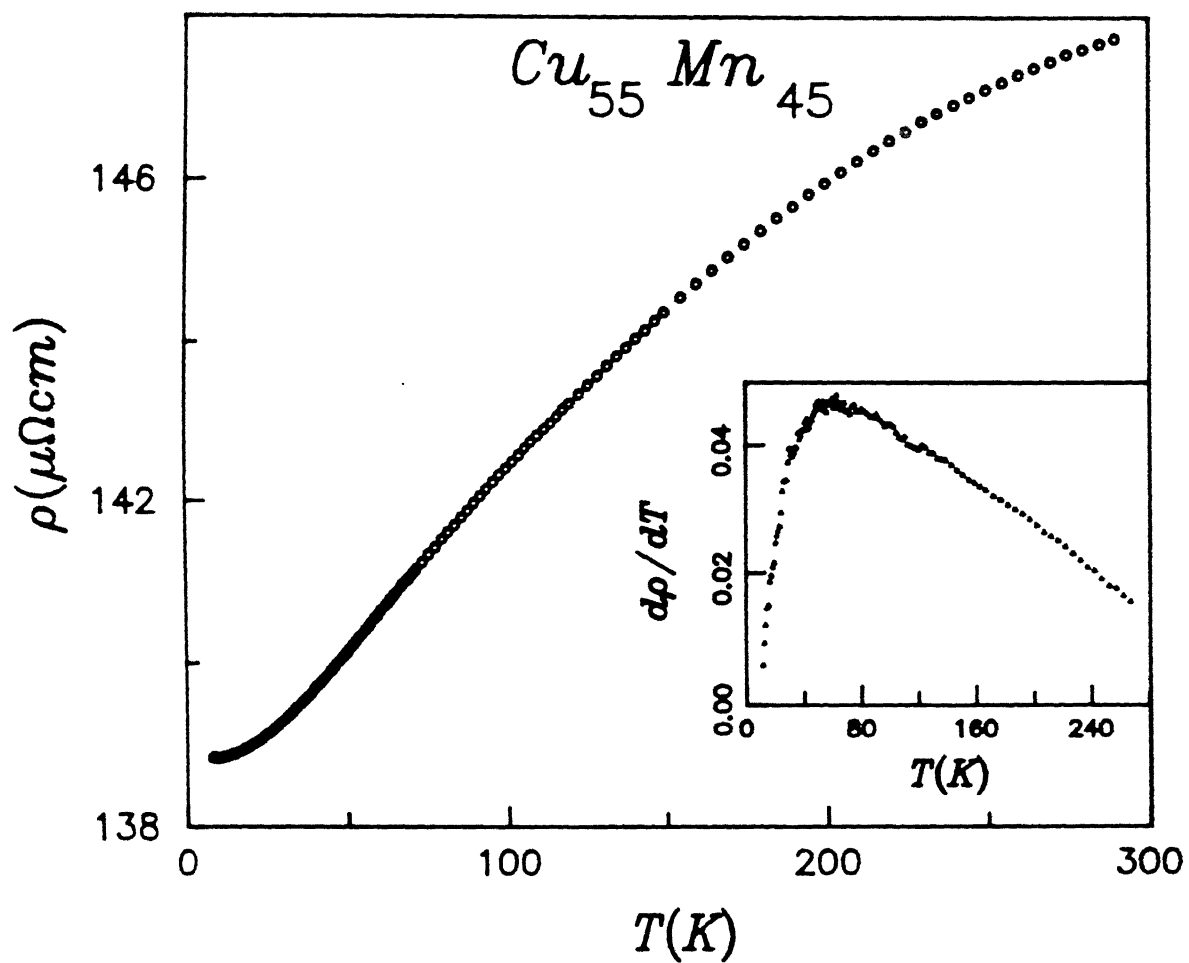Figure 3.27 Resistivity (ρ) vs temperature for sample with x = 72. Inset shows the derivative dρ/dT vs T.
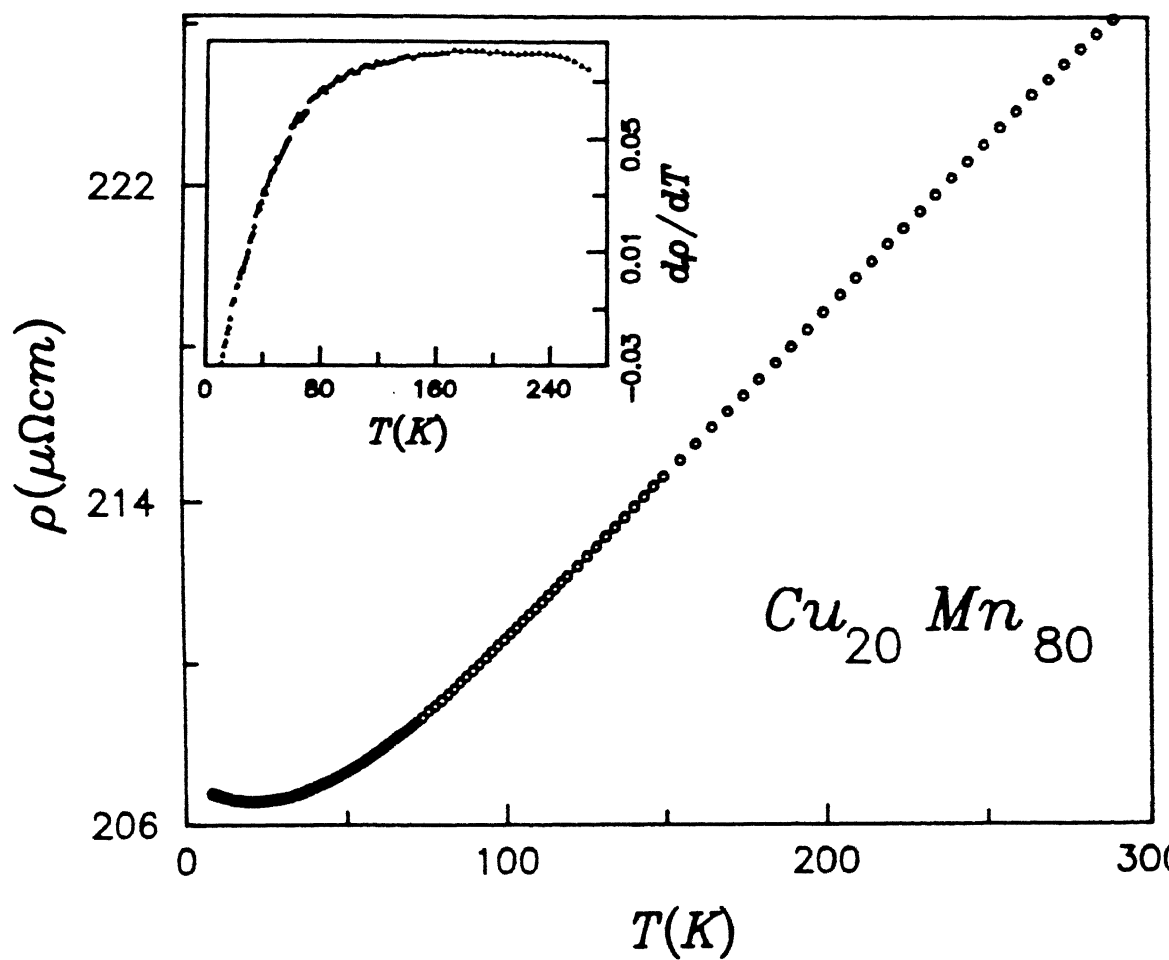
Figure 3.28 Resistivity (ρ) vs temperature for sample with x = 80. Inset shows the derivative $d\rho/dT$ vs T.
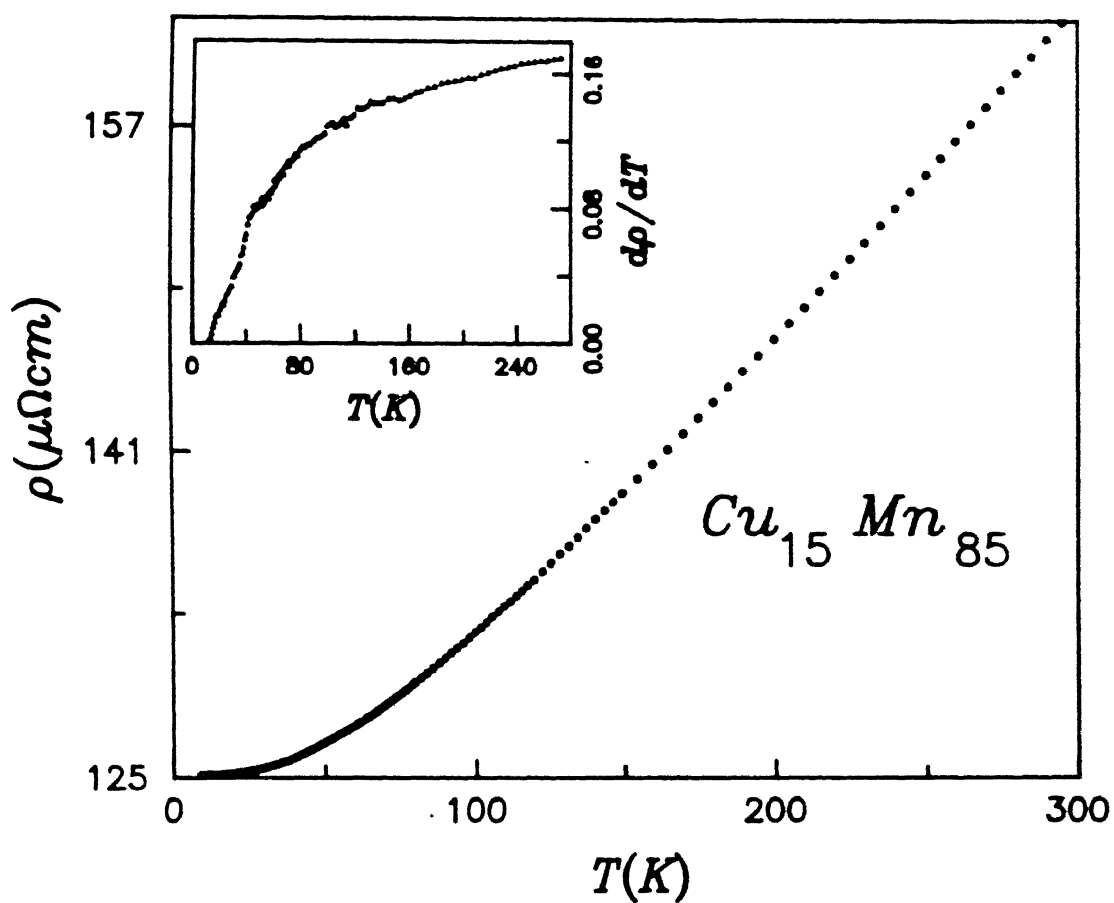
Figure 3.29 Resistivity (ρ) vs temperature for sample with x = 85. Inset shows the derivative $d\rho/dT$ vs T.

the data points and the smooth ρ vs T curves are just the raw data and not the smoothed out data. Such accurate and smooth experimental curves obviously motivate one to do a quantitative analysis of the data and squeeze out as much information as possible. We make an attempt here to analyze the $\rho(T)$ data in spite of the difficulties we face with the metastable state (crystallographic) of our samples and the general problem of interpreting the resistivity data for concentrated polycrystalline alloys. When we tried to measure the resistivity of these alloys above room temperature, we observed a decrease in resistivity from slightly above room temperature. Our x-ray analysis on some of the samples, annealed even at $100^{O}C$, shows a change in crystallographic structure with the appearance of α-phase. This has restricted us from measuring the high-temperature resistivity and using the data to extract the lattice contribution independently.

The alloys with x = 55-80 show resistivity minima at low temperatures. Earlier studies on the resistivity of concentrated CuMn alloys have also shown such minima above x = 55 [58]. The existence of resistivity minima in concentrated crystalline alloys and the associated controversies about their origin is quite a common but outstanding problem. In an attempt to check whether the minimum has got magnetic origin or not, we tried to measure the magnetoresistance in some of these alloys. But the change in resistivity at 10 kOe field was less than 1 part in 10^4 even at the lowest temperature. This prevented us from reaching any conclusion on that basis. This negligible change in

resistivity in a magnetic field may be because of very low magnetization of the samples [59]. Levin and Mill [60] have considered the effect of spin clusters in the calculation of resistivity for NiCu alloys and they predicted a resistivity minimum in concentrated crystalline alloys. Rivier [61] has shown the possibility of resistivity minimum in spin-glasses. His treatment is based upon scattering of electrons by spin diffusion modes and electrostatic potential. The criteria for resistivity minima require strong impurity scattering which is not satisfied by noble metal-transition metal canonical spin-glasses. Fischer [29] has proposed resistivity minima in spin-glasses by combining elastic scattering with inelastic scattering of electrons but the exact nature of it is not explored. Recently Mookerjee [62] has predicted the existence of resistivity minima in highly resistive alloys ($\rho \simeq$ 150 - 600 $\mu\Omega$cm) only on the basis of electron-phonon interaction. The high residual resistivity is an indication of electrons being "sluggish" near the Fermi level. These electrons can exchange energy with a phonon bath which will lead to a decrease in resistivity. If τ_e is the time scale related to the life time of electron in the vicinity of an ion and τ_0 is the time scale associated with the ground state of phonon bath, then as long as $\tau_0 \geq \tau_e$ the electron-phonon coupling will reduce the resistivity. Mookerjee has further shown that with the increase in disorder the minima in resistivity shift to higher temperatures. Our alloys, having resistivity minima, have ρ_0 in the range which satisfies the criteria ($\rho_0 \simeq$ 150 - 600 $\mu\Omega$cm) for resistivity minimum. The temperature of minima increases

monotonically from 10 to 28K with the increase in x from 45 to 72

accompanied by an increase in ρ_0. Since ρ_0 can be considered as a

measure of disorder, the shift of the resistivity minima to higher

temperature with the increase in ρ_0 for x = 45-72 gives us

confidence to apply the above theory to our alloys. Though for

x = 80 the value of ρ_0 is higher than that of x = 72 the decrease

in the temperature of the resistivity minimum may be because of

its higher Debye temperature (θ) [63], which suggests a lower τ_0

and hence the criterion $\tau_0 \geq \tau_e$ is satisfied only at a lower

temperature.

Figures 3.23 -3.29 show the following features :

a. ρ vs T curves for x = 35-72 are S-shaped whereas for x =
      80-85, they are always concave upwards.

b. $\frac{d\rho}{dT}$ vs T curves for x =35-72 show broad maxima at T_{max} which
      increases with x. For x = 80-85, $\frac{d\rho}{dT}$ increases monotonically
      with T although very slowly at high temperatures.

Both the above features, namely, the S-shaped ρ(T) curves and the

occurrence of maxima in $\frac{d\rho}{dT}$ (T) are observed in spin-glasses

[64,65]. These behaviors give indications of possible magnetic

contributions to electrical resistivity.

The measured resistivity in these alloys have

contributions from different physical phenomena. If we assume the

validity of Matthiessen's rule, then the measured resistivity

has got contributions from static disorder, i.e., the residual

resistivity (ρ_0), the electron-phonon scattering (ρ_{ph}) and the

magnetic scattering (ρ_{mag}). Hence we can write

$$\rho(T) = \rho_o + \rho_{ph}(T) + \rho_{mag}(T) . \qquad (3.17)$$

In the strong scattering regime, near the Anderson localization, the Boltzmann formalism breaks down and so is the Matthiessen's rule. This is one of the reasons for concentrating on the higher temperature region and we apply Equation (3.17) above the resistivity minima.

A theoretical calculation for the temperature dependence of resistivity in these polycrystalline materials is very difficult for various reasons. The absence of a proper band structure calculation poses the main hurdle. So we have tackled the problem in a round-about way. To estimate the magnetic contribution to resistivity from our measured $\rho(T)$, we have properly taken care of ρ_o and ρ_{ph} and assumed the validity of Matthiessen's rule in the present case. We have taken the standard Bloch-Grüneisen formula for ρ_{ph}[66] . Then $\rho(T)$ from Equation (3.17) becomes

$$\rho(T) = \rho_o + A\left[\frac{T}{\theta}\right]^5 \int_0^{\theta/T} \frac{z^5 dz}{(e^z-1)(1-e^{-z})} + \rho_{mag} , \qquad (3.18)$$

where ρ_o and A are temperature-independent constants and θ is the Debye temperature.

Rivier and Adkins [28] have shown that for spin-glass the $\rho_{mag} \propto T^{3/2}$ below the freezing temperature (T_f) but Fischer [29] found a magnetic contribution of the form $BT^2-CT^{5/2}$ below T_f with constants B and C > 0. He has also remarked that the $T^{3/2}$ variation is because of ferromagnetically ordered spins in

spin-glass.

Thus $\rho(T)$ takes the following two different forms due to ρ_{mag} predicted by the above two theories :

$$\rho(T) = \rho_0 + A\left(\frac{T}{\theta}\right)^5 \int_0^{\theta/T} \frac{z^5 dz}{(e^z - 1)(1 - e^{-z})} + BT^{3/2} \qquad (3.19)$$

and

$$\rho(T) = \rho_0 + A\left(\frac{T}{\theta}\right)^5 \int_0^{\theta/T} \frac{z^5 dz}{(e^z - 1)(1 - e^{-z})} + BT^2 - CT^{5/2} \ . \qquad (3.20)$$

We wrote a programme which can fit the experimental $\rho(T)$ data to Equation (3.18) in general, if we give the value of θ and the form of ρ_{mag}. We have checked our programme by fitting the experimental $\rho(T)$ data for pure gold taken from literature [64] to Equation (3.18) with $\rho_{mag} = 0$. Further, we have added different forms of $\rho_{mag}(T)$ (as for example, $aT^{3/2}$ or $bT^2 - cT^3$, etc.) to the $\rho(T)$ value of pure gold and fitted the resulting data to Equation (3.18) using our programme. We could retrieve the same constants ρ_0, a, b and c etc. and a normalized mean-squared deviation χ^2 consistent with the accuracy of the data. We have defined the χ^2 of the fit as

$$\chi^2 = \frac{1}{N} \sum_{i=1}^{N} \frac{(\rho_{i\ measured} - \rho_{i\ fitted})^2}{\rho_{mean}^2} \ ,$$

where N is the number of data points, $\rho_{measured}$, ρ_{fitted} and ρ_{mean}

are the measured, fitted and the mean of the measured values of the resistivity respectively. The confidence in this kind of fitting is justified by the recent work of Böttger and Hesse [67] in re-entrant spin-glasses.

We have fitted our experimental $\rho(T)$ data to Equations (3.19) and (3.20) separately taking ρ_0, A, B and C as parameters and θ of our alloys from literature [63]. The temperature range of the fit is always below T_f (determined from χ_{ac} and χ_{dc} measurements) and above the temperature of the resistivity minimum. We have tried different temperature ranges within the above specified range. We find that, for alloys with x=35,45,55 and 85 , fitting the data to Equation (3.19) gives unphysical signs of the parameters. For the others, the value of χ^2 are less by about a factor of two when fitted to Equation (3.20). Moreover, as shown in Figure 3.30 where deviations of each data point from the best fitted curves (Equations (3.19) and (3.20)) for x=72 are plotted against T, the deviations from Equation (3.19) are not only larger but also they show a systematic trend implying a poor fit. In the case of the fit to Equation (3.20) the deviation curve cuts the temperature axis much more often. On the basis of this fitting we conclude that the expression $BT^2-CT^{5/2}$ describes the magnetic contribution to the resistivity better in the spin-glass or cluster-glass range ($<T_f$) for our samples. The best temperature range of the above fit is decided on the basis of χ^2 values which are consistent with the experimental accuracy. Table 3.5 summarizes the result of this fitting procedure.
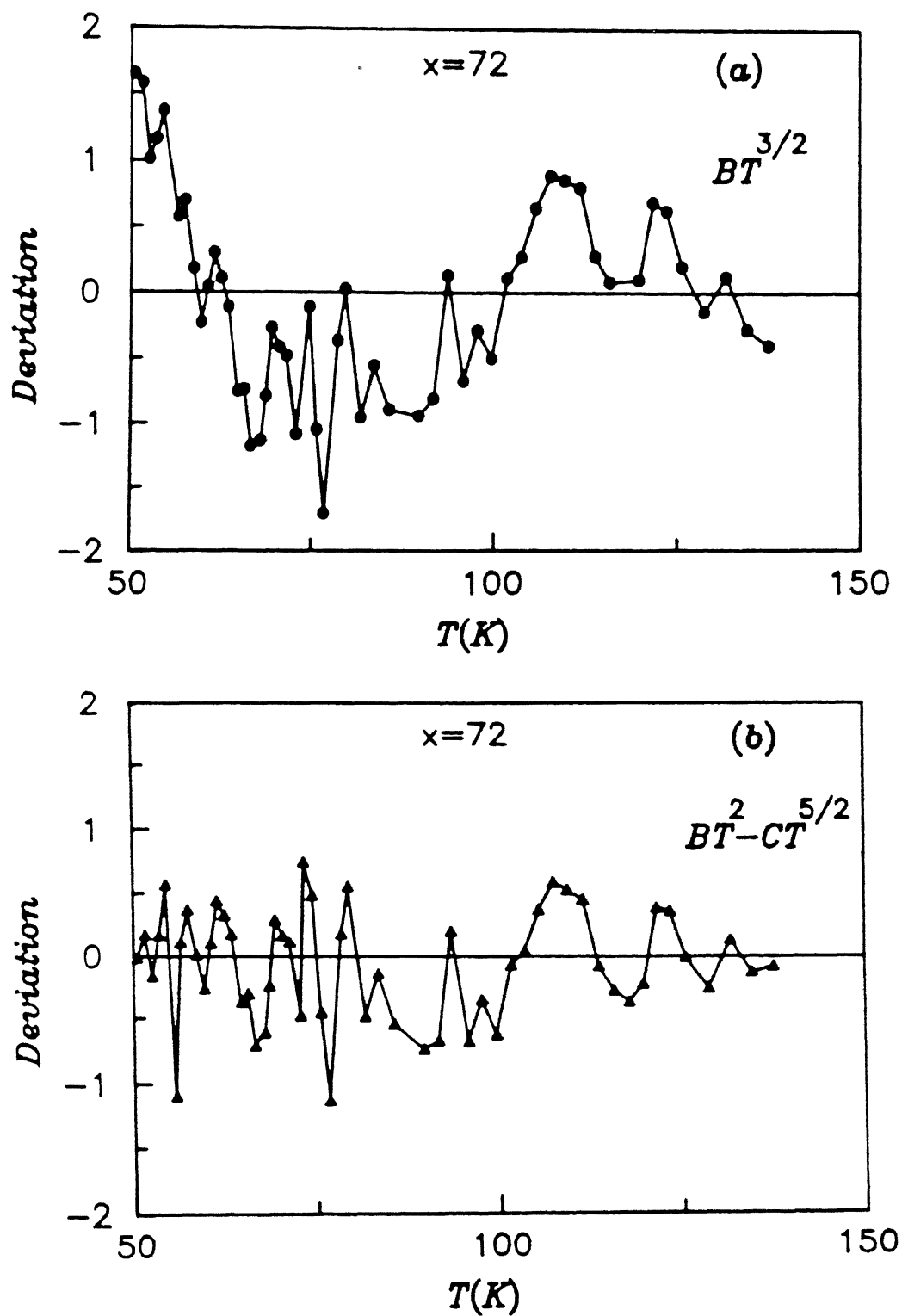
Figure 3.30 Deviation vs temperature for fits of resistivity data to Equations (3.19) and (3.20) for x = 72.

Table 3.5

Mn x (at %)	θ (K)	Range of fit (K)	χ^2 (10^{-10})	ρ_0 ($\mu\Omega$-cm)	A ($\mu\Omega$-cm)	B (10^{-4} $\mu\Omega$cmK^{-2})	C (10^{-5} $\mu\Omega$cmK$^{-5/2}$)
35	325	60-90	13.8	98	10.3	7.3	5.6
45	320	80-140	25.7	139	8.0	3.0	2.0
55	310	80-150	57.5	169	5.1	1.3	0.7
65	305	70-150	15.9	170	4.1	1.6	0.9
72	305	50-140	7.8	196	7.1	0.8	0.2
80	325	30-120	8.4	206	11.5	3.9	1.7
85	360	45-110	62.3	124	5.2	11.5	4.8

The justification for our observation of ρ_{mag} following $BT^2-CT^{5/2}$ type of relation rather than $BT^{3/2}$ type below T_f can be found in Fischer's original calculations. He has shown that the $T^{3/2}$ type of contribution in resistivity comes from the ferromagnetic clusters in spin-glasses but our system in no way can be considered to have ferromagnetic clusters. On the contrary this form of resistivity tends to the Yosida limit [59] of a dilute antiferromagnet $(V^2+S^2J^2/4)$ at zero temperature. Alongwith these Fischer's calculations hold for systems with large impurity concentration and in a temperature range where the Kondo effect may be neglected. The range of fit, especially the fitting at higher temperatures, can be rationalized from the physical consideration of spin diffusive modes which are the sources of scattering of conduction electrons. At low temperatures the spin

diffusive modes may become ineffective for bigger clusters. This is because at low temperatures the spin waves with wavelength smaller than the cluster diameter will freeze out. The absence of any experimental or theoretical input about the density of states at the Fermi level and the effective mass of electrons forbids us from making any comment about the concentration dependence of the constants A,B and C of Table 3.5. We should note that a good fit for x = 85 may indicate the presence of spin-glass type of spin diffusive modes also in this sample and hence justifies our conjecture for the presence of a mixed phase (antiferromagnetic and spin-glass) in it (dotted line in the phase diagram (Figure 3.21)).

The magnetic resistivity above T_f is predicted using ρ_0 and A from the fit below T_f and the $\rho(T)$ data above T_f as

$$\rho_{mag}(T) = \rho(T) - \rho_0 - A \left(\frac{T}{\theta} \right)^5 \int_0^{\theta/T} \frac{z^5 dz}{(e^z-1)(1-e^{-z})} \qquad (3.21)$$

$\rho_{mag}(T)$, thus obtained, shows maxima around 180K for x=35-65 , moving towards 240K for x = 72 and no maximum for x = 80 and 85 (Figures 3.31 and 3.32). The sample with x=80, however, shows a decrease in slope around 300K which may be taken as a precursor to a possible maximum in ρ_{mag} . In contrast, x=85 shows that the slope is still increasing around 300K. In canonical spin-glasses the temperature, at which ρ_{mag} is maximum, is found to increase with the addition of transition element impurities [64,65]. Inoue and Nakamura [68] have found similar behaviour of ρ_{mag} with maxima around 275K for $Cu_{100-x}Mn_x$ alloys with x=16-25.
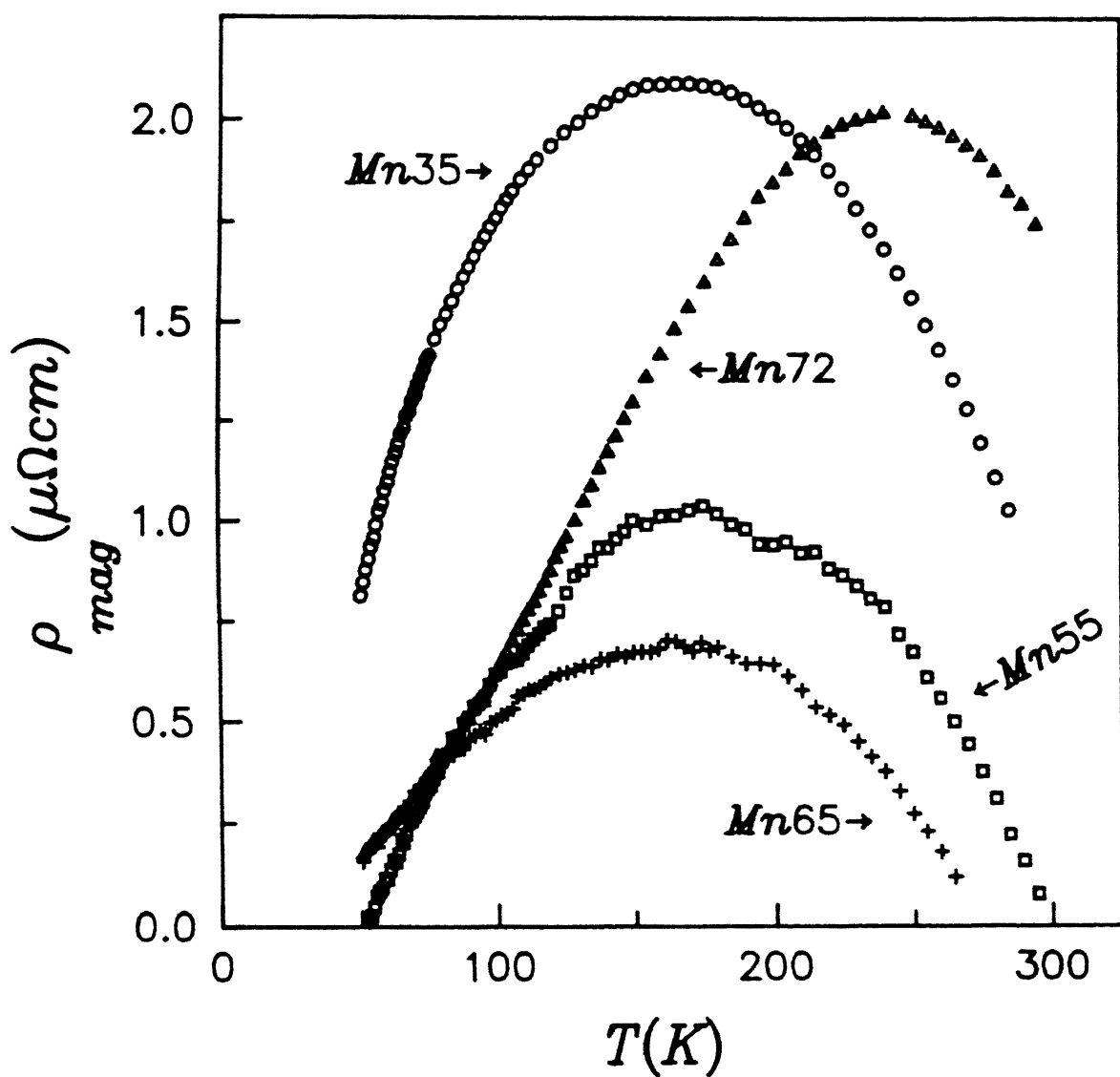
Figure 3.31 Magnetic contribution to resistivity (ρ_{mag}) vs temperature for x = 35, 55, 65and 72.

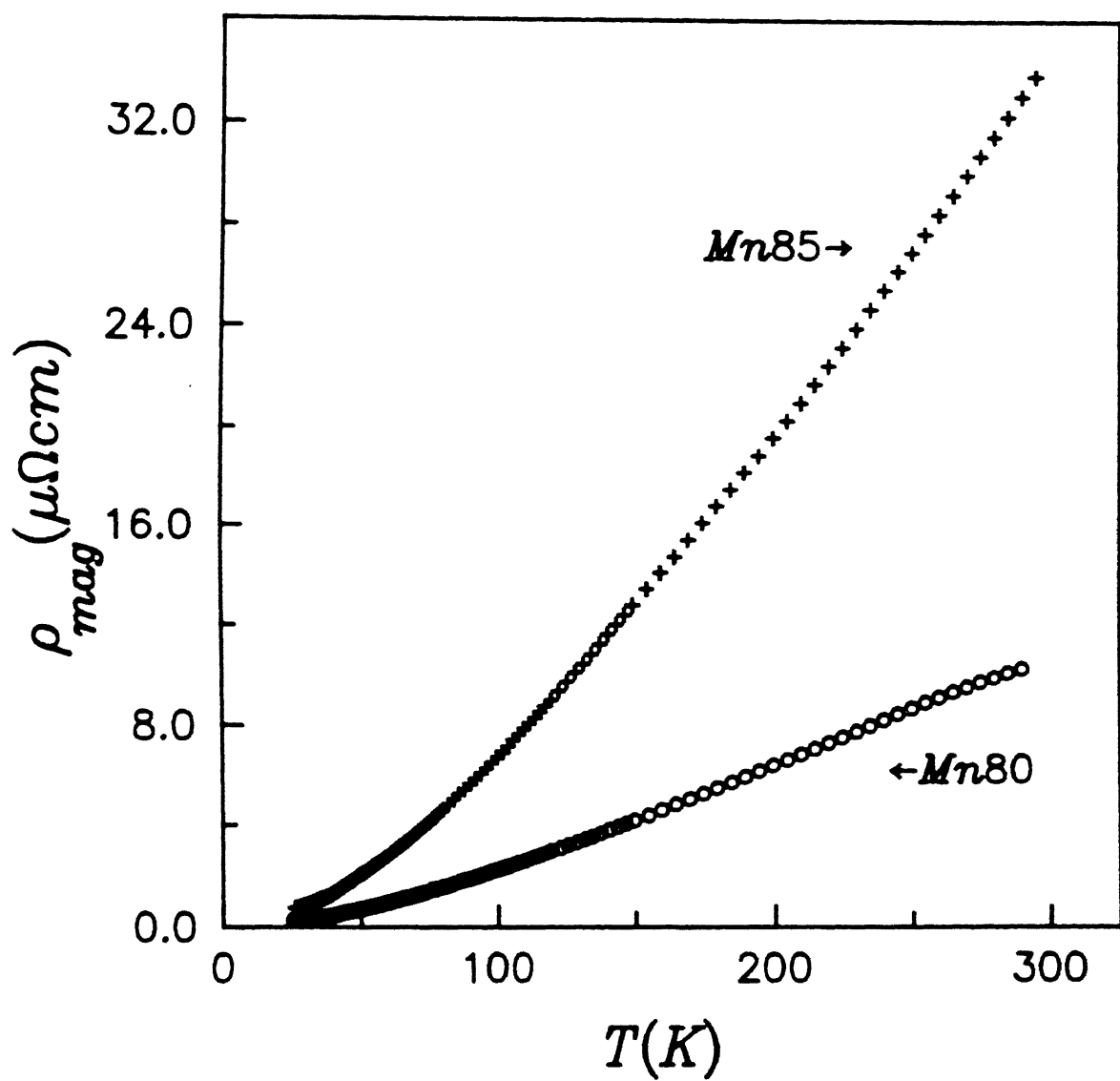Figure 3.32 Magnetic contribution to resistivity (ρ_{mag}) vs temperature for x = 80 and 85.

Thus we find that the occurance of maximum in ρ_{mag} in our concentrated alloys is very much similar to that of more dilute ones. One must realize that the extraction of ρ_{mag} in concentrated alloys is much more difficult since the estimation of phonon contribution cannot be made directly. However, our solitary attempt in the case of concentrated alloys has met with reasonable success.

The origin of the maximum in ρ_{mag} has been explained by many authors [64,65,69] in terms of "effective free" and "interacting" moments. For our alloys ρ_{mag}, beyond maximum, falls roughly as T^2 as predicted by the theory of Suhl [70].

For x = 80, $\partial\rho/\partial T$ (Figure 3.28) is almost constant for T>150K implying $\rho_{mag} \sim T$ or slightly slower since $\rho_{lattice} \sim T$ at high T. For x = 85, $\partial\rho/\partial T$ above 150K varies slower than T implying $\rho_{mag} \sim T^n$ with $1 \le n \le 2$. Any S-shaped $\rho(T)$ curve, i.e., ρ varying slower than T at high T, will yield a maximum in ρ_{mag} since $\rho_{lattice} \sim T$ at high T. Also, a $\rho(T)$ curve which is linear in T or varies faster than T at high T will have no maximum in ρ_{mag}. In other words, S-shaped $\rho(T)$ data will have a maximum in ρ_{mag} whereas a $\rho(T)$ curve which is concave upwards will have no maximum. The composition dependence of various important quantities are given in Table 3.6 and are shown in Figure 3.33. In the latter we have used the analyzed Mn concentration x.
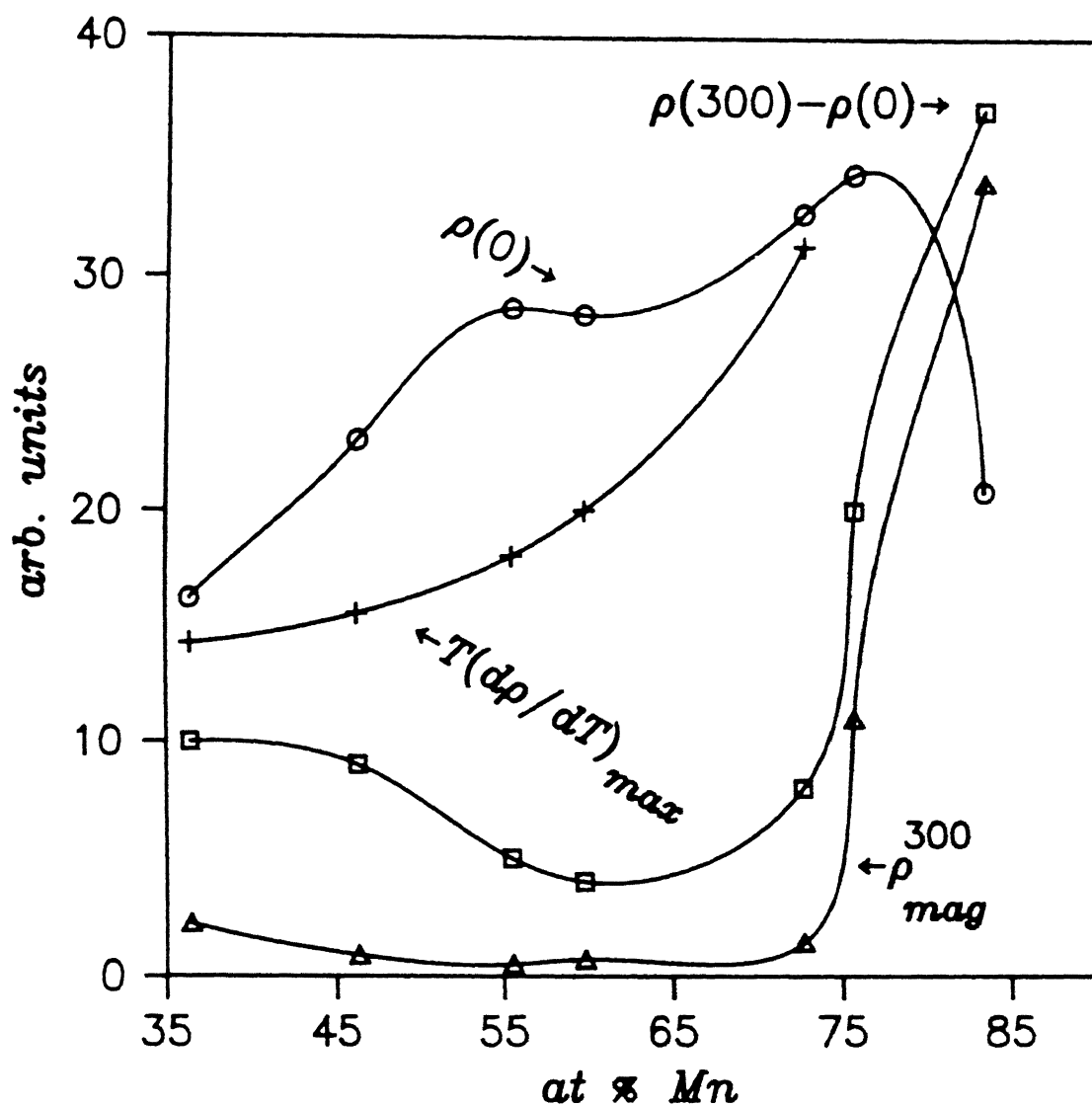
Figure 3.33 Variations of $\rho(0)$, $\rho(300)-\rho(0)$, ρ_{mag}^{300} and $T(d\rho/dT)_{max}$ with analysed Mn concentration x. The lines joining the points are just guides to the eye.

Table 3.6

Mn Conc. x (at %)	ρ_{0K} ($\mu\Omega$cm)	ρ_{300K} ($\mu\Omega$cm)	$\rho_{300K}-\rho_{0K}$ ($\mu\Omega$cm)	ρ_{mag}^{300K} ($\mu\Omega$cm)	$T(\rho_{mag}^{max})$ (K)	$T(\frac{d\rho}{dT})_{max}$ (K)
35	97	107	10	1.0	180	57
45	139	148	9	0.4	180	62
55	169	174	5	0.1	175	72
65	170	174	4	0.1	190	80
72	196	204	8	1.2	240	125
80	206	226	20	11	~300	—
85	125	162	37	34	>300	—

The values of ρ_{mag} at 300K are rather large for x=80 and 85 as compared to those for x = 35-72. This is due to the fact that in contrast to the alloys with x = 35-72, which have only short-range order, the alloys with x = 80 and 85 have long-range order (see Figure 3.21). A very similar behaviour of ρ_{mag} has been observed [64] in AuFe alloys where magnetic resistivity has a sharp increase beyond 17 at% Fe which is the percolation threshold from "mictomagnetic" to long-range ferromagnetic phases. It is rather comforting to note that the absolute values of ρ_{mag} at 300K reported in [64] agree with those of the present studies in CuMn (eg, 43 $\mu\Omega$cm for 22 at% Fe in AuFe and 34 $\mu\Omega$cm for 85 at% Mn in CuMn, both having long-range magnetic order). From Tables 3.5 and 3.6 we see that the fitted values of ρ_0 and the experimental ρ_0 (taken as the minimum ρ) are very nearly the same. We further observe that ρ_0 increases from 97 t0 206 $\mu\Omega$cm with the increase in

Mn concentration from 35 to 80 at % which implies an increase in static disorder. At the other end of concentration (x=85) we find a drop of ρ_0 to 125 $\mu\Omega$cm in confirmation to the Nordheim's rule. The difference between ρ_{300K} and ρ_{0K} is due to the lattice and magnetic scattering of electrons. This has the same x dependence as that of ρ_{mag}^{300K} implying that the lattice contribution does not depend strongly on x. This is not unexpected since the Debye temperature, θ, does not depend strongly on x (Table 3.5).

CHAPTER IV

Conclusions

The important findings of the present study are briefly summarized below :

i) Concentration fluctuations *alone* can give rise to the clustering of magnetic atoms in randomly substituted noble metal transition metal binary alloys. This is a matter of statistical chance and we have tried to show it through Figure 1.2.

The clusters thus formed in concentrated $Cu_{100-x}Mn_x$ alloys are real clusters and their response to magnetic fields dominates the magnetic properties of these alloys for all temperatures. This may be evident from the effect of dc fields on χ_{ac}, M vs H behaviors and, in general, from the variations of χ_{ac} and χ_{dc} with temperature.

On an average, bigger and bigger clusters are formed with the increase in Mn concentration x. This has been concluded from the concentration dependence of the rate of decay of the time-dependent magnetization. The same conclusion can be reached by coupling the concentration dependence of p_{eff} with the neutron diffraction results.

The decrease in the peak values of χ_{ac} and χ_{dc} with the increase in Mn concentration x and the variation of p_{eff} with x imply the presence of antiferromagnetic short-range order in the clusters. In other words, we conclude that the spins in the magnetic clusters are antiferromagnetically coupled.

ii) The magnetic phase diagram (Figure 3.21) has been obtained on the basis of various magnetic measurements. The alloys with x ≤ 72 have shown the basic signatures of spin-glass, viz, time and history-dependent dc-magnetization and peaks in ac-susceptibility (χ_{ac}). The low concentration alloys showing cusp in χ_{ac} are designated as spin-glass (SG) while the concentrated ones showing broad peaks are called cluster-glass (CG). For x =80, a double transition from paramagnetic (P) to antiferromagnetic (AF) to cluster-glass phases is observed. This, alongwith the observation of a long-range antiferromagnetic order in neutron diffraction studies at 4.2K leads to the conclusion for the existence of a *mixed* (M) phase below T_f (=130K) having properties of both antiferromagnetic and cluster-glass phases. The alloy with x = 72 seems to be very near the multicritical composition. However, the phase boundaries between CG and M and that between M and AF cannot be clearly defined.

iii) The resistivity shows qualitatively two different behaviours for x ≤ 72 and x > 72 at high temperatures ($\simeq$ 300K) as are evident from the temperature dependences of resistivity and its temperature derivative (Figure 3.23 to 3.29). This may be taken as an indication that the magnetic ordering is different for the two ranges of composition. The magnetic contribution to the electrical resistivity (ρ_{mag}) in the low-temperature range (<150K) for all the samples shows $BT^2 - CT^{5/2}$ type of spin-glass contribution. The absence of an evidence for a transition from AF to CG (or M) for x = 85 alloy in our magnetic measurements is most likely due to the very low magnetic susceptibility of the high Mn

containing alloys beyond the sensitivity of our instruments. The estimated $\rho_{mag}(T)$ at high temperature ($>150K$) shows again two different behaviours for x ≤72 and x $>$ 72. The former gives a maximum while the latter increases monotonically. The large value of ρ_{mag} , found for x = 80 and 85, indicates long-range magnetic ordering in agreement with our phase diagram. We have found for the *first* time the magnetic contribution to electrical resistivity in a concentrated crystalline alloy system.

Like any other studies the present one also has left us with a few problems for future investigations. The most striking one is about the nature of various phase boundaries in the Mn-rich region. This issue can be resolved by making more alloys with close compositions around x = 75 and studying them from $\simeq$ 4K to the required high temperatures with more sensitive and sophisticated instruments like Farady balance or SQUID magnetometer. The most puzzling problem of the present study is about the nature of the mixed phase. Whether this so-called *mixed* phase is a mixture of two magnetic phases at the same temperature or a new magnetic phase is yet to be settled. A study of magnetic anisotropy in single crystals may also throw some light on the above controversy.

REFERENCES

1. J.S.Kouvel, J. Phys. Chem. Solids $\underline{24}$, 795 (1963).

2. P.A.Beck, J. Less-Common Metals $\underline{28}$, 193 (1972).

3. E.P.Wohlfarth, Physica $\underline{86-88B}$, 852 (1977).

4. L.Néel, Adv. Phys. $\underline{4}$, 191 (1955).

5. J.L.Tholence and R.Tournier, J. de Physique $\underline{35}$, C4-229 (1974); Physica $\underline{86-88B}$, 873 (1977).

6. J.A.Mydosh and G.J.Nieuwenhuys, in *Ferromagnetic Materials*, Vol. 1, edited by E.P. Wohlfarth (North-Holland, Amsterdam, 1980), p.71.

7. A.P.Murani, S.Roth, P.Radhakrishna, B.D.Rainford, B.R.Coles, K.Ibel, G.Goeltz and F.Mezei, J. Phys. F:Metal Phys. $\underline{6}$, 425 (1976).

8. P.W.Anderson, in *Ill-Condensed Matter*, edited by R.Balian, R.Maynard, and G.Toulouse (North-Holland, Amsterdam, 1979), p.159.

9. G.Toulouse, Commun. Phys. $\underline{2}$, 115 (1977).

10. J.A.Mydosh, J. Mag. Mag. Mater. $\underline{7}$, 237 (1978).

11. N.Cowlam and A.M.Shamah, J. Phys.F:Metal Phys. $\underline{11}$, 27 (1981).

12. P.A.Bech and D.J.Chakraborti, Proc. Conf. on Amorphous Magnetism, edited by H.O. Hooper and A.M. de Graaf (Plenum Publishing Corp., New York,1973),p.273; A.M.Mukhopadhya and P.A.Beck, Solid State Commun. $\underline{16}$, 1067 (1975); R.W.Tustison and P.A.Beck, Solid State Commun. $\underline{20}$, 841 (1976); P.A.Beck, Prog. Mat. Sci. $\underline{23}$, 1 (1978).

13. *Metals Reference Book*, edited by C. J. Smithells (Butterworth, London, 1976), p.585.

14. H.Sato and R.Kikuchi, AIP Conf. Proc. $\underline{18}$, 605 (1974).

15. L.de Seze, J. Phys.C: Solid State Phys. $\underline{10}$, L353 (1977).

16. K.Binder and A.P.Young, Rev. Mod. Phys. $\underline{58}$, 801 (1986).

17. D.Chowdhury, in *Spin Glasses and Other Frustrated Systems* (Word Scientific, Singapore, 1987).

18. W.Marshall, Phys. Rev. $\underline{118}$, 1519 (1960).

19. M.W.Klein and R.Brout, Phys. Rev. $\underline{132}$, 2412 (1963).

20. J.Souletie and R.Tournier, J. Low Temp. Phys. 1, 85 (1969).

21. E.P.Wohlfarth, Phys. Lett. A70, 489 (1979); J. Phys.F: Metal Phys. 10, L241 (1980); S.Shtrikman and E.P.Wohlfarth, Phys. Lett. A85, 467 (1981).

22. E.P.Wohlfarth,in *Magnetism*, edited by G.T. Rado and H. Shuhl (Academic Press, 1963), Vol 3, p.351.

23. C.A.M.Mulder, A.J.van Duyneveldt and J.A.Mydosh, J. Mag. Mag. Mater.15-18,141 (1980).

24. A.P.Murani, J. Mag. Mag. Mater. 22, 271 (1981).

25. C.N.Guy, J. Phys.F: Metal Phys. 7, 1505 (1977); J. Phys.F: Metal Phys. 8, 1309 (1978).

26. J.Souletie, J. de Physique 44, 1085 (1983).

27. C.Y.Huang. J. Mag. Mag. Mater. 51, 1 (1985).

28. N.Rivier and K.Adkins, J. Phys.F: Metal Phys. 5, 1745 (1975).

29. K.H.Fischer, Z. Phys. B34, 45 (1979).

30. D.Meneghetti and S.S.Sidhu, Phys. Rev. 105, 130 (1957).

31. M.C.K.Wiltshire, M.M.Elcombe and C.J.Howard, J. Phys.F: Metal Phys. 15, 1595 (1985).

32. P.Gibbs, T.M.Harders and J.H.Smith, J. Phys.F: Metal Phys. 15, 213 (1985).

33. A.V.Vedyaev and V.A.Cherenkov, Sov. Phys. JETP 64, 1254 (1986).

34. *Vogel's Text Book of Quantitative Inorganic Analysis* (Longman, 4th edition, 1978), p.693.

35. L.Hartshorn, J. Sci. Instrum. 2, 145 (1925).

36. C.M.Brodbeck, R.R.Bukrey and J.T.Hoeksema, Rev. Sci. Instrum. 49, 1279 (1978).

37. S.C.Whitemore, S.R.Ryan and T.M.Sanders. Jr., Rev. Sci. Instrum. 49, 1579 (1978).

38. M.Kumano and Y.Ikegami, Rev. Sci. Instrum. 50, 921(1979).

39. M.R.Corson, Rev. Sci. Instrum. 53, 1606 (1982).

40. S. Ramakrishnan, S. Sundaram, R.S. Pandit and G. Chandra, J. Phys.E: Sci. Instrum. 18, 650 (1985).

41. M.Prasad, R.R.Rao and A.K.Raychaudhuri, J. Phys.E: Sci. Instrum. 18, 1013 (1986).

42. M.D.Rosenthal and B.W.Maxfield, Rev. Sci. Instrum. 46, 398 (1975).

43. G.Foex, C.J.Gorter and C.J.Smiths, in *Selected constants Diamagnetism and Paramagnetism, Paramagnetic Relaxatio* (Masson, Paris, 1957).

44. H.St.Rade, J. Phys. Chem. 77, 424 (1973).

45. A.K.Majumdar and P.V.Blanckenhagen, Phys. Rev. B29, 4070 (1984).

46. R.J.Cava, B.Batlogg, R.B.van Dover, D.W.Murphy, S.Sunshine, T.Siegrist, J.P.Remeika, E.A.Reitman, S.Zahurak and G.P.Espinsosa, Phys. Rev. Lett. 58, 1676 (1987).

47. A.K.Nigam and A.K.Majumdar, Phys. Rev. B29, 4040 (1984).

48. L.E.Wenger and J.A.Mydosh, Phys. Rev. B29, 4156 (1984).

49. D.Fiorani, J.L.Dormann, J.L.Tholence, L.Bessais and D.Villers, J. Mag. Mag. Mater. 54-57, 173 (1986).

50. V.Canella and J.A.Mydosh, Phys. Rev. B6, 4220 (1972).

51. D.J.Dunlop, Rev. Geophys. and Space Phys. 11, 855 (1973).

52. R.Street and J.C.Woolley, Proc. Phys. Soc. (London) A62, 56 (1949); B69, 1189 (1956).

53. P.Gaunt, Phil. Mag. 34, 774 (1975).

54. H.Claus and J.S.Kouvel, Solid State Commun. 17, 1553 (1975)

55. J.S.Kouvel and W.Abdul-Razzaq, J. Mag. Mag. Mater. 53, 13 (1985).

56. A.Mookerjee and S.B.Roy to be published in Pramana.

57. A.N.Bazhan and S.V.Petrov, Proc. Indo-Soviet Conf. on Low Temp. Phys. Jan. 11-14, 24 (1984).

58. B.R.Coles, Physica 91B, 167 (1977).

59. K.Yosida, Phys. Rev. 107, 396 (1957).

60. K.Levin and D.L.Mill, Phys. Rev. B9, 2354 (1974).

61. N.Rivier, J. Phys.F: Metal Phys. 4, L249 (1974).

62. A.Mookerjee, J. Phys.: Condens. Matter 2, 897 (1990).

63. J.L.Zimmerman and H.Sato, J. Phys. Chem. Solids 21, 7
    (1961).

64. J.A.Mydosh, P.J.Ford, M.P.Kawatra and T.E.Whall, Phys. Rev.
    B10, 2845 (1974).

65. I.A.Campbell, P.J.Ford and A.Hamzic, Phys. Rev. B26, 419ϵ
    (1982).

66. J.M.Ziman, in *Electrons and Phonons* (Oxford University Press,
    London, 1963).

67. Ch.Böttger and J.Hesse Z. Phys. B75, 485 (1989).

68. K.Inoue and Y.Nakamura J. Phys. Soc. Japan 29, 1095 (1970).

69 A.W.Sheikh and M.El-Fazani, Phys. Stat. Sol. 147, 601 (1988).

70. H.Shul, Phys. Rev. Lett. 20, 656 (1968).

APPENDIX I

Work in other areas

During the course of the thesis work the author was actively involved in research work in other branches of condensed matter physics. This resulted in the following publications:

1. Phenomenological approach to the electronic structure of glassy transition-metal alloys, A. Banerjee, Vijay A. Singh and A. K. Majumdar, Phys. Rev. B32 , 8384 (1985).

2. Effect of annealing condition on high temperature superconductivity in $La_{2-x}Sr_x CuO_4$, A. K. Rastogi, A. Banerjee, Manju Tewari and D. Bahadur, Phase Transitions 10, 123 (1987).

3. YBaCuO superconductor prepared by citrate nitrate gel method, D. Bahadur, A. Banerjee, A. Das, K. P. Gupta, Tom Mathews, A. Mitra, M. Tewari and A. K. Majumdar, Reviews of Solid State Sciences 2, 177 (1988) .

4. Structure and superconductivity in $Y^{3+} Ba^{2+}_{2-x} Na^+_x Cu^{3+}_{3-y}Cu^{2+}_y O^{2-}_{8-(x+y)/2-\delta}$, D. Bahadur, A. Banerjee, A. Das, K.P. Gupta, A. Mitra, M. Tewari and A. K. Majumdar, Advances in Ferrites (Ed. C.M.Srivastava and M.J.Patni, Oxford and IBH Publishing, New Delhi), 727 (1989).

5. Superconducting glass ceramics in Bi-Pb-Sr-Ca-Cu-O system, D. Bahadur, A. Banerjee, A. Das, K. P. Gupta, A. Mitra, M. Tewari, and A. K. Majumdar, Mater. Res. Bull. 24, 1405 (1989).

6. Effect of optimal thermal treatment in $BiSrCaCu_2O_y$, D.Bahadur, A.Banerjee, A.Das, K.P.Gupta, A.Mitra, M.Tewari and A.K.Majumdar, J. Mat. Sci., to appear (1990).